

ORIGIN OF TOURMALINE IN A POTENTIAL SEDEX-TYPE DEPOSIT,
PENRHYN GROUP, MELVILLE PENINSULA.
NUNAVUT, CANADA

Anne C. Belanger

Submitted in Partial Fulfilment of the Requirements
For the Degree of Bachelor of Sciences, Honours
Department of Earth Sciences
Dalhousie University, Halifax, Nova Scotia
April 2011


DATE: APRIL 25, 2011

AUTHOR: ANNE C. BELANGER

TITLE: ORIGINS OF TOURMALINE IN A POTENTIAL SEDEX-TYPE DEPOSIT
PENRYHN GROUP, MELVILLE PENINSULA, NUNAVUT
CANADA

Degree: B.Sc. Convocation: May Year: 2011

Permission is herewith granted to Dalhousie University to circulate and to have copied for non-commercial purposes, at its discretion, the above title upon the request of individuals or institutions.


Signature of Author

THE AUTHOR RESERVES OTHER PUBLICATION RIGHTS, AND NEITHER THE THESIS NOR EXTENSIVE EXTRACTS FROM IT MAY BE PRINTED OR OTHERWISE REPRODUCED WITHOUT THE AUTHOR'S WRITTEN PERMISSION.

THE AUTHOR ATTESTS THAT PERMISSION HAS BEEN OBTAINED FOR THE USE OF ANY COPYRIGHTED MATERIAL APPEARING IN THIS THESIS (OTHER THAN BRIEF EXCERPTS REQUIRING ONLY PROPER ACKNOWLEDGEMENT IN SCHOLARLY WRITING) AND THAT ALL SUCH USE IS CLEARLY ACKNOWLEDGED.

ABSTRACT

A suite of metamorphosed and hydrothermally altered sedimentary and chemogenic rocks was sampled from an area on the northern flank of Barrow River, Melville Peninsula (N 67°24'08.44", W 82°35'43.23"), Nunavut. The study area is in the Proterozoic Penryhn Group which lies within the Foxe Fold Belt of the Trans-Hudson orogen. On a regional scale, the Penryhn Group consists of interlayered pelitic and psammitic gneisses, amphibolites, marbles and calc-silicates, all intruded by continental arc and syn-collisional plutons and pegmatites.

In order to identify the nature and extent of superimposed hydrothermal and metamorphic processes, samples were collected from 19 outcrops spanning an area of about 400 x 100 m. Sampled lithologies include amphibolites, granites, tourmalinites, greywackes and sulphide-rich rocks, typically with abundant fine-grained, euhedral tourmaline crystals. The presence of matrix K-feldspar and fibrolitic sillimanite within tourmaline cores suggests upper amphibolite facies metamorphism. Sulphide-rich layers contain pyrrhotite and pyrite, however their abundance is highly variable throughout the sampling area.

The study area has been the focus of several mineral exploration projects, including those by Aquataine (1970), Borealis Exploration Limited (BEL; 1985-87), and BEL-BHP (1994-1996). Assays indicated concentrations of 2000-7000 ppb Au, with Zn contents locally over 9%. The area was classified as a "black shale" environment.

This report focuses on the petrography, composition, origin of tourmaline and evaluation of sedimentary-exhalative type deposit potential. At least two generations of tourmaline have been documented from petrographic and electron microprobe work; early tourmaline may be detrital while other crystals were generated in two stages of hydrothermal metamorphism and mineralization. Tourmalines range in colour from clear to light-brown, locally with darker cores that may have been inherited from originally detrital grains. Distinctive diamond-shaped oikocrysts, interpreted as pseudomorphs after tremolite, consist of medium-grained muscovite + tourmaline ± sillimanite cores with finer-grained albite + quartz + orthoclase + tourmaline rims. Tourmaline compositions are Mg-rich (dravite) with variable Mg/(Mg+Fe) from 0.57 in cores to 0.94-0.98 in rims. Boron and magnesium are believed to have been derived from pre-metamorphic sediments. Dravite tourmaline, tourmalinites and diabase intrusive, within an intercontinental basin and a possibility for local rifting and minor concentrations of Zn, Pb and Au, all suggest the study area could have been deposited with a sedimentary-exhalative environment.

Table of Contents

ABSTRACT	III
TABLE OF TABLES	VII
TABLE OF ABBREVIATIONS.....	VIII
ACKNOWLEDGEMENTS	IX
CHAPTER 1 – INTRODUCTION.....	10
1.1 OVERVIEW OF STUDY AREA	10
1.2 PREVIOUS WORK	10
1.3 TOURMALINE AS AN INDICATOR MINERAL	11
1.4 PURPOSE AND SCOPE OF THESIS.....	12
CHAPTER 2: REGIONAL GEOLOGY AND STUDY AREA.....	13
2.1 TRANS-HUDSON OROGEN.....	13
2.2 PRINCE ALBERT GROUP.....	14
2.3 PENRYHN GROUP.....	14
2.4 STRUCTURE AND METAMORPHISM	15
2.5 STUDY AREA	16
2.6 LIMITATIONS	19
CHAPTER 3: PETROGRAPHY	20
3.1 SUPRACRUSTAL ROCKS	20
3.1.1. <i>Amphibolite</i>	20
3.1.2. <i>Graphite-rich pelite</i>	23
3.1.3. <i>Tourmaline-rich pelite</i>	28
3.1.4. <i>Tourmalinite</i>	31
3.1.5. <i>Greywacke</i>	33
3.2 INTRUSIVE ROCKS.....	35
3.2.1. <i>Diabase</i>	35
3.2.2. <i>Granite</i>	38
3.3 DISCUSSION	40
3.3.1. <i>Depositional Environment</i>	40
3.3.2. <i>Stages of Deformation</i>	40
3.3.3. <i>Generation of Tourmaline and Sulphides</i>	40
3.3.4. <i>Pseudomorphs</i>	41
3.3.5. <i>Evidence for Hydrothermal Alteration</i>	41
CHAPTER 4: MINERAL CHEMISTRY.....	42
4.1 MAJOR ELEMENT ANALYSIS	42
4.2 SUPRACRUSTAL ROCKS	44
4.2.1 <i>Amphibolite</i>	44
4.2.2. <i>Graphite-rich pelites</i>	45
4.2.3. <i>Tourmaline-rich pelites</i>	45
4.2.4. <i>Tourmalinites</i>	45
4.3 INTRUSIVE ROCKS.....	45
4.3.1. <i>Granites</i>	45
4.4 DISCUSSION	46
4.4.1 <i>Tourmaline Analysis</i>	46
4.4.2. <i>Fluorine bearing minerals</i>	47
CHAPTER 5: DISCUSSION.....	50
5.1 ORIGIN OF TOURMALINE.....	50
5.1.1 <i>Pseudomorphs</i>	51

5.2.1.1 Reaction 1	52
5.1.1.2 Reaction 2	53
5.1.1.3. Reaction 3	54
5.1.1.4 Implications.....	56
5.2 SEDIMENTARY-EXHALATIVE (SEDEX) BASINS AND DEPOSITS	57
5.4 PENRYHN ECONOMIC POTENTIAL	61
CHAPTER 6: CONCLUSIONS	65
APPENDIX A: MICROPROBE ANALYSES	
APPENDIX B: MICROPROBE IMAGES.....	
APPENDIX C: SAMPLE AREA MAP	
REFERENCES	

Table of Figures

Figure 2.1: Regional geology of the Trans-Hudson Orogen and Melville Peninsula	13
Figure 2.2: Foxe Fold Belt of the Trans-Hudson Orogen	15
Figure 2.3: General study area outcrop appearance.	17
Figure 2.4: Sample area outcrops.....	18
Figure 3.1: Coarse tremolite crystals, amphibolite hand sample	21
Figure 3.2: Scanned thin section of amphibolite.....	22
Figure 3.3: Magnified diamond-shaped tremolite from amphibolite.	22
Figure 3.4: Sericitized amphibolite.	23
Figure 3.5: Graphite-rich pelite handsample.....	25
Figure 3.6: Graphite-rich oikocryst deformation	25
Figure 3.7: Scanned thin-section of fibrolitic sillimanite and muscovite pods	26
Figure 3.8: Oikocrysts in graphite-rich pelite.	26
Figure 3.9: Oikocryst formation.....	27
Figure 3.10: Tourmaline-rich pelite hand sample	29
Figure 3.11: Schistosity in tourmaline-rich pelite.....	29
Figure 3.12: Zoned tourmaline in tourmaline-rich pelites	30
Figure 3.13: Tourmalines in tourmaline-rich pelite	30
Figure 3.14: Sulfide-rich tourmalinites hand sample.....	32
Figure 3.15: Co-existentPyrrhotite and pyrite.....	32
Figure 3.16: Representative photomicrograph of tourmaline abundance in tourmalinites	33
Figure 3.17: Greywacke hand sample.....	34
Figure 3.18: Typical greywacke texture	34
Figure 3.19: Tourmaline is only visible at high magnification, greywacke.....	34
Figure 3.20: Altered fine-grained diabase.....	36
Figure 3.21: Scanned thin section of diabase in contact with possible graphite-rich pelite	36
Figure 3.22: Magnified boundary between diabase and matrix of quartz, plagioclase and tourmaline.....	37
Figure 3.23: Fine granular clinopyroxene and sulphides rimmed by chlorite	37
Figure 3.24: Alteration zoning in granite handsample.....	39
Figure 3.25: Colourless titanite adjacent to chlorite	39
Figure 4.1: Amphibole classification diagram	44
Figure 4.2: Tourmaline Na/(Na+Ca) vs. Fe/(Fe+Mg) diagram.....	47
Figure 4.3: Tourmaline compositions are dravite to alkali-free dravite: ternary diagram	47
Figure 4.4: Fluorine in all Fe-Mg bearing phases.....	48
Figure 4.5: Fluorine within study area tourmalines	49
Figure 5.1: Typical cross-section of vent proximal SEDEX-type deposit.....	57
Figure 5.2: Tourmaline alteration of the Sullivan SEDEX Deposit in British Columbia	58
Figure 5.3: Stages of oikocryst formation.....	52
Figure 5.4: The product of first reaction	53
Figure 5.5: Polished thin-section of oikocryst.	54
Figure 5.6: Proposed before and after of pseudomorph reaction.	51
Figure 5.7: Scales of pseudomorphs observation from hand sample to thin section	55
Figure 5.8: Scanned thin section of pseudomorphs within graphite-rich pelite.....	56
Figure 5.9: Tourmalines correlation to economic potential of deposits.....	63
Figure 5.10: Lake sediment samples of Au concentrations through S-E Melville Peninsula.....	Error!

Bookmark not defined.

Table of Tables

Table 4.1. Representative Tourmaline Compositions.....	42
Table 4.2 Silicate Compositions	43
Table 4.3: Accessory Compositions	43
Table 4.4. Oxide Compositions	43
Table 4.5. Sulphide Compositions	43

Table of Abbreviations

Lithology	Abbreviation
Amphibolite	Amph
Granite	Grnt
GraphitePelite	GPelite
Tourmaline-rich Pelite	TPelite
Tourmalinite	Tmlt

Mineral	Abbreviation
Chlorite	chl
Muscovite	ms
K-feldspar	kspar
Plagioclase	pl
Phlogopite	phl
Pumpellyite	pmp
Pyrrhotite	po
Quartz	qtz
Rutile	rt
Sillimanite	sil
Tourmaline	trm
Titanite	tnt

ACKNOWLEDGEMENTS

I wish to express my sincerest gratitude to my supervisors, Dr. Rebecca Jamieson and Dr. David Corrigan (GSC Ottawa) who provided me with the opportunity to work on this project and who guided me throughout the writing process. I would like to especially thank Dr. Leopold Nadeau, Saskia Erdmann and the entire crew in Barrow River camp for an amazing field season and support with this project. I would like to thank NRCAN and the Geological Survey of Canada for generously funding this project. Last but not least I would like to acknowledge my family in Ontario and the faculty and students at Dalhousie University for supporting me throughout my three years in Dalhousie Geology.

CHAPTER 1 – INTRODUCTION

1.1 Overview of Study Area

The south-eastern bedrock portion of Nunavut's Melville Peninsula is underlain mainly by continental margin deposits of the Penryhn Group (2-1.9 Ga), deposited during the Proterozoic onto Archean basement. The stratigraphically lower sections of the Penryhn Group consist of alternating layers of pelitic and psammitic gneisses, amphibolites, marbles and calc-silicates. These upper basinal psammities correlate stratigraphically to the Piling, Hoare Bay and Lake Harbour Groups of southern Baffin Island and the Karrat Group of Greenland within the Foxe Fold Belt of the Trans-Hudson Orogen and they show potential for base metal deposits (Corrigan et al. 2010).

Along the northern flank of Barrow River, Melville Peninsula (N 67°24'08.44", W 82°35'43.23"), within the Penryhn Group, samples were collected from 19 outcrops of highly metamorphosed sedimentary and chemogenic rocks to identify the original rock type, the mechanism and extent of superimposed hydrothermal alteration and metamorphism, and to propose a possible environment for deposition and mineralization.

1.2 Previous work

Previous mineral exploration of the Penryhn Group, began in the 1970s, conducted by Aquitane Company of Canada (ACC). The Geological Survey of Canada's 1977 regional lake sediment sampling program documented high values of arsenic in surrounding lakes within the area (Marmot 1994). Exploration by Borealis Exploration Limited (1985) led to the completion of the Nagvaak Project, an extensive drilling program run by BHP Minerals in 1996. Two grab samples, taken in direct proximity to my sample area, were found to contain significant Zn-Pb mineralization, associated with fine-grained galena, sphalerite, pyrite and pyrrhotite along an

approximate 1700 m strike-length horizon. Assays returned values of 9.68% Zn, 9.50% Pb, 15ppm Ag and 1200 ppm Cu. BHP Minerals proposed that the deposit may be a sedimentary-exhalative environment and SEDEX-type deposit (Marmot 1994). The Nagvaak Project, however, lacked detailed documentation of petrology and metamorphism of the area (Marmot 1994).

1.3 Tourmaline as an Indicator Mineral

Tourmaline is identified in the study and can be used as an exploration guide and an indicator mineral for deposits. The general tourmaline composition is: $XY_3Z_6B_3Si_6O_{27}(O, OH, F)_4$, where: X = Ca, Na, K, vacancy; Y = Li, Mg, Fe^{2+} , Mn^{2+} , Zn, Al, Cr^{3+} , V^{3+} , Fe^{3+} , Ti^{4+} ; Z = Al, Fe^{3+} , Cr^{3+} , V^{3+} (Clarke et al. 1989). Tourmaline usually forms trigonal habit and elongate, euhedral crystals. Tourmaline can be red, green, blue, pink, brown, colourless and almost black depending on major element substitutions. Aluminum, Mg, Fe and B are compulsory in order to form tourmaline whereas other vacancies can be occupied by a variety of different sized and charged cations to the extent that tourmaline has 14 recognized species.

Tourmalines ability to accept an extremely wide range of cations to the X, Y and Z sites also gives it a high potential to record the chemical environment in which it formed, including fluid composition and host-rock composition (Galbraith et al. 2009). Tourmaline is stable up to granulite facies metamorphism and its resistance to weathering and alteration makes it an excellent storage mineral (Galbraith et al. 2009).

Tourmaline has been proven as a useful proximity indicator mineral for a variety of mineral deposits (Galbraith et al. 2009; Henry and Guidotti 1985; Jolliff et al. 1986; Clarke et al. 1989; Pirajno and Smithies 1992; Slack 1996; Keller et al. 1999; Garda et al. 2003; Jiang et al. 2004) especially granitic, volcanic massive sulphide (VMS) and stratabound deposits types

(Slack 1994). The combination of major element, trace element and boron isotope compositions are most useful to determine mineral deposit association potential of tourmalines (Clarke et al. 1989). Tourmalines associated with granitic and VMS deposits tend to be more Fe-rich (schorl) whereas tourmalines associated with stratabound deposits tend to be more Mg-rich (dravite) (Slack 1996). Complete understanding of tourmaline as an indicator mineral to host environment and deposit potential has not been fully accomplished, however a major breakthrough is believed to be eminent (Van Hinsberg et al. 2011).

1.4 Purpose and Scope of Thesis

The specific objectives of this study are to:

1. Document mineralogy and textures
2. Determine the extent and timing of hydrothermal alteration and metamorphism
3. Relation to tourmaline generation and the sulphide mineral paragenesis
4. Test sedimentary exhalative origin hypothesis

Petrological and electron microprobe work was completed on these samples to determine mineralogy and mineral compositions, and the results are compared with data from the literature.

In Chapter 2, I present the regional geology of the Melville Peninsula, Nunavut and to document the Penryhn Group geology. Chapter 3 presents petrology, organized by lithology based on normal and polished thin sections. Chapter 4 presents electron microprobe methods and results with discussion and comparison in Chapter 3 findings. Chapter 5 discusses the results and Chapter 6 presents conclusions and recommendations for future work.

Field work for this report was conducted in early August 2010, through the GEM-minerals program on Melville Peninsula co-led by Dr. David Corrigan of the Geological Survey of Canada (GSC Ottawa) and Dr. Leopold Nadeau (GSC Quebec City).

CHAPTER 2: REGIONAL GEOLOGY AND STUDY AREA

2.1 Trans-Hudson Orogen

The Trans-Hudson Orogen (THO) is a continent-to-continent collisional orogenic belt that sutured together the Archean Rae, Hearne, Superior and Wyoming cratons. The THO took place in the Paleoproterozoic (1600 Ma to 2500 Ma) resulting in an orogenic belt comparable in scale to the Himalaya-Karakoram-Tibetan Orogen (St-Onge et al. 2007). The orogen is currently exposed over 4600 km from south-west Greenland, across Hudson Bay, and south down to Wyoming, USA (Wyoming craton) (Fig. 2.1). The Penryhn Group is located within the Foxe Fold Belt on the south-east side of Melville Peninsula and is a basal feature of the Trans-Hudson Orogen (THO).

The Neoproterozoic Rae craton is the dominant bedrock of Melville Peninsula, consisting of 2.72-2.58 Ga granitoid rocks and thin 2.73-2.70 Ga greenstone belts (Prince Albert Group) intruded by 2.6 Ga granite bodies (Berman et al., 2010).

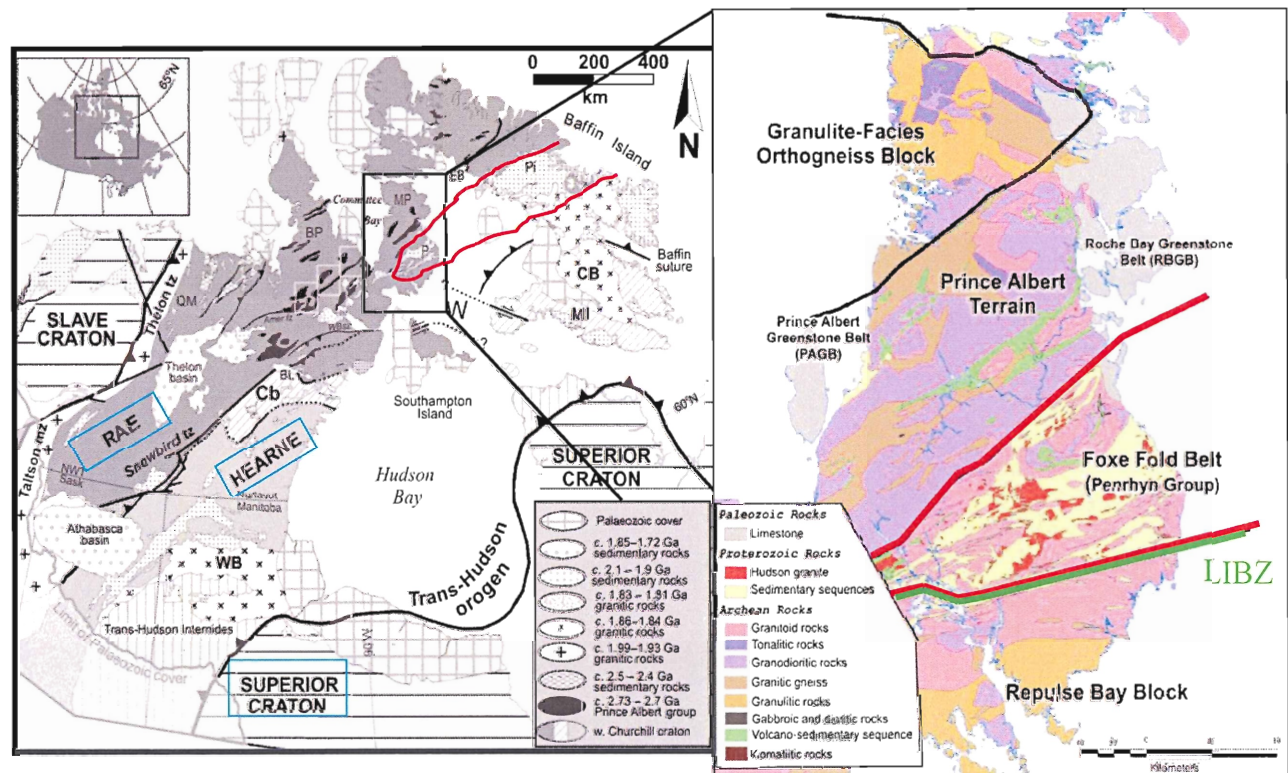


Figure 2.1: Regional geology of the Trans-Hudson Orogen and Melville Peninsula. The Trans-Hudson Orogen involved the collision of the Rae, Hearne, Superior (outlined in blue) and the Wyoming craton, which outcrops to the SW of this figure. The Penryhn Group (P) outcrops on Melville Peninsula (MP) within the Foxe Fold Belt (outlined in red) and correlates to the Piling Group (Pi) on Baffin Island. The Lyon-Inlet Boundary Zone (LIBZ, green) is referenced later in 2.4 *Structure and Metamorphism* as a suture-zone bounding the granulite-facies Repulse Bay (Trans-Hudson Orogen diagram, ages and naming modified from Berman et al. 2010. Melville Peninsula diagram modified from Houle. et al 2010.)

2.2 Prince Albert Group

The Prince Albert Group (PAG) consists of three units; a lower (2735-2728 Ma), middle (2715-2705 Ma) and upper (2690 Ma) sequence (Henderson 1983). The lower sequence consists of basalts, rhyolite lapilli tuffs, and komatiites, with the middle sequence consisting of psammities with peridotite intrusions, quartzites, intermediate tuff, and dacite. The upper PAG consists of semipelites, basalts and komatiites (Henderson 1983). Extending from south-west to north-east across Melville Peninsula, the PAG has potential for high concentrations of gold or other base metal occurrences.

2.3 Penryhn Group

Deformation during the Hudsonian Orogeny and unconformable contacts with underlying Archean granitoid gneisses indicate a Paleoproterozoic age for the Penryhn Group. It represents an accumulation of clastic and chemical sediments, within a shallow hypersaline basin (Henderson 1983). The Penryhn Group currently covers about 13000 km² of the southern area of the peninsula, stretching 200 km east to west and about 120 km north to south (Hill 1996).

The Penryhn Group consists of an interlayered succession of psammitic and pelitic gneisses, calc-silicates, marbles, amphibolites, quartzites and granitic to pegmatitic intrusions (Henderson 1983). Pelitic gneisses are typically rich in graphite with varying amounts of garnet, sillimanite and cordierite. Calc-silicates display complex deformational features with interfolding marble and silicate-rich layers. Marbles are generally diopside-rich, and massive. Amphibolite forms medium-to-fine-grained, locally foliated pods possibly accompanied by coarse-grained, serpentized ultramafic rocks. Penryhn amphibolites and other mafic volcanic and intrusive units at the bases of correlative units (Piling Group), indicate a rifting origin (Johns et al. 2006).

Metasedimentary rocks of the Penryhn Group correlate with the Piling Group on Baffin Island, as well as the Karat Group on Greenland (Fig. 2.2). Penryhn Group carbonaceous

metapelitic rocks (black shale) locally contain small disseminations of iron, zinc and nickel sulphides (Marmot 1996). Prominent zinc and lead showings in the Karat Group (Black Angel mine) and gold within the Piling Group have sparked exploration interest in the Penryhn Group, where significant gold or other base metal deposits have yet to be discovered. Exploration is difficult however, because leaching and oxidation of base metal sulphides from exposed rocks, has produced many rusty outcrops throughout the Penryhn Group succession.

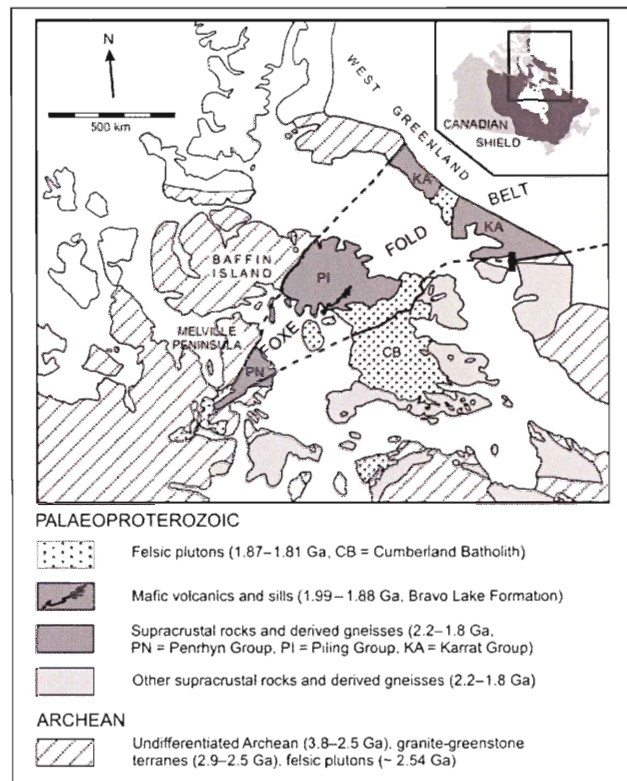


Figure 2.2: Foxe Fold Belt of the Trans-Hudson Orogen. The Penryhn Group (PN) stratigraphically correlates to the Piling Group (PI) on Baffin Island and Karat Group (KA) on Greenland all outcropping within the Foxe Fold belt. (Berman et al. 2010)

2.4 Structure and Metamorphism

The Penryhn Group has been subjected to upper amphibolite facies regional metamorphism. Mineral assemblages and textures within paragneisses suggest maximum burial

depths of 17 km with 4.9 to 5.4 kb pressures and temperatures reaching 700°C to 749°C (Henderson 1983).

Medium- to high-grade metamorphism and strong penetrative deformation of the Penryhn Group, have for the most part, obliterated primary sedimentary textures, although these can be observed locally. Deformation seems to have occurred during two distinct periods, with a first higher grade event of orogen-normal shortening involving thick-skinned north-vergent thrust imbrications, and a second higher grade event producing right-lateral transpression. Peak metamorphism is indicated by the axial-planar growth of highest grade metamorphic minerals with right-lateral (east-west) orientation. This latter event appears to have been generated by oblique collision of the Repulse Bay crustal block. The Lyon Inlet Boundary Zone represents the suture bounding the granulite-facies Repulse Bay block to the south and the amphibolite facies Rae Craton *sensu stricto* with Paleoproterozoic cover to the north (Fig. 2.1).

2.5 Study Area

The rolling flat hills of the Melville Peninsula tundra reflect the underlying predominately metasedimentary rocks and their susceptibility to weathering and erosion. Along the Barrow River, at N 67°24'08.44", W 82°35'43.23", a generally flat 400m by 100m rectangular sample area encompasses continuous pods of rusty outcrops and frost-heave zones (Fig. 2.3). The study area was chosen because previous exploration suggested the potential for mineralization. Outcrops are generally about 3m in length and 1m to 2m wide and spaced about 2m to 4m apart (Fig 2.4). Lithologies are metasedimentary rocks, with light-brown to brown weathered surfaces, with a rusty purple tone for the more sulphur-rich outcrops. Metasedimentary rocks are predominately fine-grained (typically <1mm), where as amphibolites are medium-to coarse-grained (0.3cm-2cm). Minerals distinguishable in hand sample include

coarse-grained tremolite crystals in amphibolites; quartz, feldspar, and micas within greywackes, and disseminated or medium-grained pyrite within tourmalinites. Outcrops lack distinctive mesoscopic structures as a result to their low relief and weathering.



Figure 2.3: General study area outcrop appearance. Outcrops throughout the sample area were brown to rusty orange with adjacent frost heave samples. Deformation indicators on outcrop scale were for the most part absent.

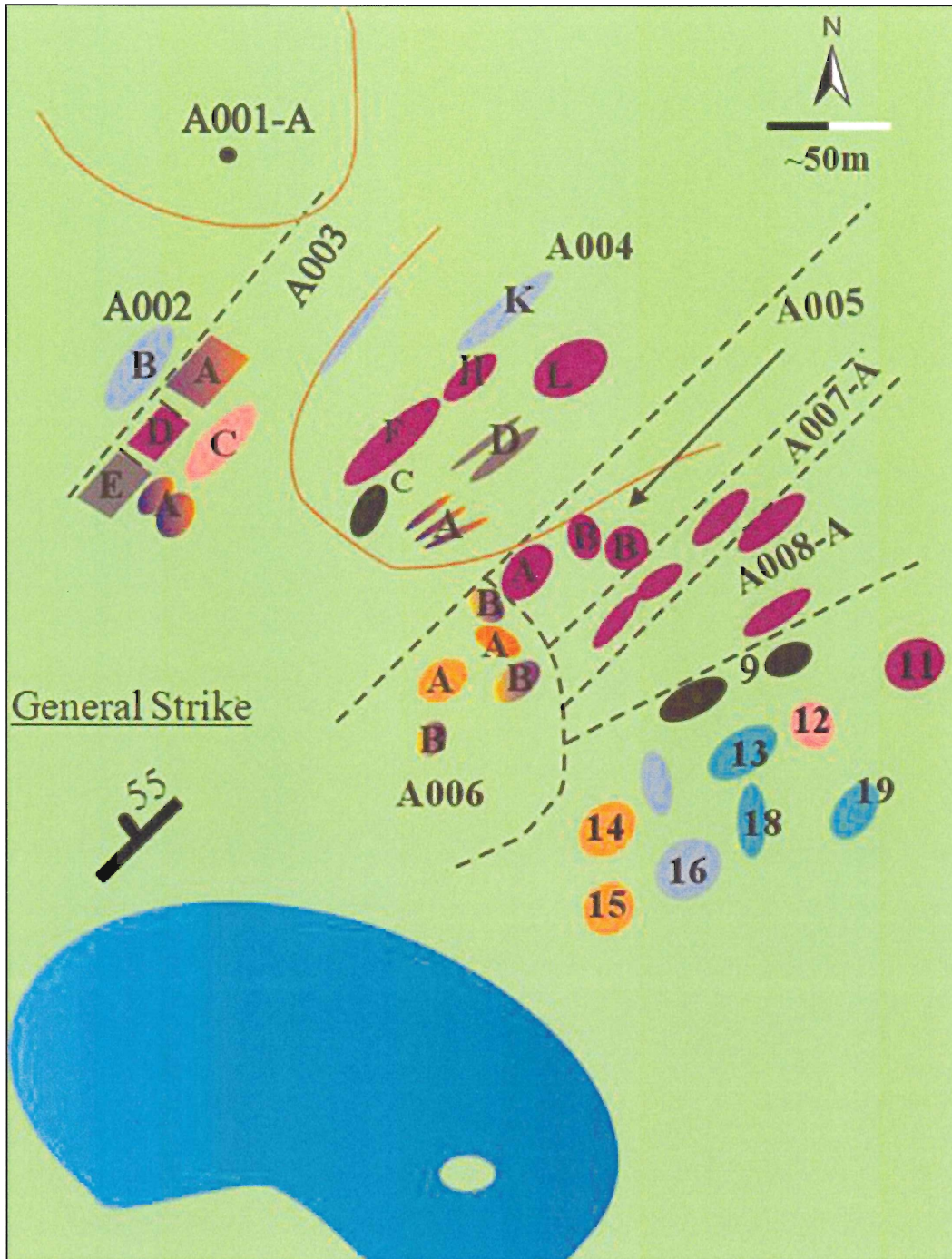


Figure 2.4: Sample area outcrops. Dashed lines separate clusters of outcrops defined during the mapping and indicate the general trend of sampled units. Samples were taken at $N67^{\circ}24'08.44''$, $W82^{\circ}35'43.23''$ +/- 200m.

- | | | |
|--|--|---|
| ● Graphite-rich pelite | ● Granite | ● Tourmaline-rich pelite |
| ● Amphibolite | ● Tourmalinite | ● Greywacke |
| ● Musc-schist | ● Gabbro | |

2.6 Limitations

Limitations to this project include the classification of the type of sedimentary basin from which the study area originates and the sources of B, Mg and hydrothermal fluids that facilitated tourmaline growth and metamorphism. Sedimentary basin type hypotheses can only be inferred from previous studies because the study area is not large enough to provide sufficient information needed in order to deduce my own hypothesis.

ICP-MS would be especially useful to document B and S-isotope values for tourmalines and sulphides which could provide valuable insight into sedimentary basin chemistry. Enrichment in ^{34}S is characteristic of Proterozoic SEDEX-type deposits and indicates high retention of H_2S in the bottom of the water column, indicating anoxia.

Boron isotope values indicative of seawater influence on clastic sedimentary rocks are -15.4 to -1.7‰, however B-isotopes are also influenced by temperature and alkalinity of the water that interacted with the sediments, Rayleigh fractionation, post-depositional alteration and metamorphism and skewing the possibility for a quantitative conclusion.

Hydrothermal fluids could be sourced from basin circulating waters, saturated sediments, prograde dehydration reactions and compression induced fluid migration from distant areas.

CHAPTER 3: PETROGRAPHY

A detailed petrographic study was conducted to determine the sequence of mineral formation, sulphide-mineral paragenesis, mineral assemblages and corresponding deformation history in samples from the study area. In this chapter, protolith rock names have been used wherever possible, with metamorphic rock names used where no primary features survive. Rocks are grouped based on similar hand sample appearances and mineralogical abundances and have been separated into two categories: supracrustal and intrusive rocks. Supracrustal rocks, originally deposited within the Paleoproterozoic basin, have been classified as greywackes, graphite-rich pelites, tourmaline-rich pelites, tourmalinites and amphibolites. Intrusive units that have retained primary characteristics include Proterozoic granite and diabase.

3.1 Supracrustal Rocks

Rock types from the region are described from most to least abundant within the sample area. Lithology is indistinguishable from outcrop features as the entire area consisted of small, rounded mounds of crumbly or unstructured rock of rusty-brown colour.

3.1.1 Amphibolite

In hand sample, amphibolites are grey to dark-grey with coarse (5-10 mm) tremolite crystals poorly aligned on fresh and weathered surfaces (Fig 3.1). Amphibolites generally consist of coarse-grained diamond- or oblate-shaped tremolite (45-60%, Fig 3.2) accompanied by graphite (15-10%), fine-grained tourmaline (10%), phlogopite (7%), titanite (2%), apatite (1%), quartz (10-5%) and potassium feldspar (10-5%). Tremolite crystals are idioblastic to subidioblastic (2 x 5mm to 0.3 x 0.5mm), with cores containing graphite and minor tourmaline (Fig 3.3). Tremolite crystals (Sample A004-L) show little tendency to be aligned where as matrix graphite crystals define a weak fabric. Tourmalines are fine to very-fine-grained crystals (0.5mm

to 0.01mm) with both elongate and basal sections. Cores of tourmalines are generally dark green, sharply contrasting with the light brown to colourless rims; no other zonal layers are present. Quartz and potassium feldspar are matrix minerals (0.2 mm). Matrix phlogopite crystals (0.1 mm) are aligned in the foliation. Titanite and apatite are scattered throughout the matrix as xenoblastic clusters (0.3 mm). More altered tremolites (A004-F, A011-A) are pokiloblastic, irregular crystals in a sericitized matrix (Fig 3.4).

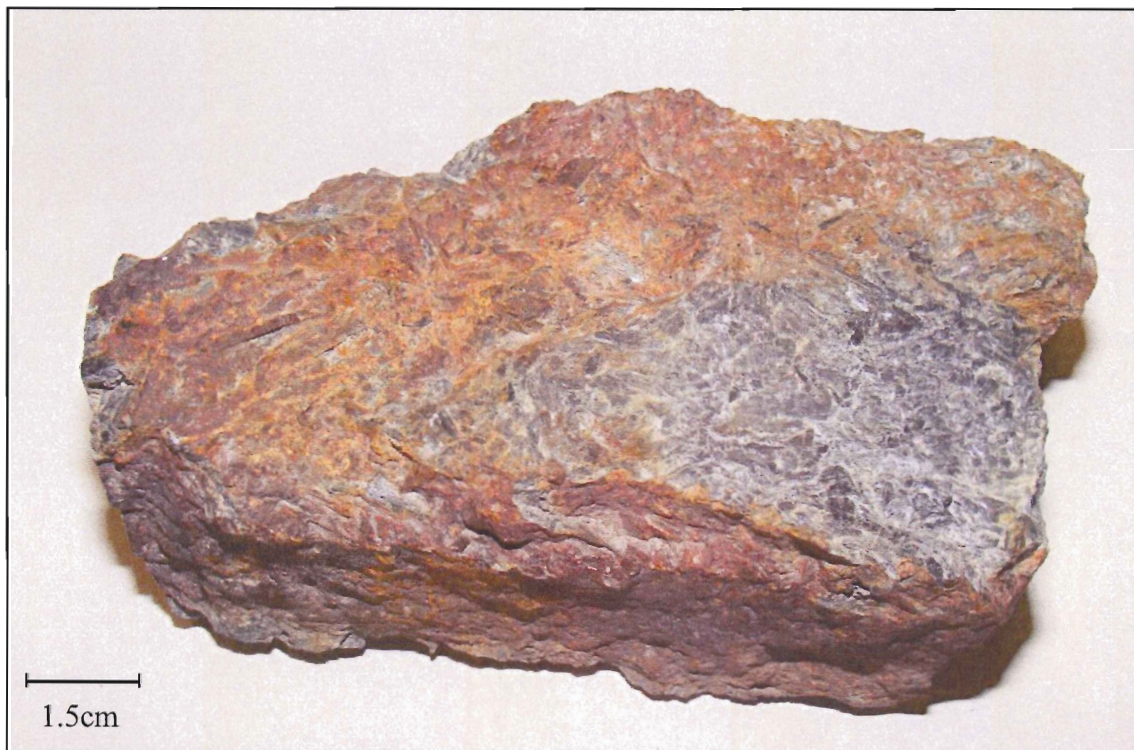


Figure 3.1: Coarse tremolite crystals in amphibolite hand sample. Coarse tremolite is visible both on the brown, weathered surface and dark-grey fresh surface. (Sample A011-A)



Figure 3.2: Scanned thin section of amphibolite. Diamond-shaped tremolite crystals are aligned with weak foliation defined by phlogopite and graphite. (Sample A004-L)

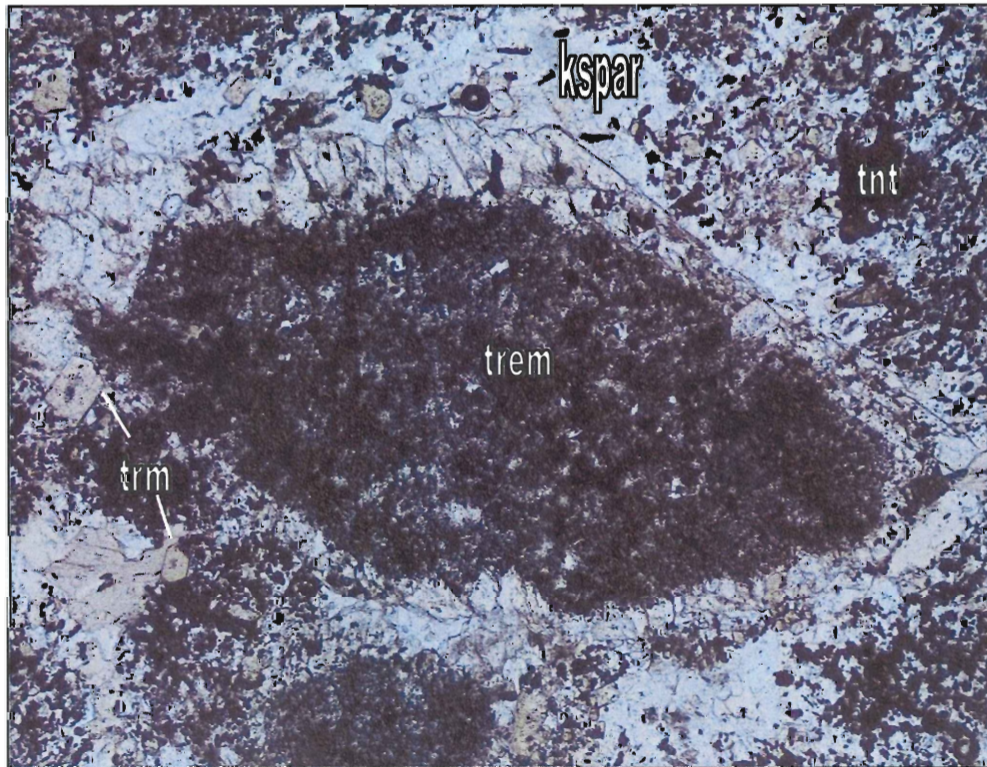


Figure 3.3: Magnified tremolite crystal from amphibolite sample. Single idioblastic tremolite crystal (trem) with abundant graphite inclusions and colourless rim. Tourmaline (trm) and titanite (tnt) are in the matrix. (PPL, Sample A004-L)

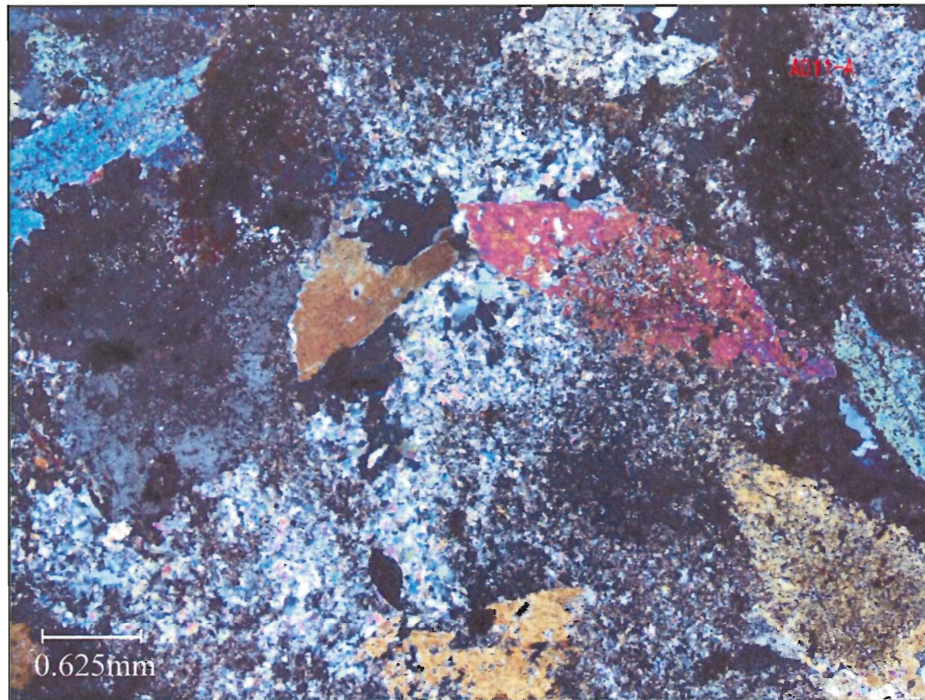


Figure 3.4: Sericitized amphibolites. Pokiloblastic tremolite crystals are roughly diamond-shaped in a sericitized matrix. (XPL, Sample A011-A)

3.1.2. Graphite-rich pelite

In hand sample, graphite-rich pelites are light-grey to medium-grey (Fig 3.5), generally fine-grained with local white spots on fresh surfaces (<1 mm). In thin section, graphite-rich pelites are equigranular, with matrix minerals dominated by quartz (20%), plagioclase (20%), graphite (25%), tourmaline (4%), muscovite (23%), sillimanite (6%) and titanite (2%). Oblate pods of fibrolitic sillimanite and medium-grained muscovite reach up to 4 mm in length (Fig 3.7). These pods lack graphite, and commonly contain small clusters of fibrolitic sillimanite. Fibrolites are crenulated or parallel within clusters of subidioblastic to xenoblastic muscovite (0.7 mm).

Xenoblastic quartz, plagioclase (0.3 mm) and graphite (<0.05 mm) make up most of the matrix. Matrix muscovite ranges from xenoblastic to subidioblastic (0.4 to <0.1 mm). Tourmaline crystals are idioblastic to subidioblastic (0.1 to 0.3mm), with basal and elongate

sections. Inner core and outer rim colours generally differ over a sharp boundary, with cores olive green and rims colourless. Titanite is present within the matrix. Matrix muscovites define a schistosity that wraps around pods, while muscovites within pods have variable orientations. Graphite and tourmaline are aligned with the schistosity along S_1 .

Diamond-shaped oikocrysts (Sample A004-K, Fig. 3.6, 3.8, 3.9) are present in some graphite-rich pelite outcrops. The term oikocryst refers to an aggregate of crystals or minerals that form in a specific pattern characteristic to that oikocryst. These oikocrysts consist of aggregates of medium-grained muscovite and idioblastic tourmaline rimmed by fine-grained K-feldspar, plagioclase and tourmaline.

Oikocrysts range from 0.5mm to 4mm in length. The cores of the oikocrysts are dominated by medium-grained xenoblastic muscovite (0.05 mm to 0.5 mm) and medium-grained subidioblastic tourmaline (0.1-0.3 mm). Elongate sections of tourmaline can reach lengths up to 2mm. Cores of larger tourmalines are medium-brown with inclusions of fibrolitic sillimanite, while the rims are colourless and lack fibrolite. The oikocrysts are generally 7% albite in the rim, 63% white mica, and about 30% tourmaline, and resemble pseudomorphs of diamond-shaped tremolite crystals. This possibility is considered further in Chapters 4 and 5.



Figure 3.5: Graphite-rich pelite handsample. The fresh face exposes white pods that contain sillimanite and muscovite. The white pods are scattered in the rock but planar. (Sample A002-B)

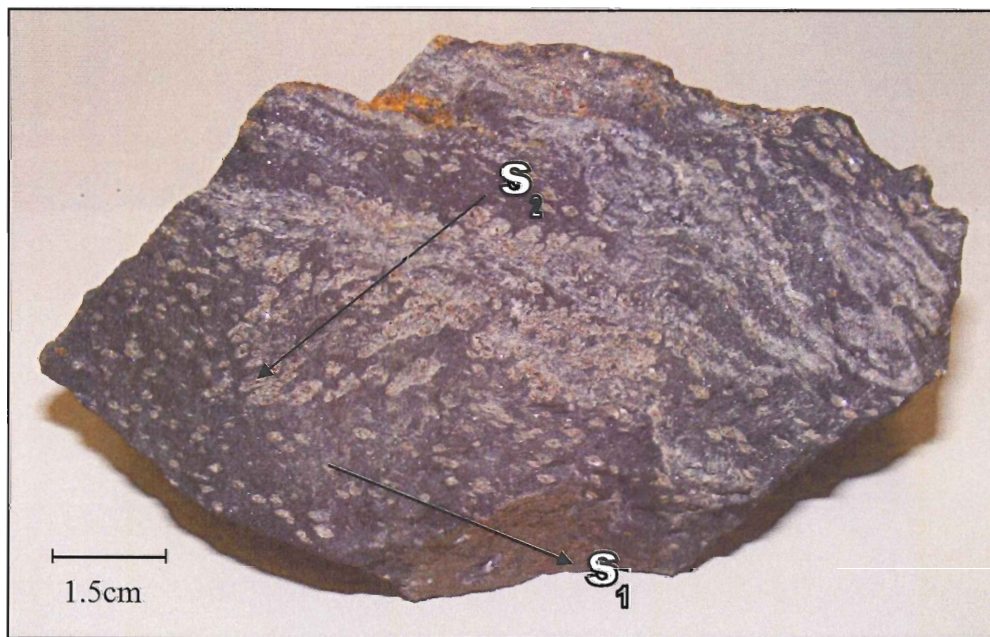


Figure 3.6: Graphite-rich oikocryst deformation. Two deformation stages are visible with the distribution of porphyroblasts in hand sample. First stage planarly aligned oikocrysts (S_1) while the second stage re-oriented (S_2) diamond oikocrysts about 55° from S_1 . (Sample A004-K)

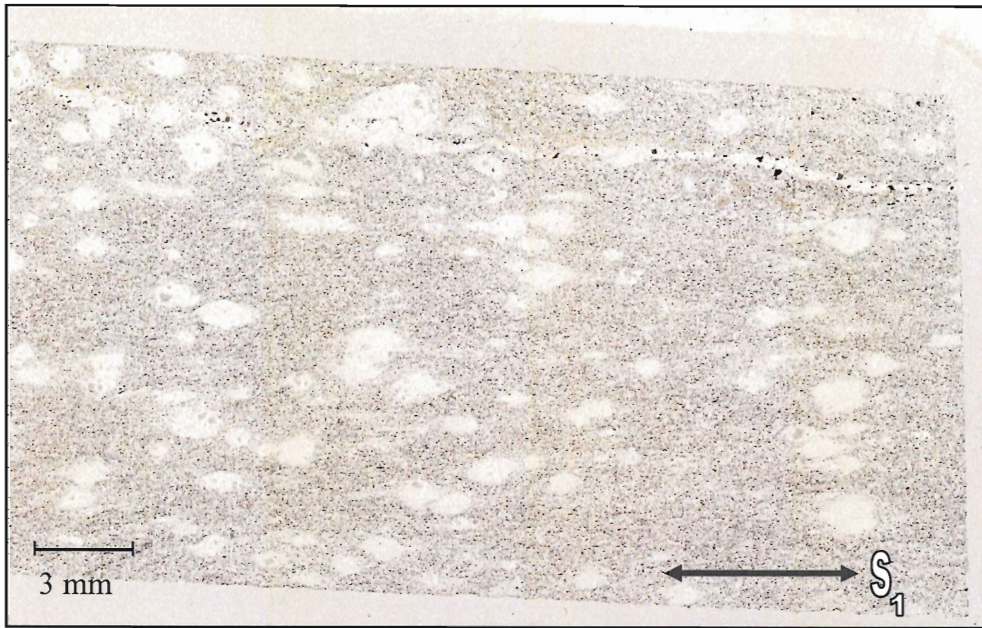


Figure 3.7: Scanned thin-section of fibrolitic sillimanite and muscovite pods. Pods are aligned along similar plane, S₁, which is defined by graphite, muscovite and phlogopite matrix. (Sample A002-B)

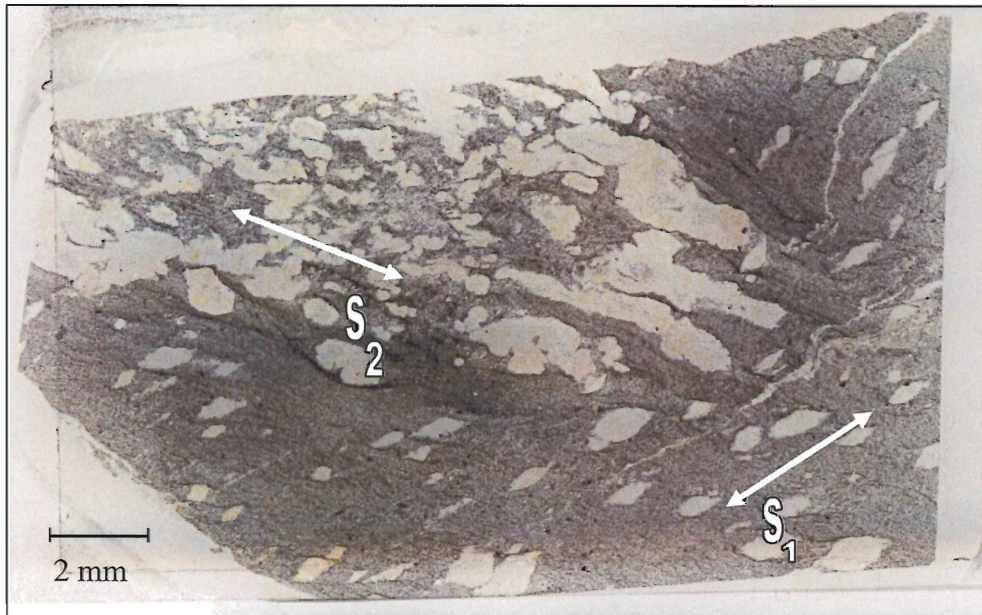


Figure 3.8: Oikocrysts in graphite-rich pelite. Stage two locally deforms oikocrysts obliquely to stage one orientation. (Sample A004-K)

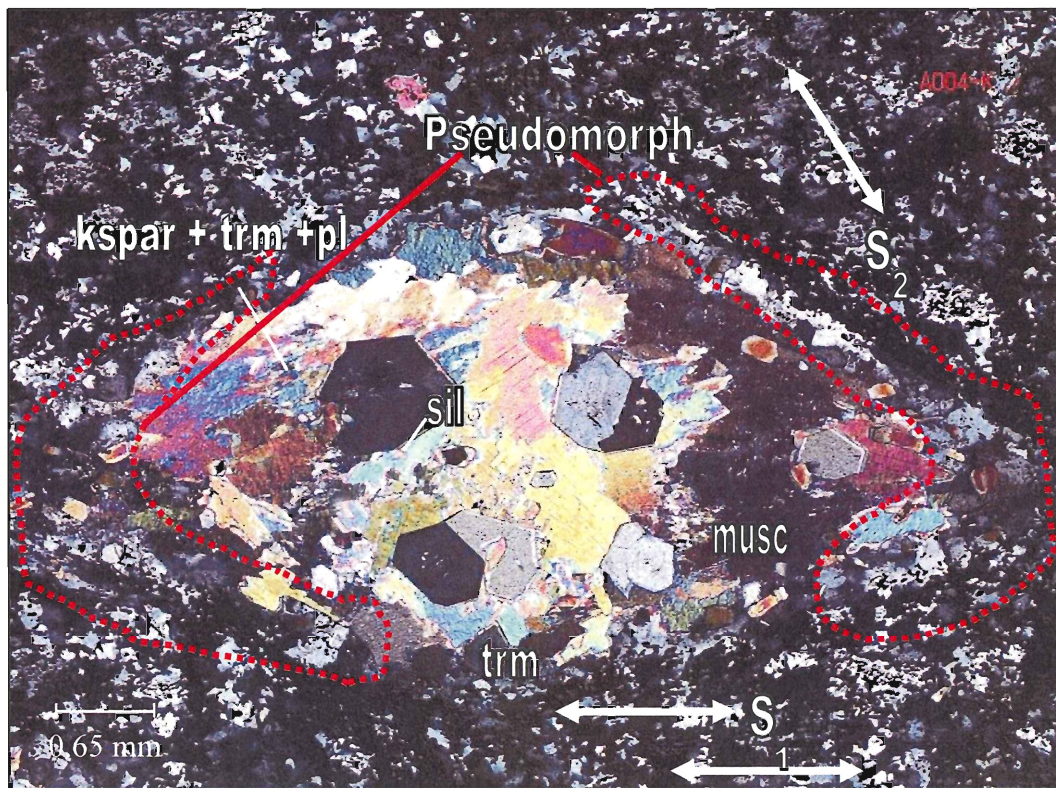
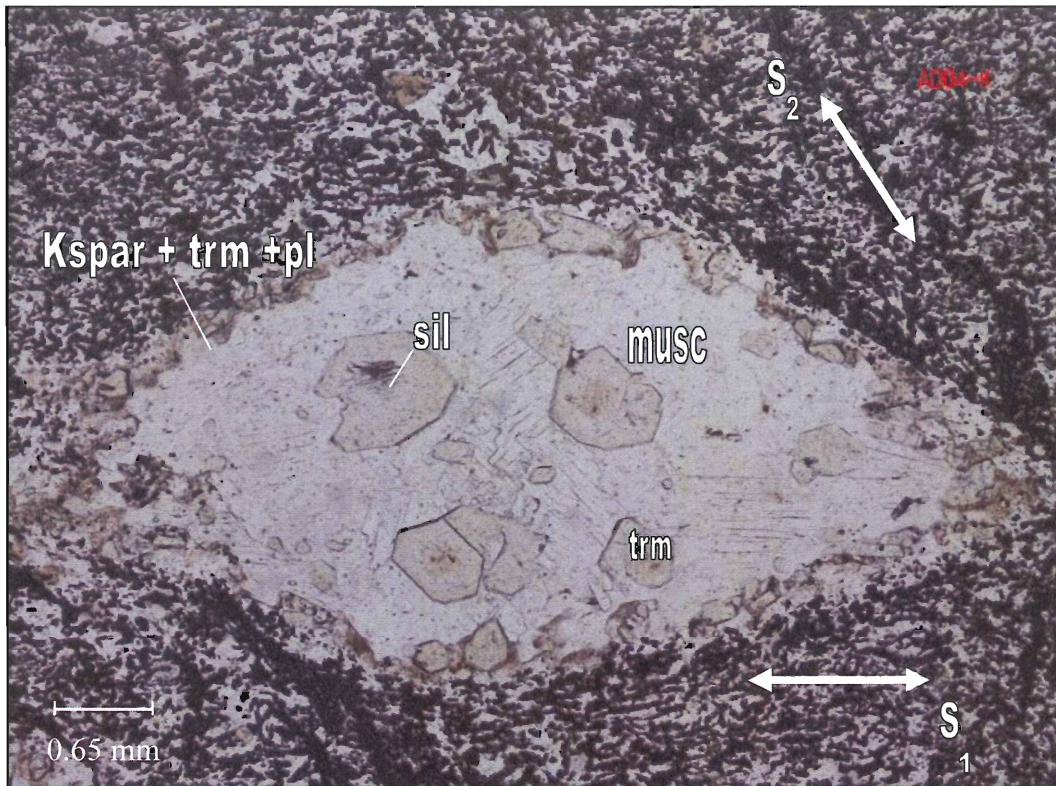


Figure 3.9: Oikocryst formation. Oikocryst has a rim of fine-grained k-feldspar (kspar) and tourmaline (trm) with medium grained muscovite and tourmaline crystals in the inner region. In PPL medium, brown core contrasts with colourless rim. Sillimanite (sil) is within cores of tourmalines. Two different deformation stages are represented by S_1 and S_2 . In XPL, apparent relict colourless rim of tremolite crystal outlined with red dotted line. Inner region, which once held graphite and tourmaline, now consists of muscovite and an additional generation of tourmaline. (Sample A004-K)

3.1.3. *Tourmaline-rich pelite*

In hand sample, tourmaline-rich pelites are light-grey on fresh surfaces but are too fine-grained to distinguish any minerals (Fig. 3.10). In thin section, tourmaline-rich pelites consist of quartz (45%), muscovite (20%), tourmaline (10%), rutile (1%), plagioclase (4%), sericitized K-feldspar (10%), phlogopite (10%) and minor graphite. Quartz crystals (0.1-1 mm) are xenoblastic with larger quartz crystals displaying undulose extinction, and are locally poikiloblastic with tourmaline inclusions (<0.1 mm). Subidioblastic to xenoblastic muscovite crystals (<0.4 mm) are generally aligned defining a schistosity (Fig. 3.11). Tourmalines range from coarse (0.5 mm) to extremely fine (0.01 mm) crystals. Coarse tourmalines have olive-green cores, which are commonly zoned, and colourless rims. This zoning could be evidence for a detrital tourmaline nucleus (Fig. 3.12). Smaller (<0.1 mm) tourmalines, concentrated in pods (<1.5 mm) are aligned in the schistosity. Rutiles (0.2 mm) are scattered throughout the matrix. Xenoblastic sericitized K-feldspar (0.2 to 0.1 mm) and plagioclase (0.1 mm) crystals comprise the remainder of the rock.

Some samples contain up to 77% graphite (Sample A019-A; Fig. 3.13) with tourmaline (10%) distributed through the entire sample as idioblastic 0.2 mm diameter crystals. Zoning is present in tourmalines with core inclusions of graphite or darker green colour. Oblate aggregates of amphibole (10%) are 4 mm long, with isolated crystals up to 0.2 mm large. Apatite (1%) and K-feldspar (2%) forms subidioblastic crystals about 0.1 mm across.



Figure 3.10: Tourmaline-rich pelite hand sample. Fresh face is grey and fine grained and the weathered surface is beige to rusty. (A018-A)

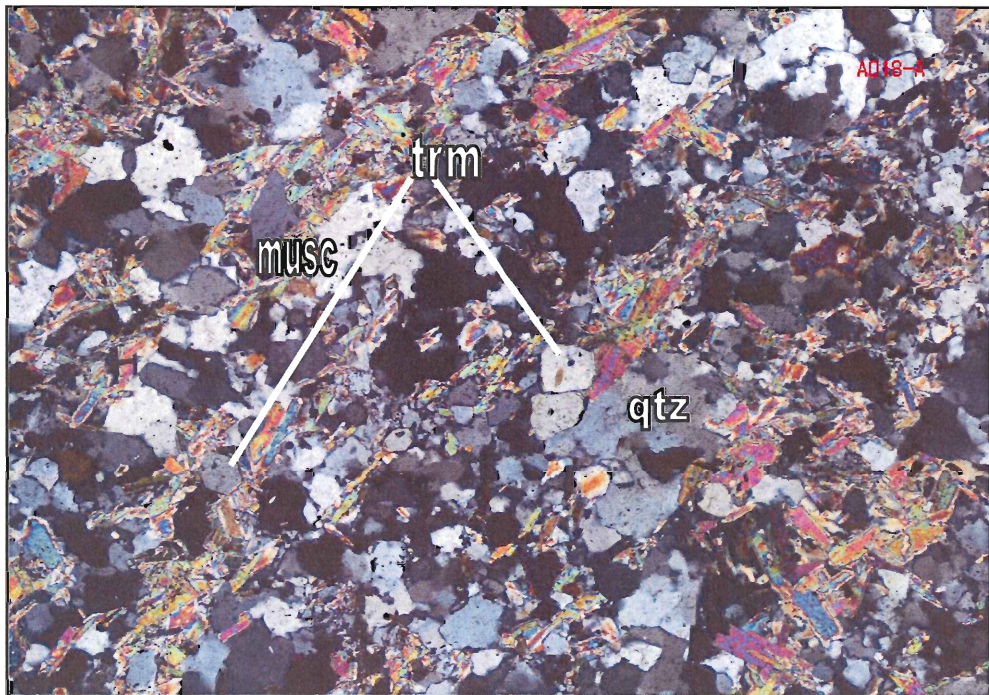


Figure 3.11: Schistosity in tourmaline-rich pelite. Muscovite and phlogopite are aligned to define schistosity. Medium-grained tourmalines are subidio- to idioblastic in matrix. (XPL, Sample A018-A)

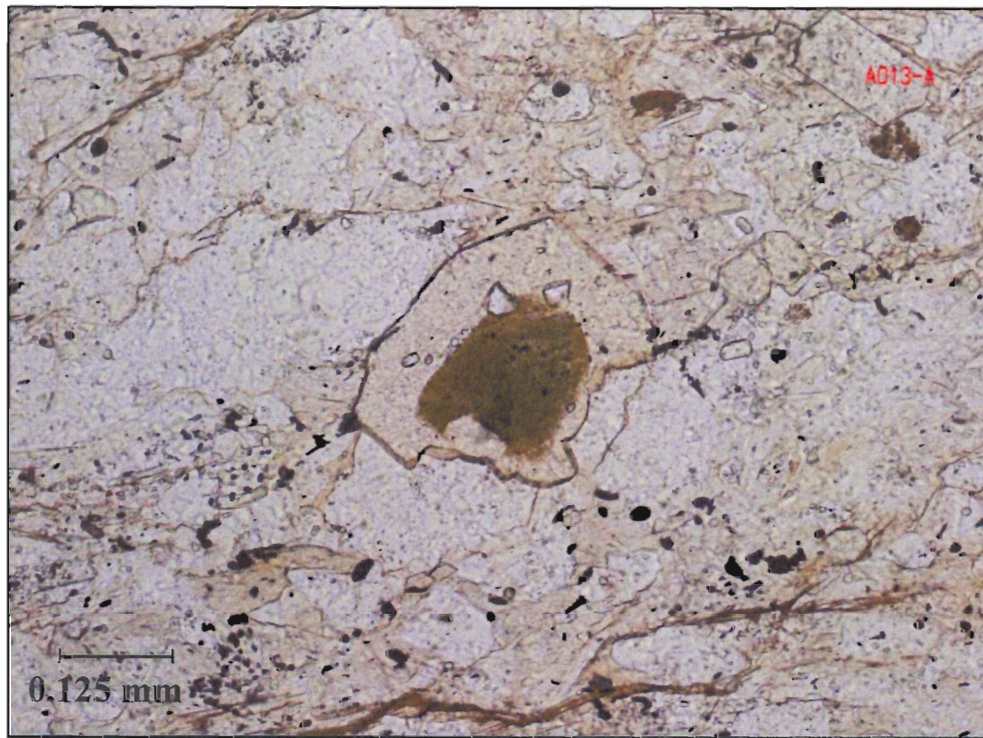


Figure 3.12: Zoned tourmaline in tourmaline-rich pelites. Distinct colour change between dark core and pale rim is interpreted to represent metamorphic overgrowth of detrital nucleus. (PPL, Sample A013-A)

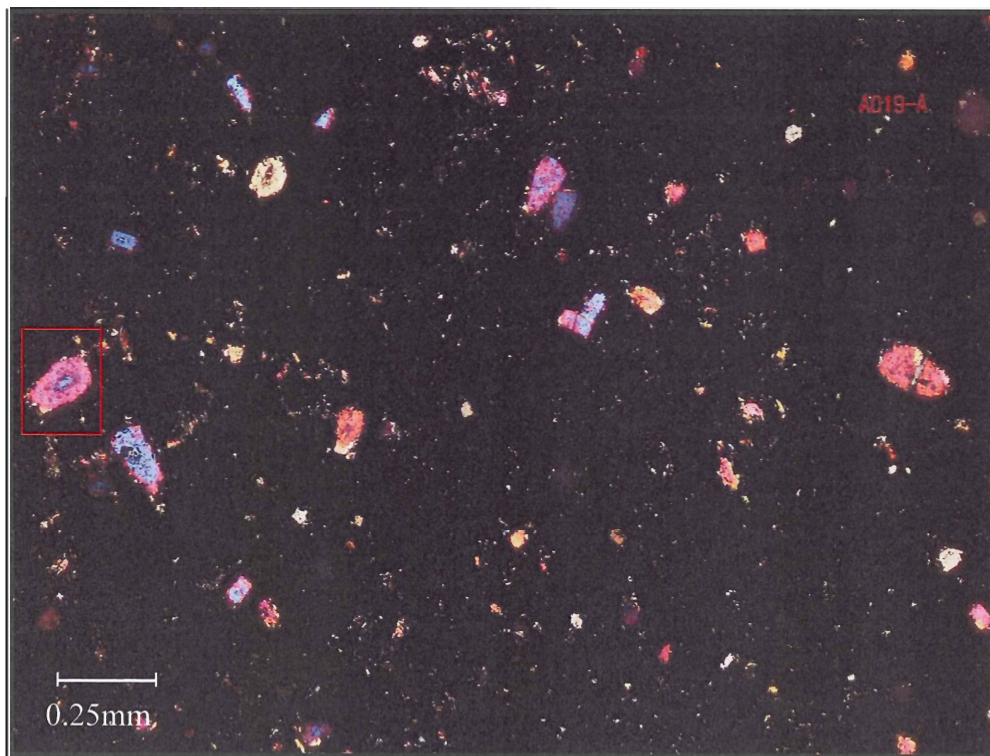


Figure 3.13: Tourmalines in tourmaline-rich pelite. Tourmalines are subidio- to idioblastic and can display core-to-rim zoning (outlined in red). (XPL, Sample A019-A)

3.1.4. *Tourmalinite*

Tourmalinites are the most weathered and rusty rocks of the sample area; hand samples are dense and contain visible pyrrhotite and pyrite (Fig. 3.14). In thin section tourmalinites are equigranular and fine-grained, consisting of quartz (47%), tourmaline (18%), muscovite (9%), titanite (4%), phlogopite (8%), apatite (1%), pyrrhotite (8%) and pyrite (5%). Fine-grained quartz (0.1 mm) is granoblastic and medium-grained quartz (<0.6 mm) is xenoblastic. The main sulphide is pyrrhotite, with accessory pyrite. Textural relationships between the two sulphides suggest pyrrhotite replaces pyrite (Fig. 3.15). Tourmaline (0.1 mm) is pervasive as disseminated, idioblastic crystals with elongate sections aligned along foliation planes (Fig. 3.16). Tourmalines are colourless with no zoning. Muscovite crystals are idioblastic to subidioblastic (<1 mm - 4 mm) and define the schistosity. Titanite and phlogopite are adjacent to fractures and within the matrix. Phlogopites are 4mm in size and subidioblastic. Sulphides are large xenoblastic aggregates (7 mm) adjacent to veins or within the matrix or deposited as isolated crystals (>0.9 mm). Sulphide deposition appears to be post-matrix crystallization as pyrrhotite cuts quartz, plagioclase and phlogopite crystal boundaries and occurs within veins.

In some tourmalinites, sillimanite forms large pods, knots or clusters of fibrolitic crystals. Pods (5 mm x 0.2 mm) are aligned and resemble faserkiesel texture with minor graphite and tourmaline adjacent to the rim in the matrix. Retrogression of sillimanite fibres is evident with muscovite crystals overgrowing fibrolites. Sillimanite is rare outside pods. Disseminated (<0.1 mm) tourmalines are elongated parallel to the fabric.

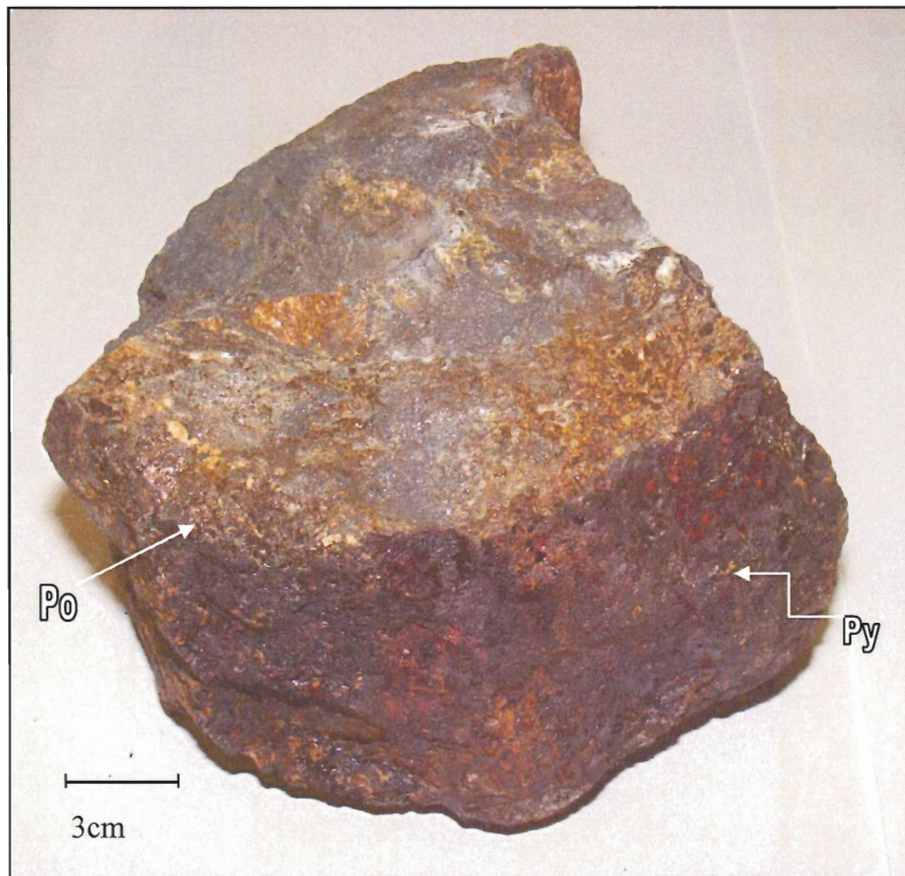


Figure 3.14: Sulfide-rich tourmalinites are most the most rusty samples from the study area. Dark brown pyrrhotite (Po) blends in with brown staining whereas pyrite provides yellow-brown colour. (Sample A003-A)

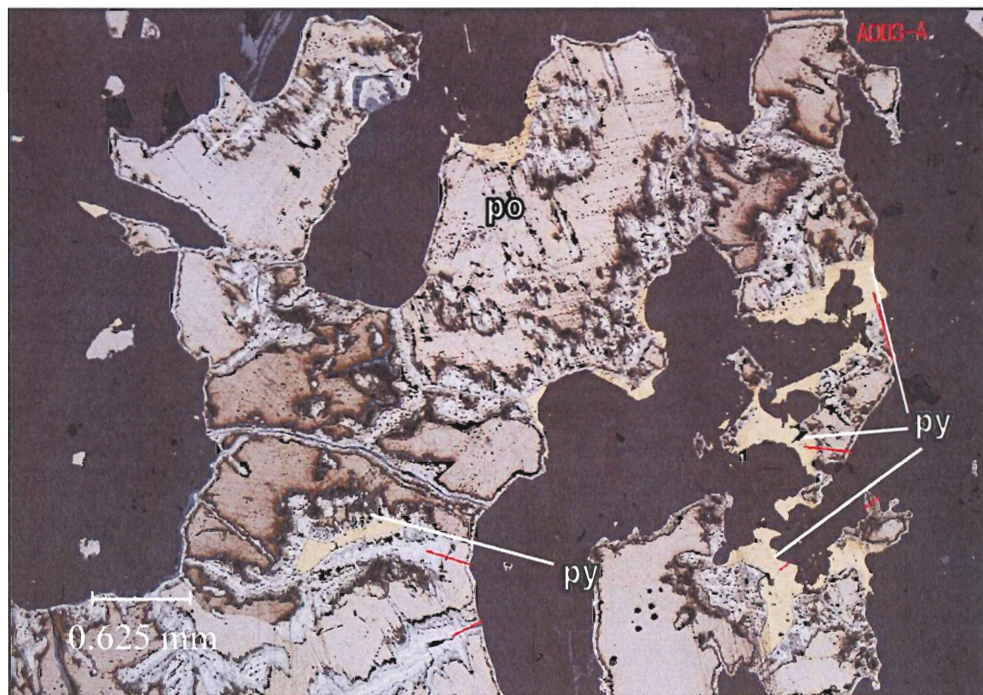


Figure 3.15: Pyrrhotite and pyrite co-exist in most samples. The largest aggregates of pyrrhotite and pyrite are within tourmalinites. Pyrite lines the edges and interstitial areas of larger concentrations of pyrrhotite. (Reflected light, Sample A003-A)

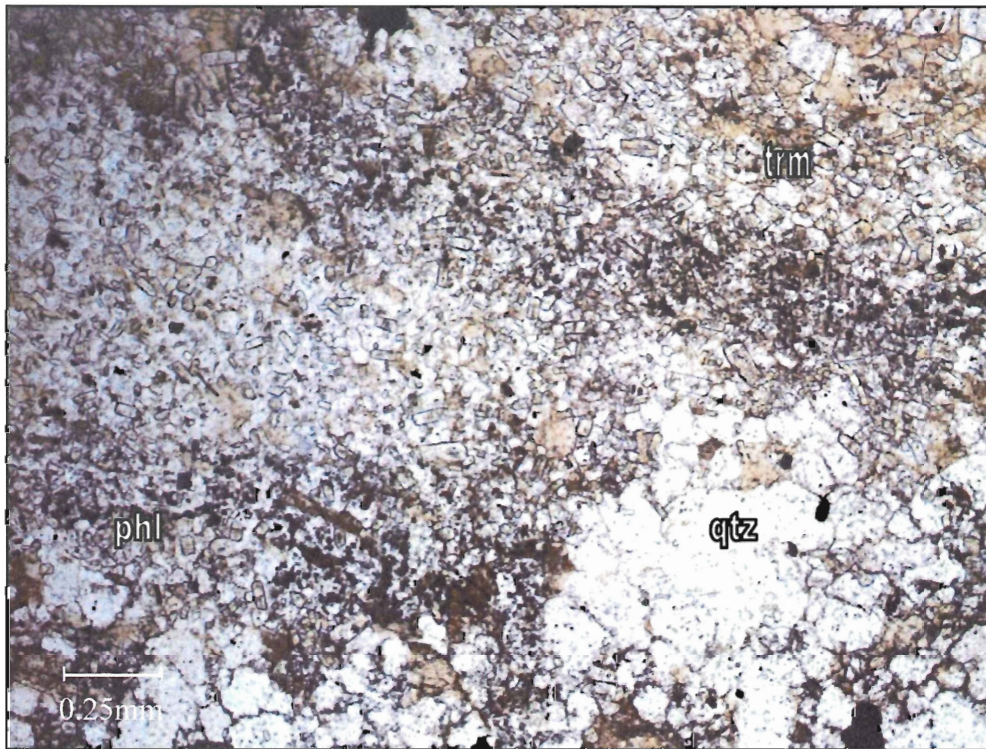


Figure 3.16: Representative photomicrograph of tourmaline abundance in tourmalinites. Tourmalinites are defined as containing more than 10-15% tourmaline. The fine idioblastic colourless crystals are tourmalines and average abundance in study area tourmalinites is 18%. (PPL, Sample A003-A)

3.1.5. Greywacke

In hand sample, greywackes are white on fresh surfaces with quartz-rich bands (0.7 mm) distinguishable on weathered surface (Fig. 3.17). In thin section, the greywackes are fine-grained and equigranular (Fig. 3.18), consisting largely of polygonal quartz (55%), plagioclase (20%), potassium feldspar (15%) and fine-grained tourmaline (5%), with rare tremolite and disseminated sulphides (5%) (Sample A006-A; Fig. 3.18, 3.19). The protolith is interpreted to have had a matrix-dominated texture. A weak foliation is defined by aligned sillimanite, tourmaline, and sulphides, and the rock is cut by quartz veins (4 mm). Tremolite forms medium-grained (0.2 mm) subidioblastic crystals associated with sulphides and veins. Sillimanite forms small fibrous aggregates ($\leq 1 \text{ mm} \times 0.4 \text{ mm}$), and is also associated with veins and sulphides.

Pyrites are fine-grained, xenoblastic, and generally disseminated, although they locally form 2 x 1 mm clusters.



Figure 3.17: Greywackes are white to light-grey in hand sample. Abundant quartz and plagioclase are organized in the matrix with bands of quartz showing minor deformation. (Sample A014-A)

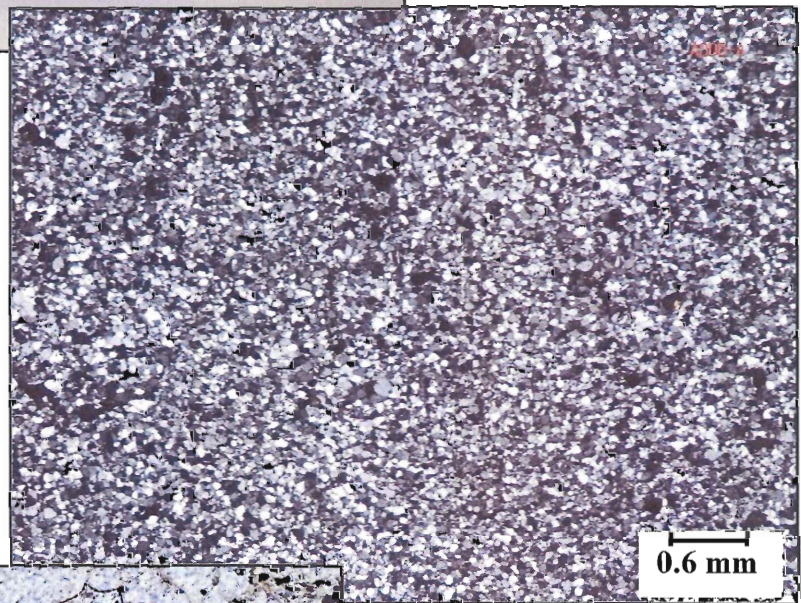


Figure 3.18: Typical greywacke texture with clastic rounded quartz and plagioclase crystals. Interstitial sulphides are also present. (XPL, Sample A006-A)

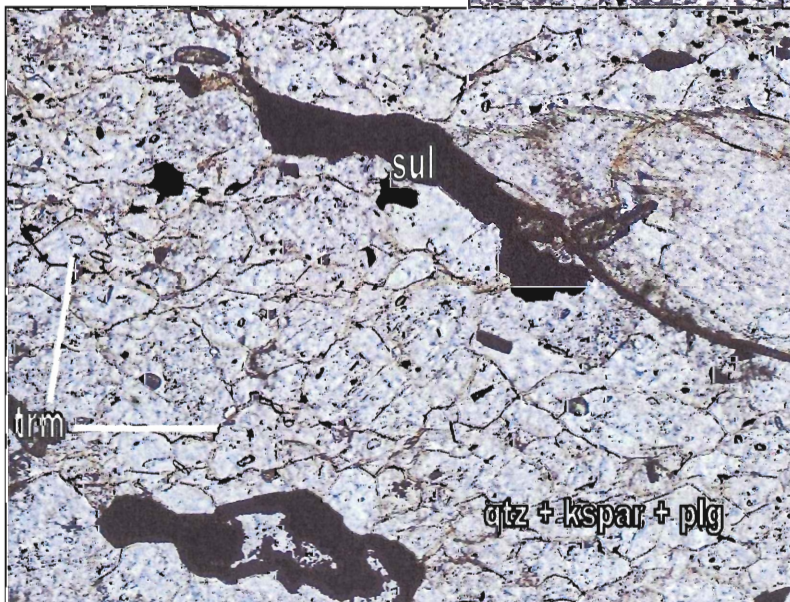


Figure 3.19: Tourmaline (trm) is only visible at high magnification. Grains maintain idioblastic shape but are disseminated within matrix quartz (qtz), potassium feldspar (kspar) and plagioclase (plg) crystals, along with sulphides (sul). (PPL, Sample A006-A)

3.2 Intrusive Rocks

3.2.1. Diabase

In hand sample, diabases are fine grained (<1mm) and yellow-green in colour (Fig. 3.20). In thin section diabases are equigranular and consist of clinopyroxene (50%), quartz (7%), tremolite (3%), chlorite, plagioclase (20%), potassium feldspar (15%), titanite (2%) and sulphides (3%). Clinopyroxenes (4 mm to <0.3 mm) are xenoblastic and partly replaced by aggregates of fine equant crystals. Quartz is subidioblastic polygonal (0.5mm to 0.1mm), however edges of crystals in some places are poorly defined and irregular. Xenoblastic amphiboles are generally 0.5 mm in size. Plagioclase crystals are subidioblastic or xenoblastic, with extensive sericitization (Fig. 3.23). Titanites are fine (0.3 mm to 0.1 mm), subidioblastic, oval crystals scattered throughout the rock. Sulphides (0.4 to <0.1 mm) are xenoblastic and form scattered clusters concentrated within veins throughout diabases within veins.

The sample A004-C contains a compositional boundary, which is possibly the contact between diabase and pelite. The contact is defined by the loss of clinopyroxene over a 1 mm gradient, where quartz, plagioclase and tourmaline become dominant (Fig. 3.21, 3.22). Tourmalines (0.1 mm) are idio-to subidioblastic isolated crystals which also form clusters.

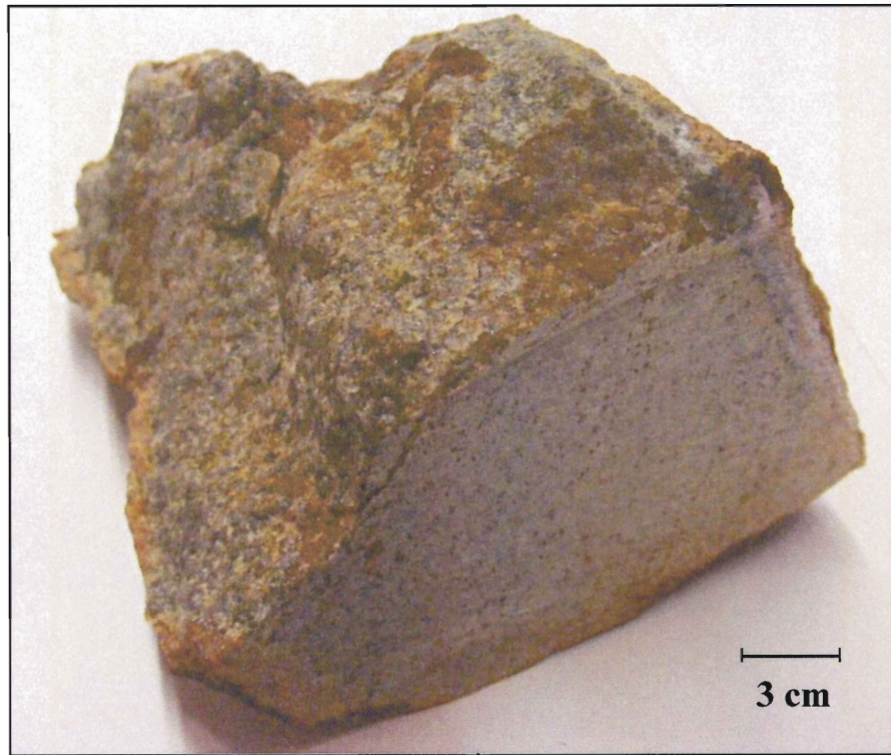


Figure 3.20: Altered fine-grained diabase. General colour is yellow to brown with fine-grained sulphides spotting the fresh face. (Sample A009-A)



Figure 3.21: Scanned thin section of diabase (right) in contact with possible graphite-rich pelite (left). Boundary is sharp indicating a low volatile content intrusive. Sulphides are present in both rock type matrixes. (Sample A004-C)

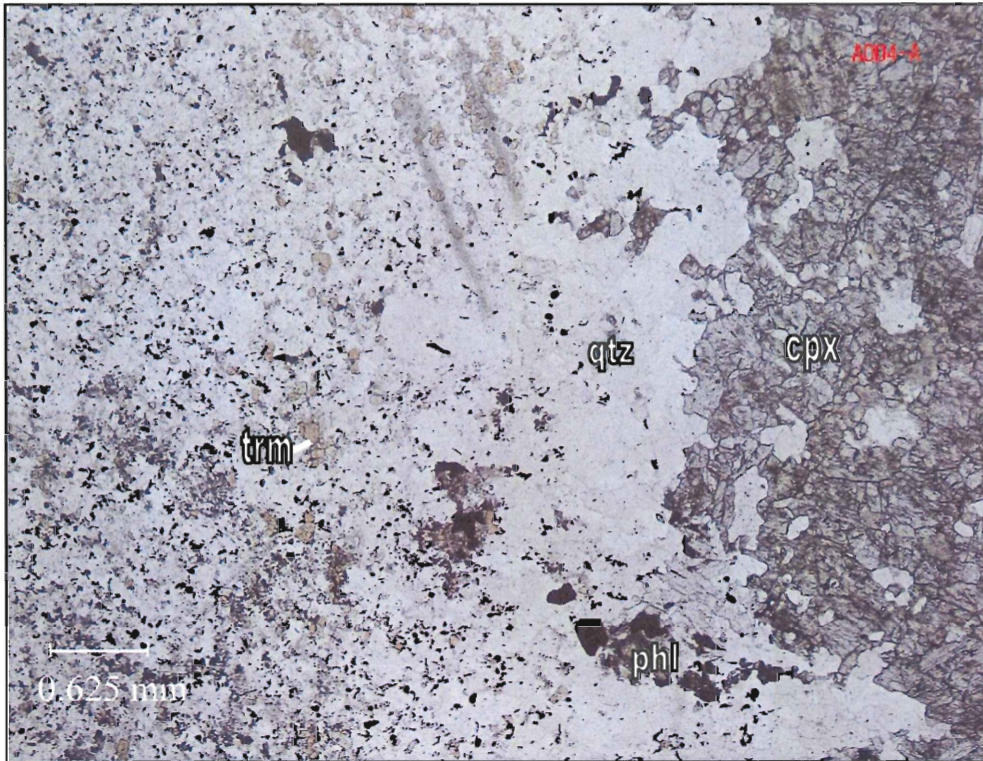


Figure 3.22: Magnified boundary between clinopyroxene-rich zone (cpx) zone and matrix of quartz (qtz), plagioclase and tourmaline (trm). Coarse-grained recrystallized quartz creates a thin rim with clinopyroxene possibly indicating low fluid content in diabase. (PPL, Sample A004-C)

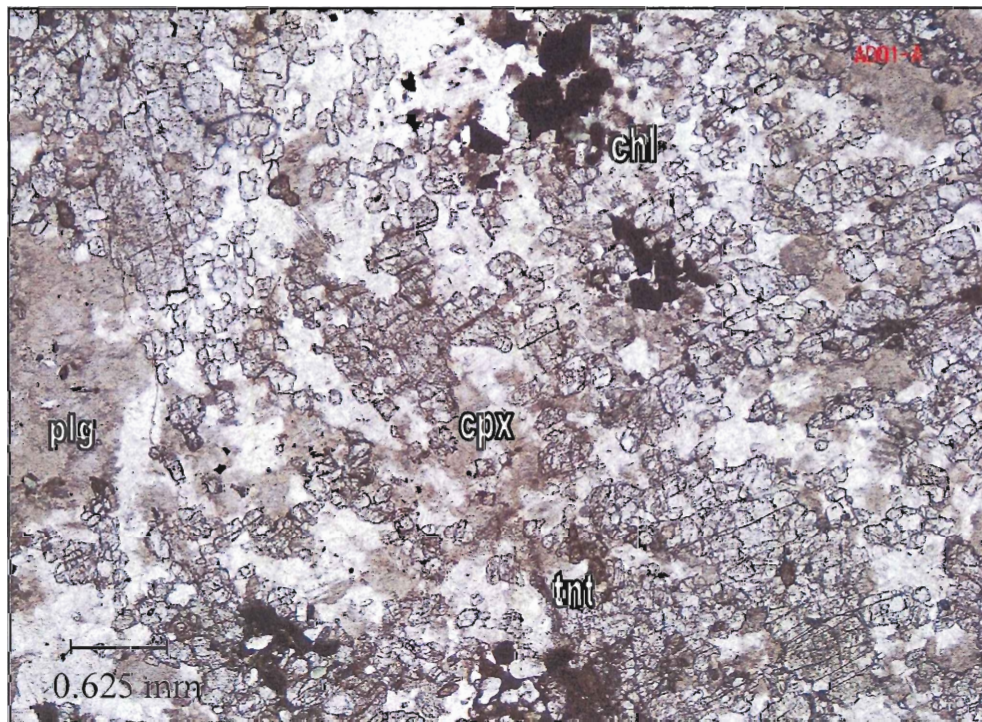


Figure 3.23: Fine granular clinopyroxene(cpx) with titanite (tnt) and sulphides rimmed by chlorite (chl). Sericitized plagioclase (plg) suggests potassic fluid alteration.

3.2.2. Granite

In hand sample, granites are white to light grey with coarse plagioclase, feldspar and quartz, as well as sulphides (Fig. 3.24). In thin section, granites are equigranular and consist of medium-grained anhedral plagioclase (40%), quartz (20%) and K-feldspar (30%) with accessory apatite (1%), titanite (<1%), sulphides (4%) and secondary chlorite (4%), pumpellyite (<1%) and accessory actinolite. Plagioclase crystals are 1.5 mm to 0.2 mm large while alkali feldspars are mostly microcline (0.7 mm). Quartz exhibits undulose extinction, and forms up to 1 mm diameter crystals. Chlorite (1 mm) is secondary after major minerals. Apatite (0.1 mm) is sparsely scattered in the sample as isolated grains. Idioblastic titanite (0.2 mm) is adjacent to sulphides, chlorite or amphibole. Rare secondary pumpellyite (about 0.2 mm) is proximal to chlorite and titanites (Fig. 3.25). Pumpellyite (0.2 mm) possibly replaces actinolite adjacent to chlorite.

More altered granites have been sericitized (Sample A012-A) with feldspars ranging from 0.1 mm to 1 mm and exsolution blebs speckling the faces of other coarse feldspar crystals. Graphic texture is sparsely present within isolated crystals of quartz (0.5 mm). All minerals are xenoblastic. Xenoblastic pyrite and pyrrhotite are only locally present.

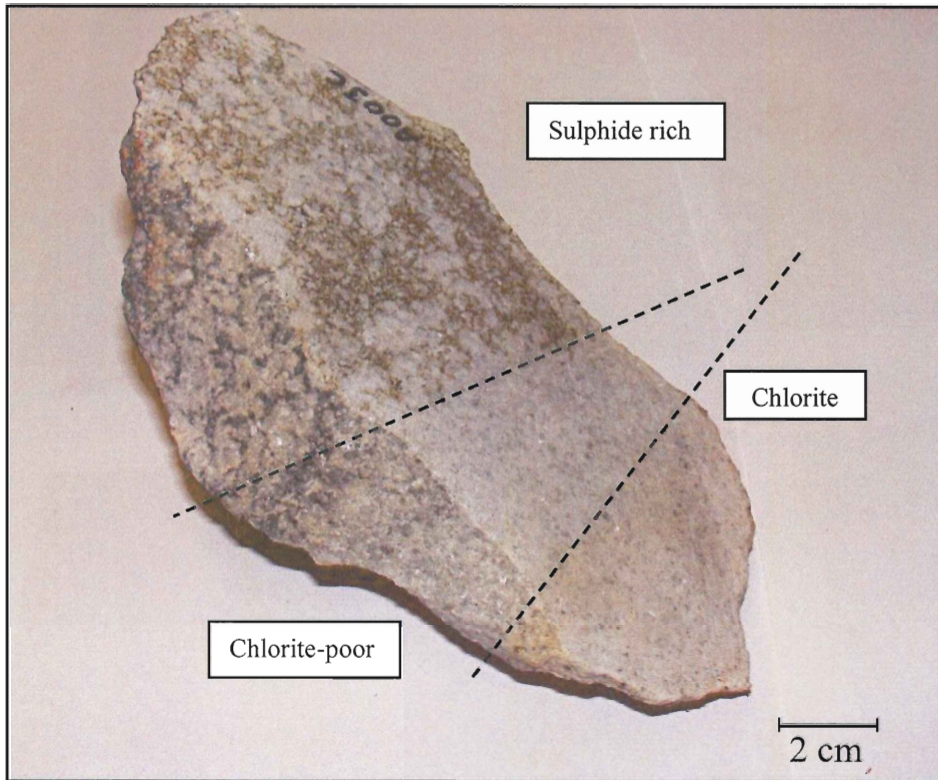


Figure 3.24: Alteration zoning in granite handsample. Three different zones of alteration with a more sulphide-rich area (top-left) sharply in contact to chlorite-poor zone (middle). The final zone (bottom-right) is more chlorite-rich. Varying alteration in hand sample scale indicates high hydrothermal alteration. (Sample A003-C)

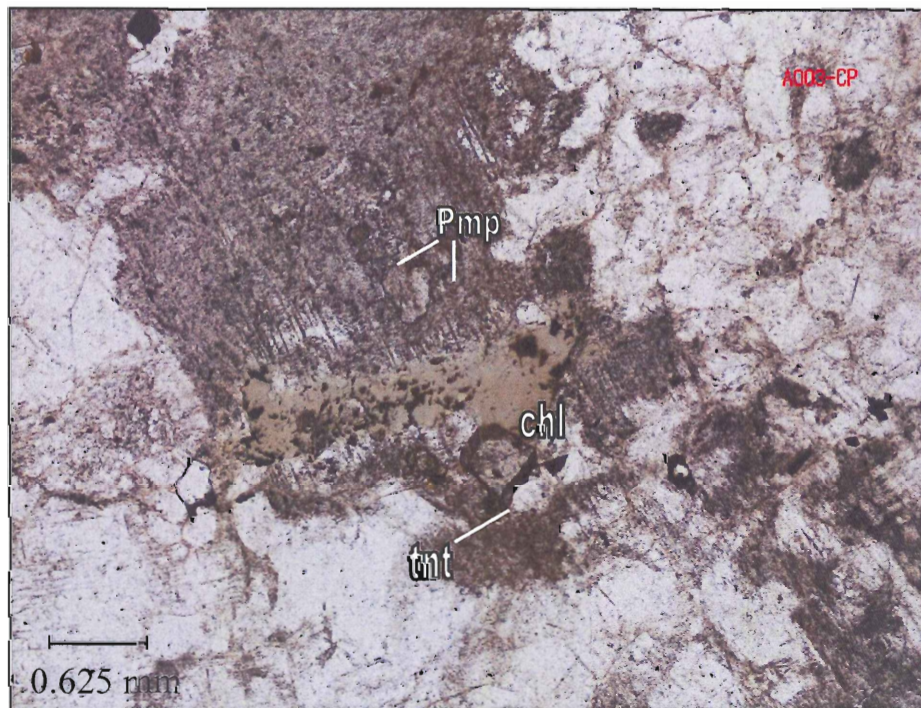


Figure 3.25: Colourless titanite (tnt) adjacent to chlorite (chl). Pumpellyite (pmp) lies within sericitized k-feldspar, and chlorite clusters are generally spatially associated with titanite. (PPL, Sample A003-C)

3.3 Discussion

The petrographic observations offer insights into the depositional environment of these rocks, sequences of deformation and metamorphic grade, timing of mineral deposition, and changes in mineralogy which are related to hydrothermal alteration. Further discussion of these topics will be presented in chapter 5.

3.3.1. Depositional Environment

The primary clastic and pelitic rocks differ in minerals and textures over a small geographic area, which could indicate an energetic depositional environment involving multiple chemical inputs. Clear and light brown tourmalines are pervasive throughout many samples and sulphide abundance (pyrite & pyrrhotite) is sporadic, commonly associated with tourmalinite outcrops, consistent with typical proximal exhalative fumarole characteristics.

3.3.2. Stages of Deformation

Evidence for at least two stages of deformation are preserved in these rocks. In graphite-rich pelites, two foliations are defined by alignment of graphite. S_1 is the dominant fabric, and both oikocrysts and matrix graphite are aligned and elongated in this fabric. S_2 is not as well developed. It is defined by realignment of some matrix graphite at high angle to S_1 with S_2 wrapping around oikocrysts.

3.3.3. Generation of Tourmaline and Sulphides

In all lithologies, most tourmalines have dark-green cores and colourless or light-brown rims, suggesting either two stages of growth or a change in chemical environment during growth. Possible detrital cores with colourless rims indicate at least two stages of tourmaline mineralization. The second possibility cannot be ruled out by petrographic data alone, however,

as compositions of hydrothermal fluids inferred to be responsible for tourmaline growth in some samples may have changed with time or changing temperature.

Sulphides are pervasive in tourmalinites, where they cross-cut grain boundaries of both matrix minerals and tourmalines. In other rock types (diabases, greywackes), sulphides, mainly pyrrhotite, are adjacent to, or within veins, suggesting secondary hydrothermal deposition.

3.3.4. Pseudomorphs

Through visual comparison, I interpreted oikocrysts in graphite-rich pelites to be pseudomorphs of diamond-shaped tremolite crystals. Tremolites are idioblastic with graphite and tourmaline inclusions and colourless rims. Oikocrysts mimic the diamond shape of tremolites, with fine-grained tourmaline and albite rims and medium-grained muscovite and tourmaline core regions. The former presence of tremolite is still distinguishable by alignment of graphite grains along edges of oikocrysts; however, no tremolite remains within the rock. Pumpellyite and chlorite may also be retrograde replacements of amphibole in granites.

3.3.5. Evidence for Hydrothermal Alteration

Evidence of secondary hydrothermal alteration in these samples can be drawn from lithologic variation over short distances, pervasive tourmaline, possibly the tourmaline core-to-rim deposition, sulphide deposition within veins, and the seritization of matrix minerals. Lithologic variation over short distances could indicate that localized hydrothermal fluids distributed ions over short distances to precipitate different minerals. The inferred pseudomorph replacement would require extensive fluid-rock alteration during or after the metamorphic peak.

CHAPTER 4: MINERAL CHEMISTRY

Mineral chemistry reflects the temperatures, pressures and chemical influences rocks are subjected to during deposition and metamorphism. In order to constrain mineral compositions extensive electron microprobe (EMP) data were obtained from the sample area. Samples were selected from a broad spectrum of rock compositions including tourmalinite, granite, graphite-rich pelite, amphibolite and tourmaline-rich pelite. Emphasis was placed on tourmaline, amphibole and sulphide compositions, focusing on texturally complex regions.

4.1 Major Element Analysis

Major element analyses were conducted using the JEOL JXA 8200 electron microprobe in the Dalhousie Regional Electron Microprobe Laboratory with the assistance of Mr. Dan MacDonald. Polished sections were scanned and carbon-coated prior to analysis by wavelength dispersive spectrometry (WDS). Operating conditions were 15kV acceleration voltage, 2 μ m spot size and 20nA beam current. Boron was assumed to be 10.5% of tourmaline weight percent and plagioclase totals are low due to Na burn-off during analysis. Five representative samples were chosen for silicate, oxide and sulphide analysis. The results are summarized in Tables 4.1 to 4.4 and complete analyses, photos and BSE images are available in Appendix A.

Table 4.1. Representative Tourmaline Compositions				
Lithology	Mineral	Structural formula (Nesse, 2000)	Area	Mg#
	Dravite	Na(Mg, Fe, Li, Al) ₃ Al ₆ (Si ₆ O ₁₈)(BO ₃) ₃ (O,OH,F) ₄ NaMg ₃ Al ₆ (Si ₆ O ₁₈)(BO ₃) ₃ (O,OH,F) ₄		
Amphibolite	trm	Na _{0.57} Ca _{0.08} Fe _{1.10} Ti _{0.11} Mg _{1.60} Al _{5.99} (BO ₃) _{3.07} (Si _{6.02} O ₁₈)(OH) ₄ F _{0.08}	Core	0.59
		Na _{0.28} Ca _{0.53} Fe _{0.13} Ti _{0.14} Mg _{2.94} Al _{5.56} (BO ₃) _{3.02} (Si ₆ O ₁₈)(OH) ₄ F _{0.16}	Rim	0.96
Graphite-rich Pelite	trm	Na _{0.48} Mg _{1.64} Fe _{0.67} Al _{6.53} (BO ₃) _{3.03} Si _{5.96} O ₁₈ (OH) ₄ F _{0.14}	Core	0.71
		Na _{0.43} Mg _{2.27} Ca _{0.19} Fe _{0.15} Al _{6.49} (BO ₃) _{2.98} Si _{5.94} O ₁₈ (OH) ₄ F _{0.19}	Rim	0.96
Tourmaline-rich Pelite	trm	Na _{0.42} Ca _{0.2} Fe _{0.52} Ti _{0.05} Mg _{2.05} Al _{6.2} (BO ₃) _{2.97} (Si _{6.05} O ₁₈)(OH) ₄ F _{0.05}	Core	0.80
		Na _{0.41} Ca _{0.16} Fe _{0.1} Ti _{0.05} Mg _{2.39} Al _{6.35} (BO ₃) _{2.93} (Si _{6.03} O ₁₈)(OH) ₄ F _{0.07}	Rim	0.96
Tourmalinite	trm	Na _{0.5} Ca _{0.04} Fe _{0.38} Ti _{0.06} Mg _{2.06} Al _{6.3} (BO ₃) _{2.94} (Si _{6.08} O ₁₈)(OH) ₄ F _{0.18}	Core	0.84
		Na _{0.39} Ca _{0.22} Fe _{0.07} Ti _{0.07} Mg _{2.35} Al _{6.36} (BO ₃) _{2.91} (Si ₆ O ₁₈)(OH) ₄ F _{0.18}	Rim	0.97

Table 4.2 Silicate Compositions			
Lithology	Mineral	Structural formula (Nesse, 2000)	End-Members
Amphibolite	kspar	$K_{0.97}Na_{0.03}AlSi_3O_8$	Or ₉₇
	trem	$Ca_{2.10}Al_{0.31}(Mg_{4.88}, Fe_{0.20})Si_8O_{22}(OH)_2$	
	phl	$K_{0.87}Mg_{2.5}Fe_{0.16}Al_{1.33}Si_{2.89}O_{10}(OH)_4F_{0.16}$	
Granite	chl	$(Mg_{5.2}, Fe_{1.03})(Si_{3.8}Al_{2.62})O_{10}(OH)_8$	Or ₉₈
	kspar	$K_{0.97}Na_{0.02}AlSi_3O_8$	
	ms	$K_{1.94}Al_4(Al_{1.66}Si_{6.23}O_{20})(OH)_4$	
	pl	$Na_{0.5}Ca_{0.23}K_{0.04}Al_{1.24}Si_{2.82}O_8$	
	trem	$Ca_{2.08}Al_{0.14}(Mg_{4.36}, Fe_{0.77})Si_8O_{22}(OH)_2$	
Graphite-rich Pelite	kspar	$K_{0.92}Na_{0.05}AlSi_{3.01}O_8$	Or ₉₅
	ms	$K_{1.79}Al_4(Al_{1.54}Si_{6.27}O_{20})(OH)_4$	
	phl	$K_{0.98}Mg_{2.35}Fe_{0.2}Al_{1.35}Si_{2.83}O_{10}(OH)_4F_{0.37}$	
	pl	$Na_{0.81}Ca_{0.19}Al_{1.19}Si_{2.88}O_8$	
Tourmaline-rich Pelite	kspar	$K_{0.94}Na_{0.04}AlSi_{2.99}O_8$	Or ₉₆
	phl	$K_{0.89}Mg_{2.40}Fe_{0.25}Al_{1.61}Si_{2.77}O_{10}(OH)_4F_{0.06}$	
	pl	$Na_{0.50}Ca_{0.19}Al_{1.21}Si_{2.85}O_8$	
Tourmalinite	phl	$K_{0.95}Mg_{2.38}Fe_{0.16}Al_{1.32}Si_{2.89}O_{10}(OH)_4F_{0.38}$	

Table 4.3: Accessory Compositions		
Lithology	Mineral	Structural formula (Nesse, 2000)
Amphibolite	ap	$Ca_{10.81}(PO_4)_3F_{2.08}$
	tnt	$CaTi_{0.95}OSiO_4$
Granite	ap	$Ca_{10.85}(PO_4)_3F_{2.23}$
	pmp	$Ca_{2.29}Mg_{0.71}Al_{2.63}(Si_{3.46}O_{12})(OH)_2F_{0.14}$
	tnt	$Ca_{1.03}Ti_{0.9}Al_{0.1}OSiO_4F_{0.04}$
		$Ca_{1.03}Ti_{0.74}Al_{0.24}OSiO_4F_{0.17}$
Tourmaline-rich Pelite	ap	$Ca_{10.84}(PO_4)_3F_{1.55}$
Tourmalinite	ap	$Ca_{10.79}(PO_4)_3F_{2.11}$

Table 4.4. Oxide Compositions		
Lithology	Mineral	Structural formula (Nesse, 2000)
Graphite-rich pelite	Rutile	TiO ₂
	Titanite	Ca _{1.3} Ti _{1.09} Al _{0.18} Si _{0.64} O ₅
Granite		Rutile: TiO ₂ Titanite: CaTiSiO ₅

Table 4.5. Sulphide Compositions		
Lithology	Mineral	Structural formula (Nesse, 2000)
Tourmalinite	Pyrite	Pyrite: FeS ₂ Pyrrhotite: Fe _{1-x} S _x
	Pyrrhotite	FeS _{1.98}
Granite	Pyrite	Fe _{0.94} S _{1.06}
	Pyrrhotite	FeS _{1.98}
	Pyrrhotite	Fe _{0.94} S _{1.06}

4.2 Supracrustal Rocks

Minerals were analyzed in representative samples from all supracrustal rock types except greywackes. The dominant minerals in these samples are plagioclase, quartz and K-feldspar, with tremolite dominant in amphibolites. The microprobe study focused on tourmaline, tremolite and closely associated minerals as an aid to understanding the origin of the tourmaline-bearing pseudomorphs.

4.2.1 Amphibolite

The compositions of apatite, phlogopite, titanite, tremolite, tourmaline, plagioclase and potassium feldspar were measured in amphibolites. Feldspar, titanite and apatite compositions show little variation in composition (Tables 4.2 and 4.3). K-feldspars are close to the orthoclase end-member (Or₉₇). Amphiboles lack Na and K and have high Ca and Mg/(Mg+Fe) and are thus categorized as tremolite, with actinolite in granites (Fig. 4.1). Fluorine content in tremolite is generally consistent at 0.05 to 0.10 apfu (Fig 4.2).

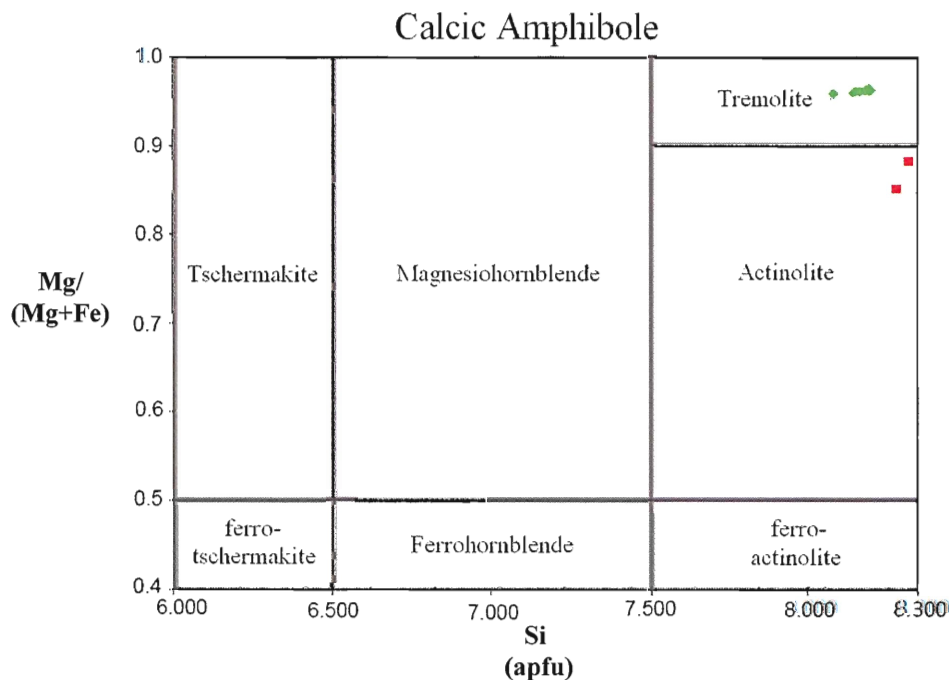


Figure 4.1: Tremolite is present in amphibolite samples from the study area whereas actinolite is in the granites. (Classification diagram from Yavuz 1999)
 Amphibolite ◆ Granite ■

4.2.2. *Graphite-rich pelites*

Graphite-rich pelites are dominated by quartz, plagioclase, K-feldspar, graphite, phlogopite and muscovite, with accessory tourmaline. Phlogopite, muscovite, plagioclase, K-feldspar and tourmaline were analyzed. Phlogopite compositions have Mg/(Mg+Fe) from 0.92-0.87 and Al 1.23-1.31 apfu. Tourmaline compositions are dravitic with Mg/(Mg+Fe) predominately from 0.94-0.96. Iron ranges from 0.9-0.12 apfu and locally reaches 0.67 apfu within cores of tourmalines.

4.2.3. *Tourmaline-rich pelites*

Tourmaline-rich pelites consist mainly of quartz, mica, tourmaline, rutile and feldspar. K-feldspar is close to the orthoclase end member (Or₉₆). Phlogopites are Fe-deficient with Mg/(Mg+Fe) ratios from 0.94 to 0.87, and 0.05-0.07 apfu F. Tourmalines vary from Mg/(Mg+Fe) of 0.79 to 0.96, 0.16-0.34 apfu Ca and 0.04-0.08 apfu F. Tourmaline cores are higher in Fe, with 0.52 apfu compared to 0.1 apfu in rims.

4.2.4. *Tourmalinites*

Tourmalinites are sulphide-rich and iron-stained rocks consisting of quartz, feldspar, mica, tourmaline, apatite and titanite. Tourmalines range in composition from 0.84 to 0.98 Mg/(Mg+Fe) and 0.39-0.5 Na. Fluorine abundance ranges from 0.17-0.21 apfu. Phlogopites range 0.91 to 0.94 Mg/(Mg+Fe) and 0.24-0.45 apfu F.

4.3 *Intrusive Rocks*

4.3.1. *Granites*

Granites are coarse-grained with plagioclase, K-feldspar and quartz and minor secondary chlorite, pumpellyite and actinolite. Actinolite composition ranges from 0.85-0.88 Mg/(Mg+Fe)

while Al varies from 0.11 to 0.14 apfu. Minor apatite contains 0.52-0.77 apfu F whereas pumpellyite varies from 0.1 to 0.23 apfu F. Tourmalines are absent from granite.

4.4 Discussion

Tourmaline chemistry presents some interesting trends and variations between cores and rims. All tourmaline rim compositions are similar whereas cores vary throughout study area.

4.4.1 Tourmaline Analysis

The main substitutions in tourmalines from the study area are X=Na; Y=Al, Mg, Fe; Z=Mg, Al, Fe; B=B, V=OH and W=OH, F and compositions are mostly dravite to alkali-free dravite. Tourmalines in amphibolites are distinctly different from those in other rock types, with a lower Na/(Na+Ca) vs. Fe/(Fe+Mg) ratio and highly contrasting core to rim compositions (Fig.4.3). Cores are significantly higher in Fe with concentrations up to 1.10 apfu whereas rims are as low as 0.08 apfu and are closer to alkali-free tourmaline (Fig. 4.4). Tourmaline-rich pelite, tourmalinite and amphibolite tourmalines are approximately equal in Fe/(Fe+Mg) values of 0.05. However, Na/(Na+Ca) values range from ~0.95 in graphite-rich pelites, to ~0.7 in tourmalinites and ~0.4 in amphibolites. Tourmaline in graphite-rich pelites is closest to alkali-free dravite.

Tourmaline Analyses

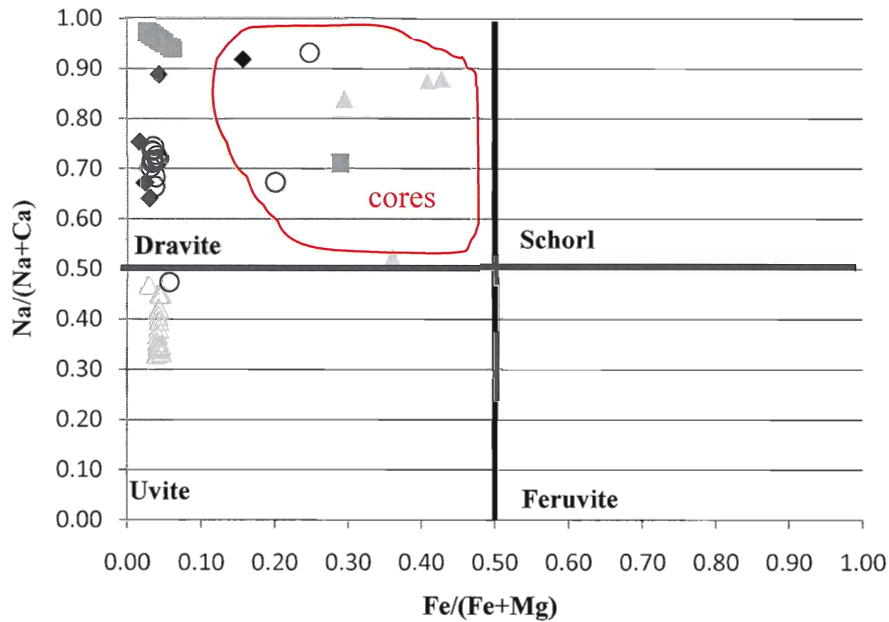


Figure 4.2: Tourmaline rims are uniformly Fe-poor. Na values vary for tourmaline rims from different rock types but all are consistently Fe-poor. Cores vary in Na as well but are more Fe-rich than rims. (Classification diagram from Henry and Dutrow 1996)

◆ Tourmalinite ■ Graphite-rich Pelite △ Amphibolite Rims ○ Tourmaline-rich Pelite ◊ Amphibolite Cores

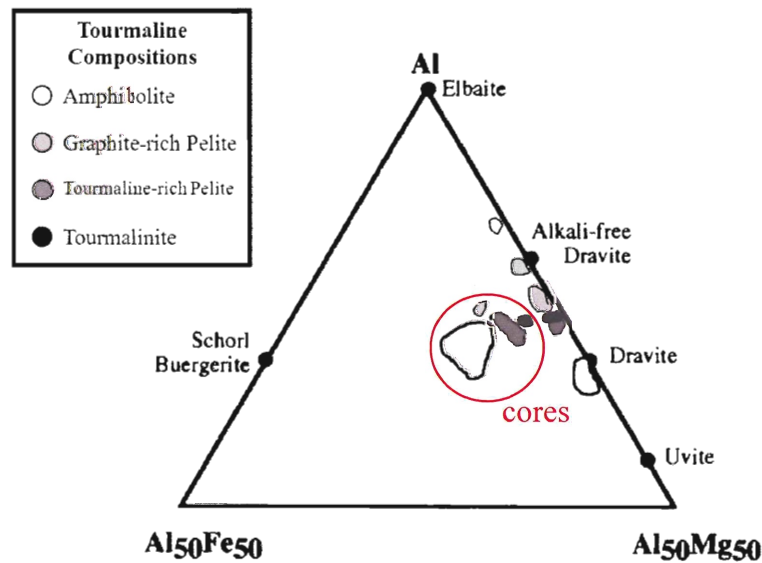


Figure 4.3: Tourmaline compositions are dravite to alkali-free dravite. Tourmaline rim compositions plot mostly along the dravite to alkali-free dravite solid solution sequence. Iron is almost absent from rims whereas cores contain up to 7.8wt% Fe. (Classification diagram from Slack 1996)

4.4.2. Fluorine bearing minerals

Fluorine content in F-bearing minerals is mainly influenced by the temperature of crystallization and presence of other F-bearing minerals (Edgar & Arima 1985). Common F

content for phlogopites in metamorphosed pelites is 0.05-2 wt% (0.02-0.9 apfu). If F-bearing minerals co-exist, F is partitioned between them (Edgar & Arima 1985). Fluorine substitutes for at most 1 O site in the tourmaline structure and in general, most tourmalines contain less than 0.2 apfu F (Henry & Dutrow 1996). Phlogopites in tourmalinites and graphite-rich pelites are comparatively higher in F (0.45 apfu to 0.23 apfu) than phlogopite in tourmaline-rich pelites (0.07 apfu) and amphibolites (0.16 apfu) (Fig 4.5).

Fluorine and Rock Assemblages

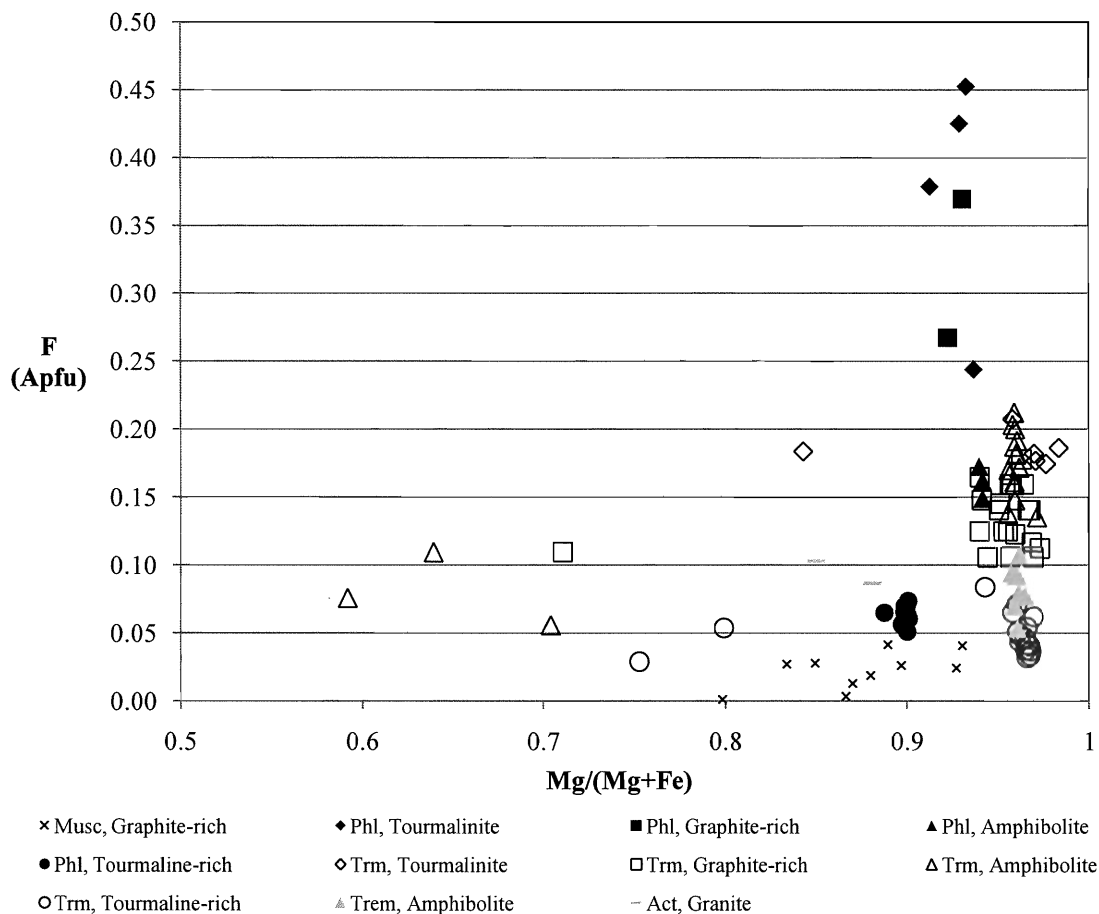


Figure 4.4: Fluorine in all Fe-Mg bearing phases. Values for tourmalines range from 0.03 in tourmaline-rich pelites to 0.21 in amphibolites. Open symbols are tourmalines and closed symbols are phlogopite.

Fluorine becomes enriched in granitic tourmalines: however, in low-to medium-grade pelites, tourmalines typically contain less than 0.2 apfu (Henry & Dutrow 1996). Fluorine in tourmalines from the study area are generally lower than 0.2 apfu, consistent with other data suggesting granites are not the source of fluids.

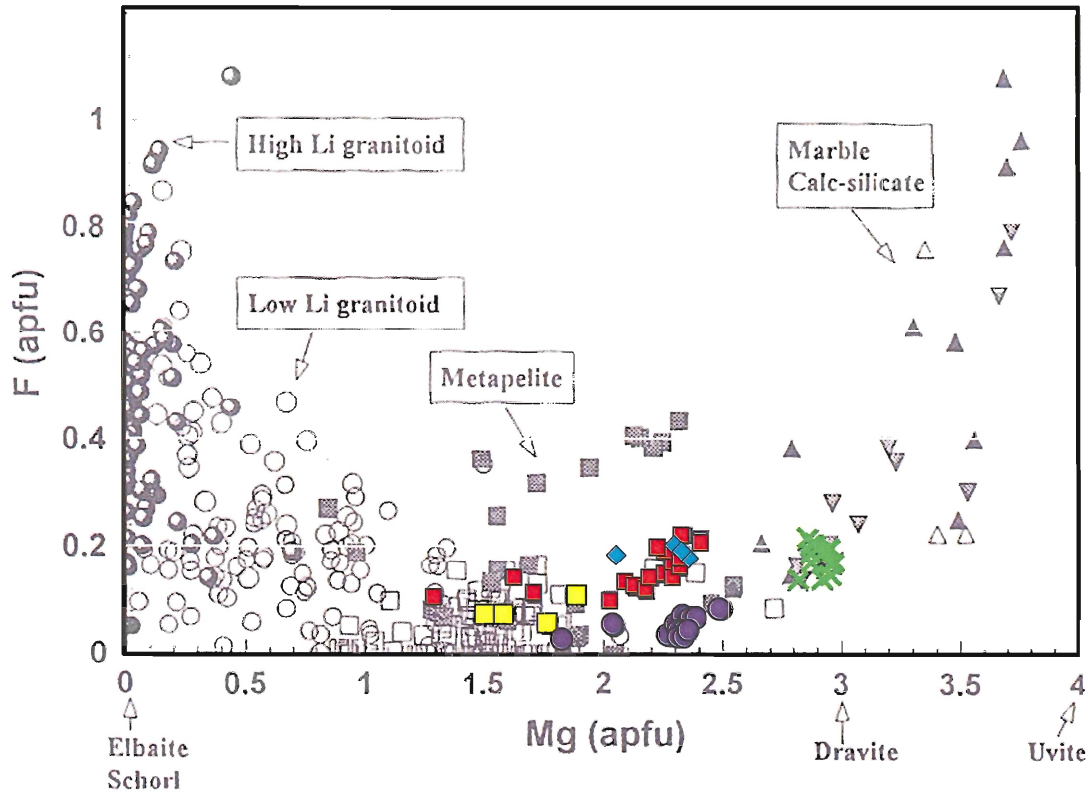


Figure 4.5: Fluorine within study area tourmalines (legend below) compared with other data from Henry and Dutrow (1996). Fluorine of study area tourmalines falls mostly below 0.2 apfu in the metapelite division, contrasting with tourmalines in granitoid and marble protoliths (Henry & Dutrow 1996)

- ◆ Tourmalinite ● Tourmaline-rich Pelite ✕ Amphibolite Rims
- Graphite-rich Pelite ■ Amphibolite Cores

CHAPTER 5: DISCUSSION

The purpose of this chapter is to test the working hypotheses from Chapter 1, including tourmaline genesis and that the rocks of the study area were deposited in a sedimentary-exhalative environment. First I discuss the possible donors which enabled tourmaline generation and the stages of pseudomorph generation, proposed through a progression of 3 reactions. The characteristics of sedimentary exhalative environments will also be described, with focus on characteristics of Proterozoic basins, leading into a comparison with rocks from my study area. Based on the comparison, the validity of the working hypothesis is assessed and modifications and alternatives proposed.

5.1 Origin of Tourmaline

Supracrustal rock samples contain fine-grained (0.01 mm) to medium-grained (1 mm) tourmaline (4-18%), whereas tourmaline is absent from intrusive lithologies. Tourmalines are dravite to alkali-free dravite. They are zoned from Fe-rich ($Mg/[Mg+Fe]=0.57$) and F-poor (0.07 apfu) dark olive-green olive cores, to Fe-poor and Mg-rich ($Mg/[Mg+Fe]=0.96$) and higher F (0.2 apfu) colourless rims. Multiple stages of tourmaline deposition are suggested by changes in Fe, Mg and F content.

Magnesium in tourmalines and other metamorphic minerals (tremolite, phlogopite) suggests the sedimentary protoliths were Mg-enriched prior to metamorphism. The first stage of tourmaline deposition could have been from compaction of sediments and exhalative or infiltrated sedimentary fluids from the sedimentary sequence. Boron could be provided from the leaching of surrounding sediments and concentration in hydrothermal fluids that precipitated ($Mg/[Mg+Fe] = 0.57-0.87$) tourmaline on cooling. Continued B-leaching and progressive tourmaline crystallization from a Fe-depleted system could have precipitated colourless, Mg-rich

[Mg/(Mg+Fe) = 0.96] tourmaline rims. It is likely that the B needed to grow new tourmaline came from hydrothermal fluid or fluid derived by continued prograde metamorphism of sediments because tourmaline is stable to granulite facies metamorphism whereas k-feldspar and sillimanite suggest the study area was only subjected to upper-amphibolite grade.

5.1.1 Pseudomorphs

The shapes of tremolite crystals closely resemble the diamond-shaped tourmaline-sillimanite-muscovite oikocrysts in the graphite-rich pelite, suggesting an interesting replacement process (Fig 5.1). There appears to be an intermediate reaction in which phlogopite, plagioclase, K-feldspar and sillimanite are first produced from tremolite and muscovite (Fig 5.2, 5.3).

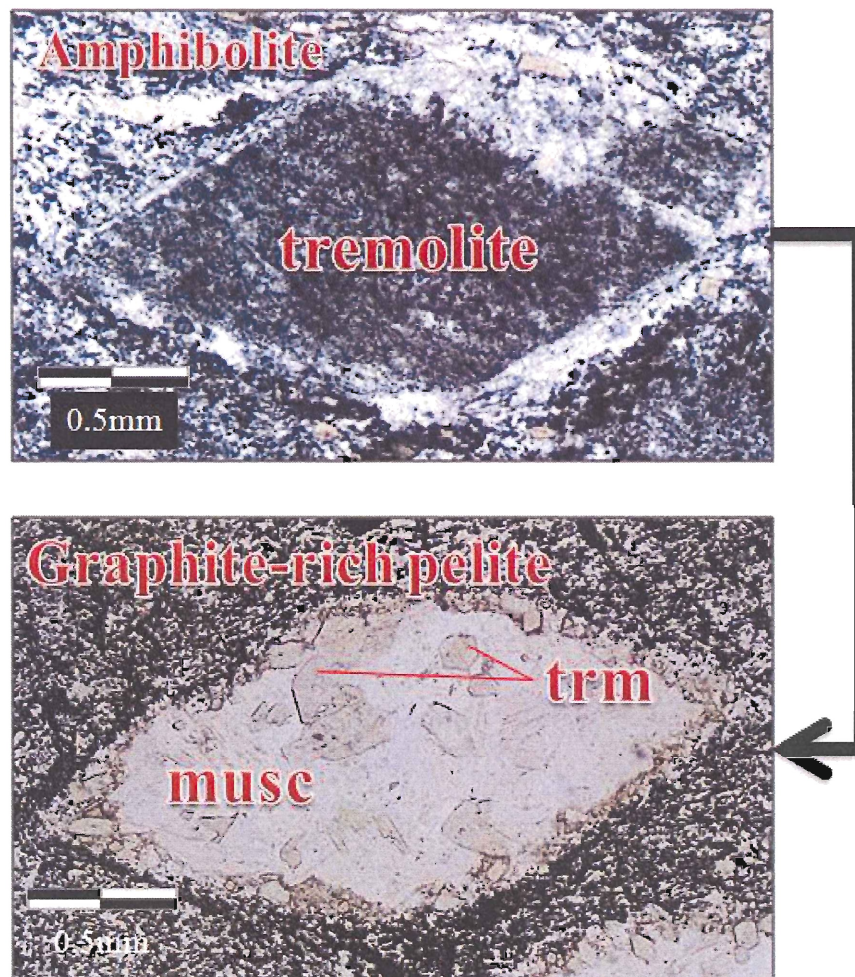


Figure 5.1: Proposed “before” (tremolite, top) and “after” (oikocryst, bottom) of pseudomorph reaction. The tremolite crystal rim now consists of fine grained tourmaline, k-feldspar and plagioclase through reactions 1 to 3 (see text). Note one basal section containing fibrolitic sillimanite, emphasizing core to rim contrast. (top: PPL, Sample A004-L. bottom: PPL, Sample A004-K)

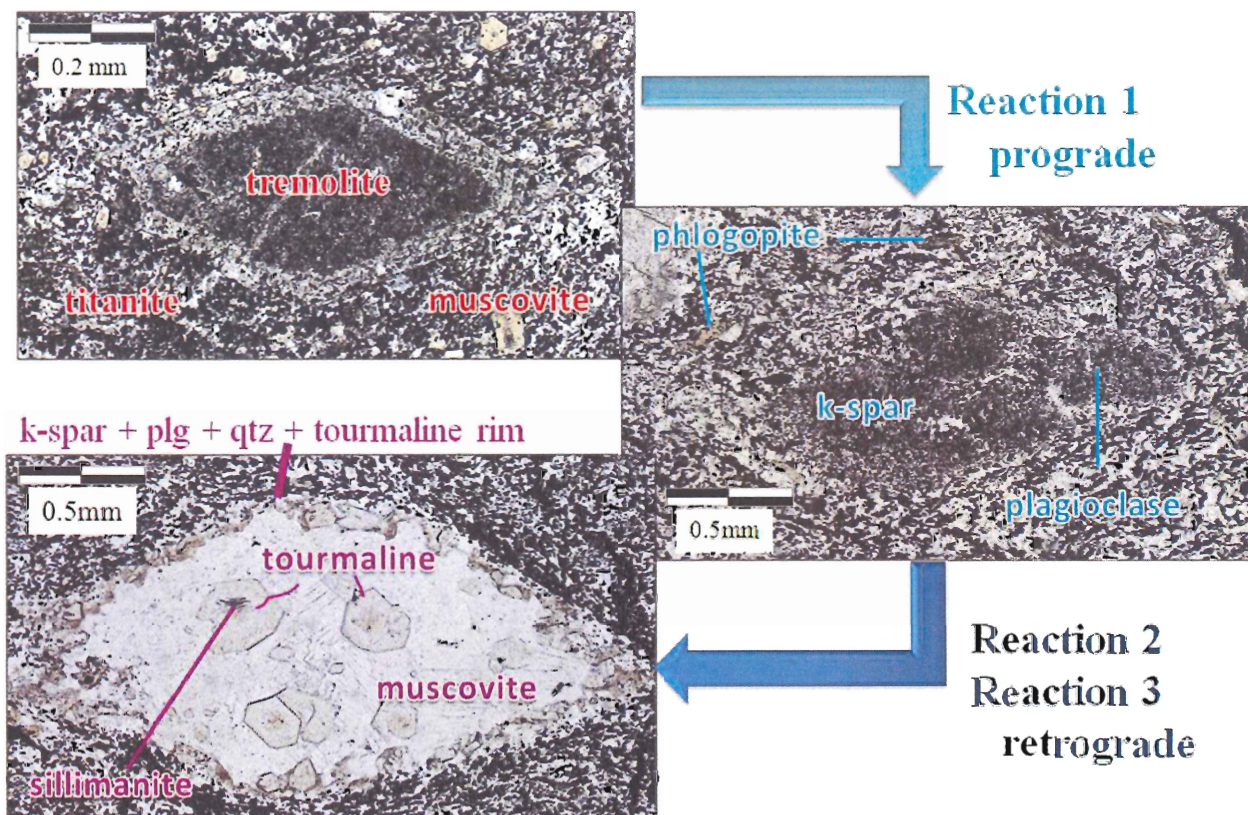
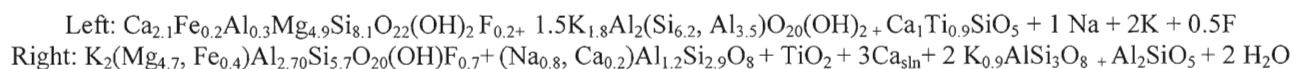
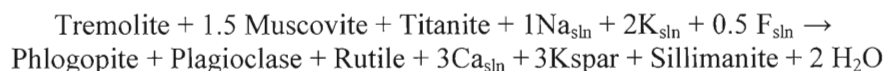


Figure 5.2: Stages of oikocryst formation. The first stage involves a prograde reaction that breaks down muscovite and tremolite to create phlogopite, k-feldspar and plagioclase. Reactions 2 and 3 are retrograde and involve the generation of tourmaline with the first stage creating tourmaline cores and the second stage creating the tourmaline rims.

5.2.1.1 Reaction 1



Reaction 1 involves prograde replacement of tremolite and muscovite by phlogopite, plagioclase, K-feldspar and sillimanite (Fig 5.4). Titanite breaks down to rutile and releases Ca. Associated fluids contributed to Na, K and F in solution and leached Ca from the rocks.

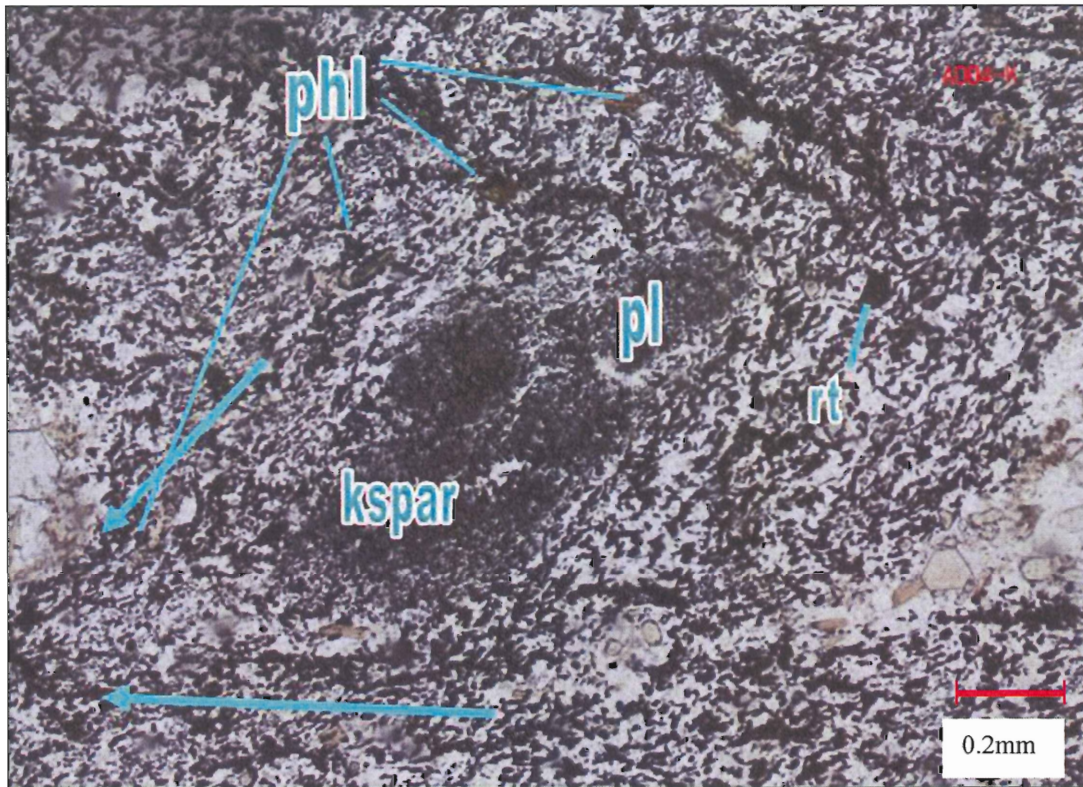
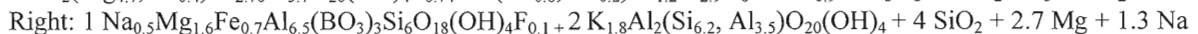
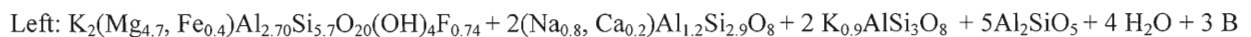
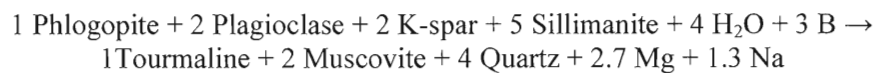


Figure 5.3: The product of first reaction. Secondary phlogopite surrounds the diamond-shape imprint outlined by the red arrows. Phlogopite (phl) is aligned with orientation of the proposed original tremolite rim. Plagioclase (pl) and k-feldspar (k-spar) form inside the original tremolite. Rutile (rt) lies adjacent to the primary crystal area in similar abundance and habit as titanite in the amphibolite. (PPL, Sample A004-K)

5.1.1.2 Reaction 2



The second reaction consumed sillimanite and led to the nucleation of tourmaline cores and muscovite in the oikocrysts with quartz placed into the rim. Fluids added B to the system and liberated Mg and Na. Sillimanite is restricted to the idioblastic tourmaline cores but is absent from rims (Fig 5.5) however, suggesting that it was mostly consumed by this process.

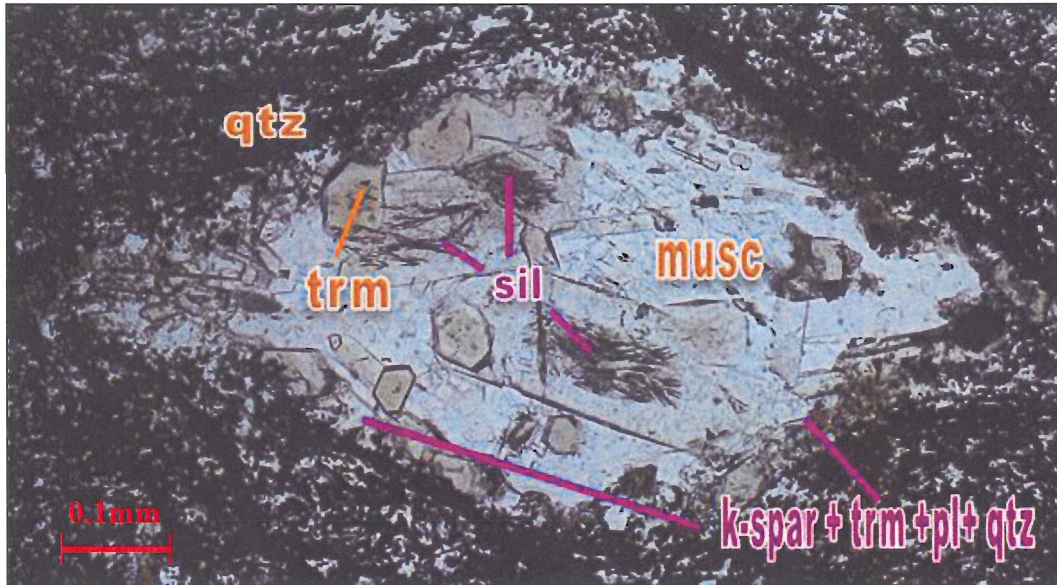


Figure 5.4: Polished thin-section of oikocryst. Sillimanite fibres are clearly confined to euhedral tourmaline brown core in basal section. Sillimanite and tourmaline crystals are generally aligned with oikocryst and fabric orientation. (Polished section, PPL, Sample A004-K)

5.1.1.3. Reaction 3



Left: $1 \text{ K}_2(\text{Mg}_{4.7}, \text{Fe}_{0.4})\text{Al}_{2.70}\text{Si}_{5.7}\text{O}_{20}(\text{OH})_4\text{F}_{0.74} + 2(\text{Na}_{0.8}, \text{Ca}_{0.2})\text{Al}_{1.2}\text{Si}_{2.9}\text{O}_8 + 2 \text{ K}_1\text{AlSi}_3\text{O}_8 + 6 \text{ Al}_2\text{SiO}_5 + 4 \text{ H}_2\text{O} + 3 \text{ B}$

Right: $2 \text{ Na}_{0.4}\text{Mg}_{2.3}\text{Ca}_{0.2}\text{Fe}_{0.2}\text{Al}_{6.5}(\text{BO}_3)_3\text{Si}_6\text{O}_{18}(\text{OH})_4\text{F}_{0.19} + 1 \text{ K}_{1.8}\text{Al}_2(\text{Si}_{6.2}, \text{Al}_{3.5})\text{O}_{20}(\text{OH})_2 + 2 \text{ SiO}_2 + 1 \text{ Na}^+ + 2 \text{ K}^+ + 3.5 \text{ Si}$

Reaction 3 is similar to Reaction 2 but creates Fe-depleted and more Mg-rich tourmaline rims. Fluids leach Na, K, Si but provides B. Pseudomorphs of tourmaline, muscovite, plagioclase, K-feldspar and quartz have fully replaced tremolite (Fig 5.6).

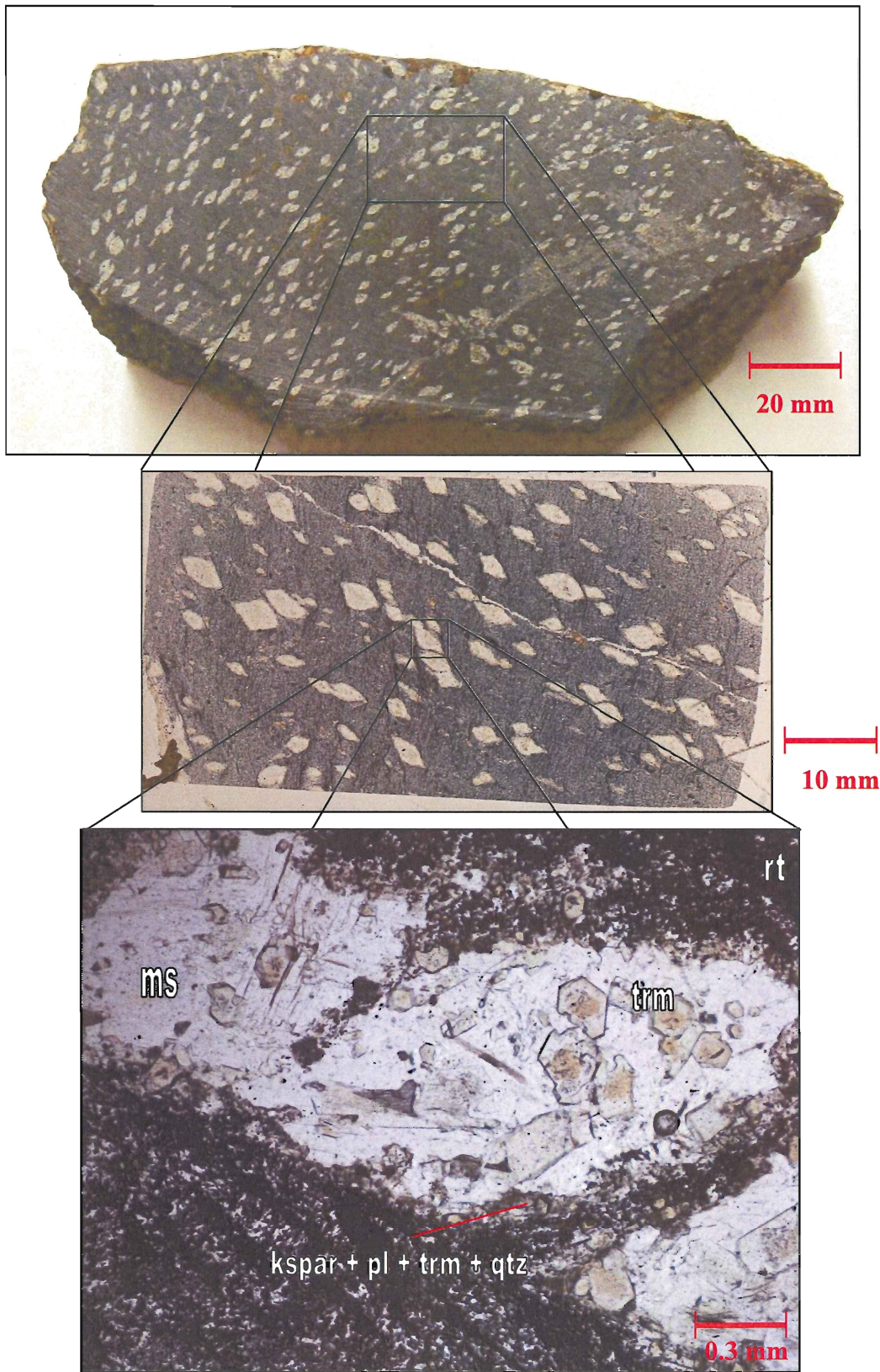


Figure 5.5: Scales of observation from hand sample to thin section. Oikocrysts are abundant in hand sample but constituent crystals are indistinguishable. Zonation of fine grained k-feldspar-plagioclase-tourmaline rim with medium-grained muscovite (ms) and zoned tourmaline (trm). (Sample A004-K)

5.1.1.4 Implications

Fluids contributing to metamorphism in Reaction 1 could have been derived from sediments during dehydration accompanying prograde metamorphism. There is no evidence that partial melting or intrusion of granites at this stage could have contributed fluids. Calcium leached could have been deposited elsewhere as calcite veins, but no direct evidence is preserved.

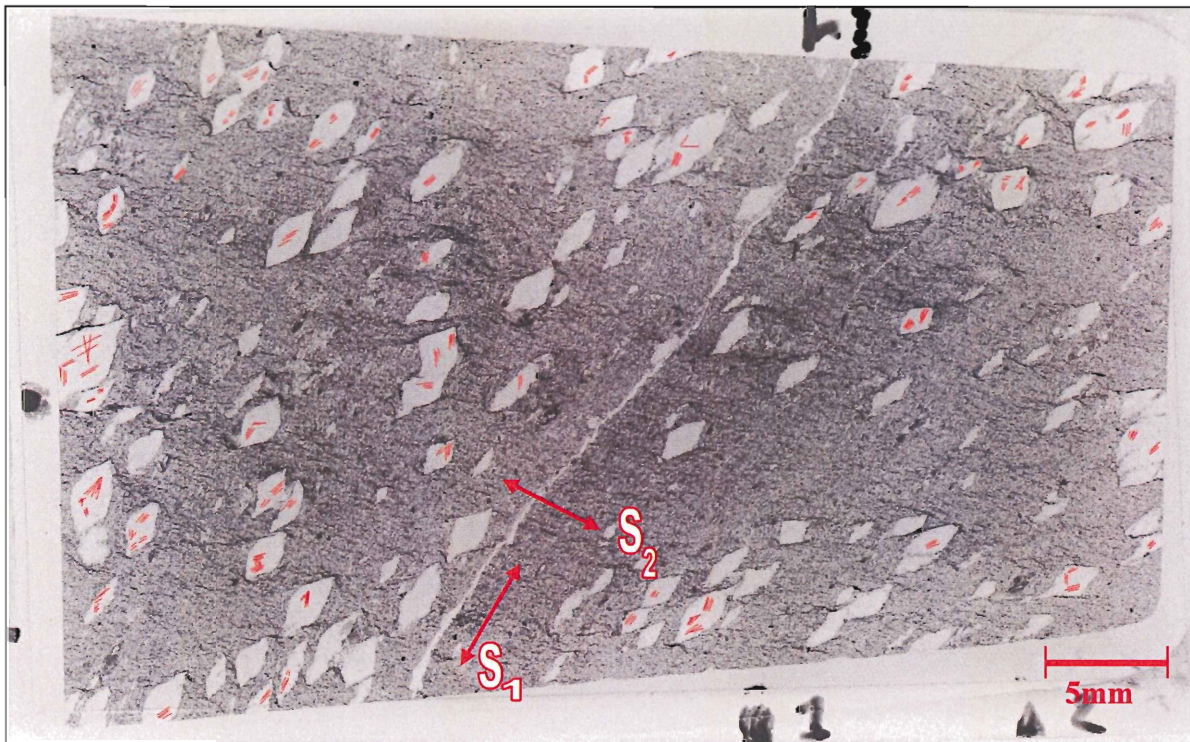


Figure 5.6: Scanned thin section of pseudomorphs within graphite-rich pelite. Red lines portray orientations of sillimanite fibres within the cores of tourmalines. Long axis of pseudomorphs and most sillimanite fibres are aligned with S_1 . (Sample A004-K)

Reaction 2 releases Mg and Na into solution and Reaction 3 releases Na, K and Si into solution. Minor veins throughout samples predominately consist of phlogopite and K-feldspar providing evidence for Mg and K rich fluids. Fluids could have been derived from external areas as regional thrusting and shortening will cause displacement, movement and infiltration of fluids (Barnes 1997). Right lateral transpression along the Lyon Inlet Boundary zone may have also

caused some fluid migration. As fluids moved through sediments B could have been partitioned into fluids. Further work is needed to resolve this question.

5.2 Sedimentary-exhalative (SEDEX) basins and deposits

Sedimentary-exhalative deposits form in continental rift basins and are dominated by graphite-rich host rocks. Most deposits formed during Proterozoic and Phanerozoic times within anoxic and H₂S-rich basins. Metals of interest are Zn, Pb and Ag. Sulphide minerals of interest and abundance are galena, sphalerite, pyrite and pyrrhotite. Clastic rocks and related volcanics usually lie at the base of the depositional sequence, and are overlain by post-rift shales or carbonates (Fig. 5.1). Basaltic rocks, dykes or sills may be spatially or temporally associated with ore deposits but are not present in all such deposits (Goodfellow & Lydon 2007).

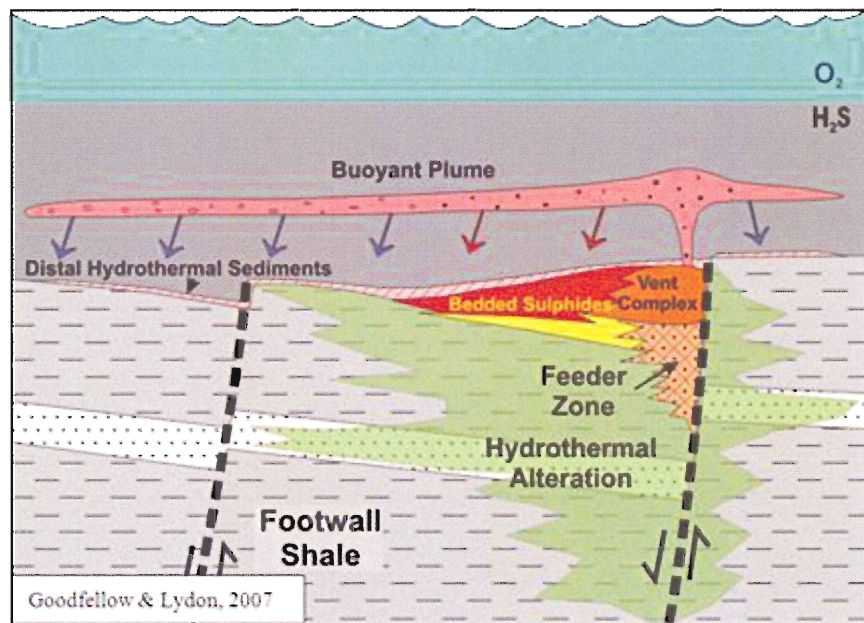


Figure 5.7: Typical cross-section of vent proximal SEDEX-type deposit. Hydrothermal fluids flow up through basin floor extensional and transpressional faults where fluids exhale into an anoxic bottom stratified basin. Bedded sulphides are deposited in footwall alteration zone. (Goodfellow and Lydon, 1997)

Transform and extensional faults in the basin floor allow hydrothermal fluids to rise through conduits and discharge at the seafloor. The source of reduced S is most likely bacteria-reduced SO₄⁻² in SEDEX-seawater. Basin temperatures, acidity, metal content and redox

conditions vary largely, but in most cases metal sulphides are precipitated at or just above the seafloor, where they react with the H₂S-rich water column (Goodfellow & Lydon 2007).

Hydrothermal alteration in SEDEX environments is poorly documented, but non-sulphide alteration minerals include quartz, muscovite, chlorite, ankerite, siderite and tourmaline. Pyrite, pyrrhotite, galena, sphalerite, chalcopyrite, tetrahedrite and arsenopyrite may be present (as alteration) but usually at low concentrations. Hydrothermal alteration around SEDEX deposits can extend for up to 7km laterally and hundreds of metres around ore-bearing sediments (Fig. 5.2). Alteration can continue after sulphide formation by convection where cold fluids descend into the sedimentary sequence, are subsequently heated, and rise to the seafloor again, continuing alteration on their ascent (Goodfellow & Lydon 2007).

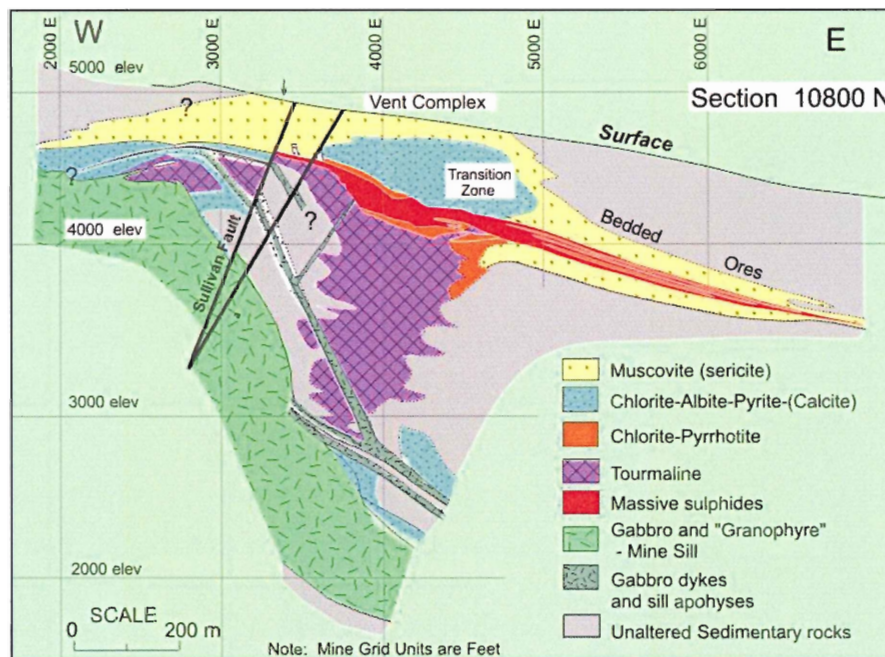


Figure 5.8: Tourmaline, muscovite and chlorite alteration of the Sullivan SEDEX Deposit in British Columbia. Tourmaline is present in a 250m x 500m pipe adjacent to faults as well as other deposits proximal to faults. (Goodfellow & Lydon 2007)

Tourmalines in SEDEX-environments are largely produced by secondary metamorphism and metasomatism, and it reflects the bulk composition of the rock in which it forms (Alonso 1997). Boron is usually derived from the sediments in these deposits. Graphite-rich schists and

shales contain twice as much B as graphite-poor rocks and B is generally easily leached from water-rock interfaces at relatively low temperatures ($\geq 150^{\circ}\text{C}$) and then partitioned into hydrothermal fluids (Henry & Dutrow 1996). Anoxic basin water concentrates B and promotes its precipitation.

Dravite, or Mg-rich tourmaline, is used as an exploration guide, especially for stratabound mineral deposits (Slack 1996). Where associated with stratabound deposits or sedimentary rocks, dravite or Mg-rich tourmaline indicates deposition within an exhalative fumarole environment (Deer et al. 1997). High Mg concentrations in tourmaline indicate high Mg-bulk compositions suggesting either Mg-rich pre-metamorphic sediments that may have contained dolomite or Mg-rich clays, such as sepiolite and palygorskite, which are most commonly found in peri-marine evaporitic settings or in alkaline lakes (White 2009). Magnesium can also be provided in marine hydrothermal settings from the sea water that was partitioned into clays (Slack 1996).

Tourmalinites are common in SEDEX environments. They consist of conformable layers of quartz and tourmaline, with tourmaline exceeding 15-20% of the rock (Slack et al. 1994). Tourmalinites are interpreted to form by metasomatic modifications of volcanic exhalative deposits during sedimentation or by the early diagenesis of B-rich chemical precipitates (Henry and Dutrow 1996). Where tourmalinites are present within ore deposits, the most Mg-rich tourmalines are associated with larger sulphide deposits; however concentrations of tourmaline and tourmalinites also occur without any adjacent ore deposit (Slack 1996).

5.3 Sedimentary Exhalative Assessment

The sample area lies within the Paleoproterozoic Penryhn Group, which was deposited within an intracontinental hypersaline basin (Henderson 1983). Primary sedimentary structures

are mostly absent from the Penryhn Group as a result of medium-to high-grade metamorphism and penetrative deformation (Corrigan et al. 2010). Samples contain abundant graphite indicating an organic-rich shale protolith.

Although my samples were not deposited within a purely continental rift setting, similarities can be drawn with the characteristics of sedimentary-exhalative environment rocks. Crustal thinning and local rifting are documented within the Piling Group, possibly correlating to other interlaying Foxe Fold Belt groups, including the Penryhn Group (Johns et al. 2006). Diabase and granite are the proximal intrusive units and could be associated with minor rifting.

Pyrite, pyrrhotite, and tourmalinites with abundant Mg-rich tourmaline are consistent with deposition in an exhalative system. Study area tourmaline rim compositions provide particularly interesting points of comparison, as they are among the most Mg-rich reported from hydrothermal environments (Slack 1996). Most SEDEX deposits have tourmalines with $Mg/(Mg+Fe)$ as high 0.85. The Sullivan Zn-Pb SEDEX-deposit in British Columbia ranges from $Mg/(Mg+Fe)$ 0.15 to 0.90 and tourmaline in Appalachian-Caledonian massive sulphide deposits averages $Mg/(Mg+Fe)$ 0.79 (Taylor and Slack 1984). Tourmalines of the Rampura Agucha Zn-Pb-(Ag) SEDEX deposit in India average $Mg/(Mg+Fe)$ of 0.98 in the footwall of the ore-deposit but 0.32 to 0.57 in the hanging wall (Holler & Gandhi 1997). Where stream samples have been used for exploration, tourmalines with $Mg/(Mg+Fe) > 0.76$ correlate with larger sulphide deposits (Slack 1996). Tourmalines from the study area most closely resemble those of global stratabound deposits, exclusive of massive sulphides (Fig 5.9). The tourmaline compositions do not resemble those from granitoid hydrothermal systems, consistent with the absence of tourmaline from the minor granite in the area.

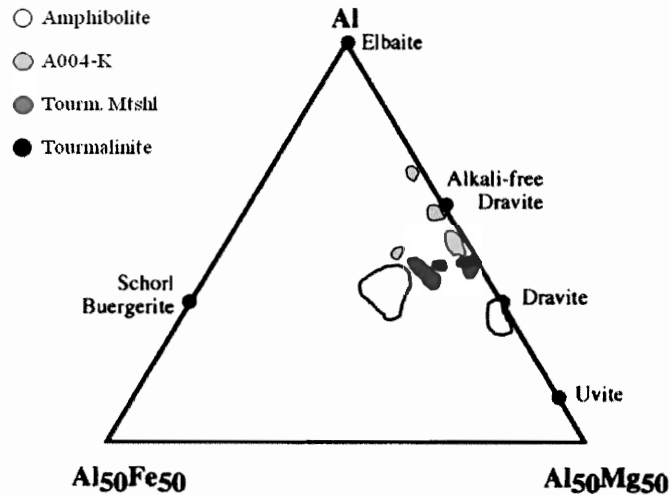
While the study area lacks some features of SEDEX-type deposits, it could have been deposited in a sedimentary-exhalative environment. Minor concentrations of base metal minerals and gold lake sediment anomalies however have sparked exploration in the area in search of a sulphide deposit. Lake sediment samples from the region show anomalies of higher Au, Zn and As concentrations encouraged mineral exploration projects adjacent to and within the study area. Aquitaine Company of Canada reported concentrations of 2-8% Zn within rock samples. Borealis Exploration reported soil samples with 2319 ppm Au and 62000 and 4200 ppm Zn. BHP Billiton's Nagvaak Project (1994-1996) documented the most significant results. Zn levels reached 9.68%, Pb 9.5%, 1220 ppm Cu and 6940 ppb Au in frost-heave rock samples. These values indicate some concentrations of valuable metals; however concentrations may not be economically viable. Study area rocks only contain pyrite and pyrrhotite in trace amounts except for tourmalinites which hold up to 10% sulphides. Sulphides overprint matrix minerals and are concentrated in veins indicating secondary deposition.

5.4 Penryhn Economic Potential

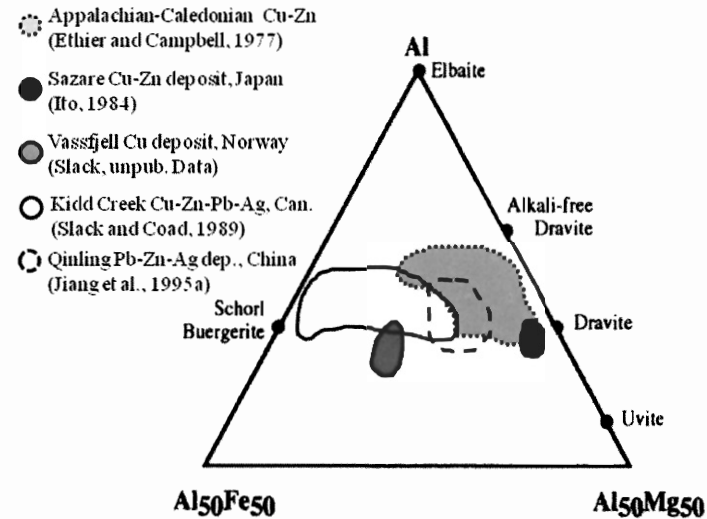
No economically viable deposit has yet been discovered within the Penryhn Group although rusty sulphur-stained gossanous outcrops are common (Henderson 1983). Dravitic tourmalines, tourmalinites, high concentrations of Zn and Au in lake, soil and rock samples (Fig 5.10) and minor Pb concentrations suggest some further exploration should be conducted. BHP Billiton, Aquitaine and Borealis Exploration all suggested further exploration in the area, but the isolation of Canada's north discouraged further work. Exploration of northern Canada is gaining interest again with the government and mining companies providing easier access to the area. A frost-heave sample returned the highest assay (6940 ppb Au) so if a deposit is present, it may be at depth. Graphite-and pyrrhotite-rich rocks promote leaching and oxidation of base metal

sulphides from exposed rock and may account for the relatively high concentrations within soil and lake sediments. I suggest that a systematic drilling project be conducted within the study area, in a 2km x 2 km grid, and drilling every 500m, N-S and E-W, including areas north where Au-rich grab samples were found. If drill cores show potential, further drilling should be conducted.

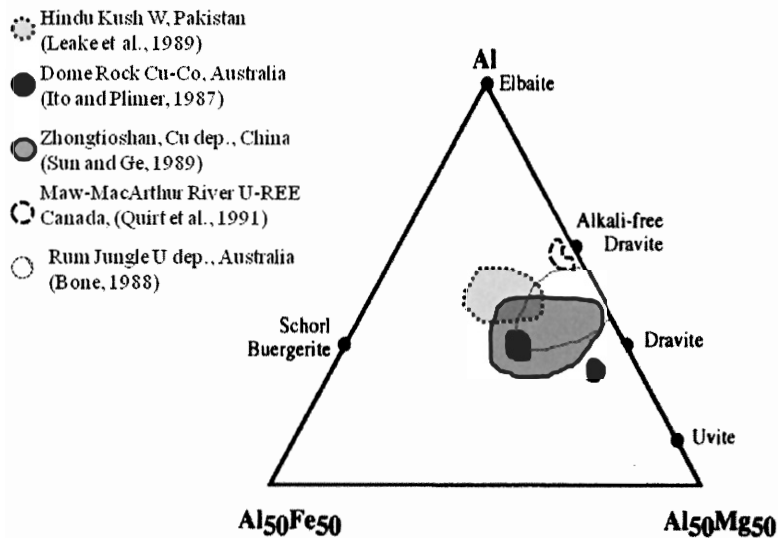
Sample Area Tourmalines



Massive Sulphide Deposits



Stratabound Deposits



Granitic Deposits

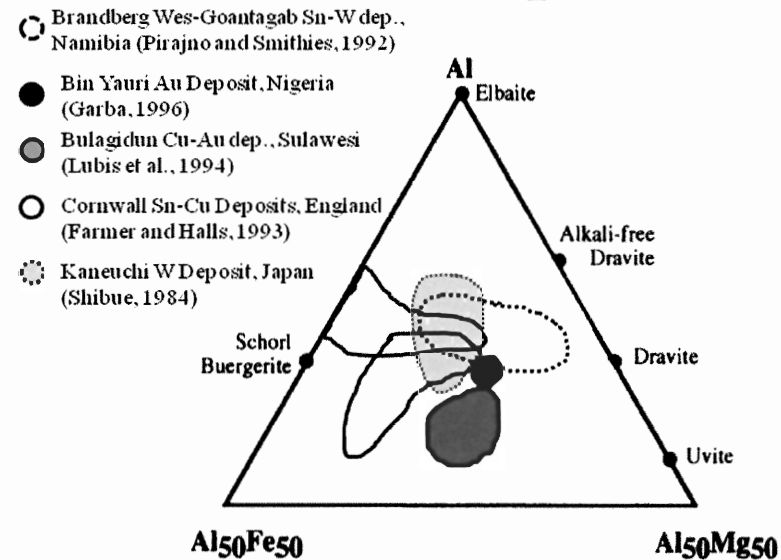


Figure 5.9: Tourmalines have been used in many studies to examine their correlation to economic potential of deposits. Tourmaline can be used as an indicator mineral for many types of deposits including massive sulphide, granitic generated and stratabound deposits. Study area tourmalines (top left) correlated best with tourmalines from stratabound deposits but are Fe-poor in comparison to granitic deposits. (Classification diagrams from Slack, 1996)

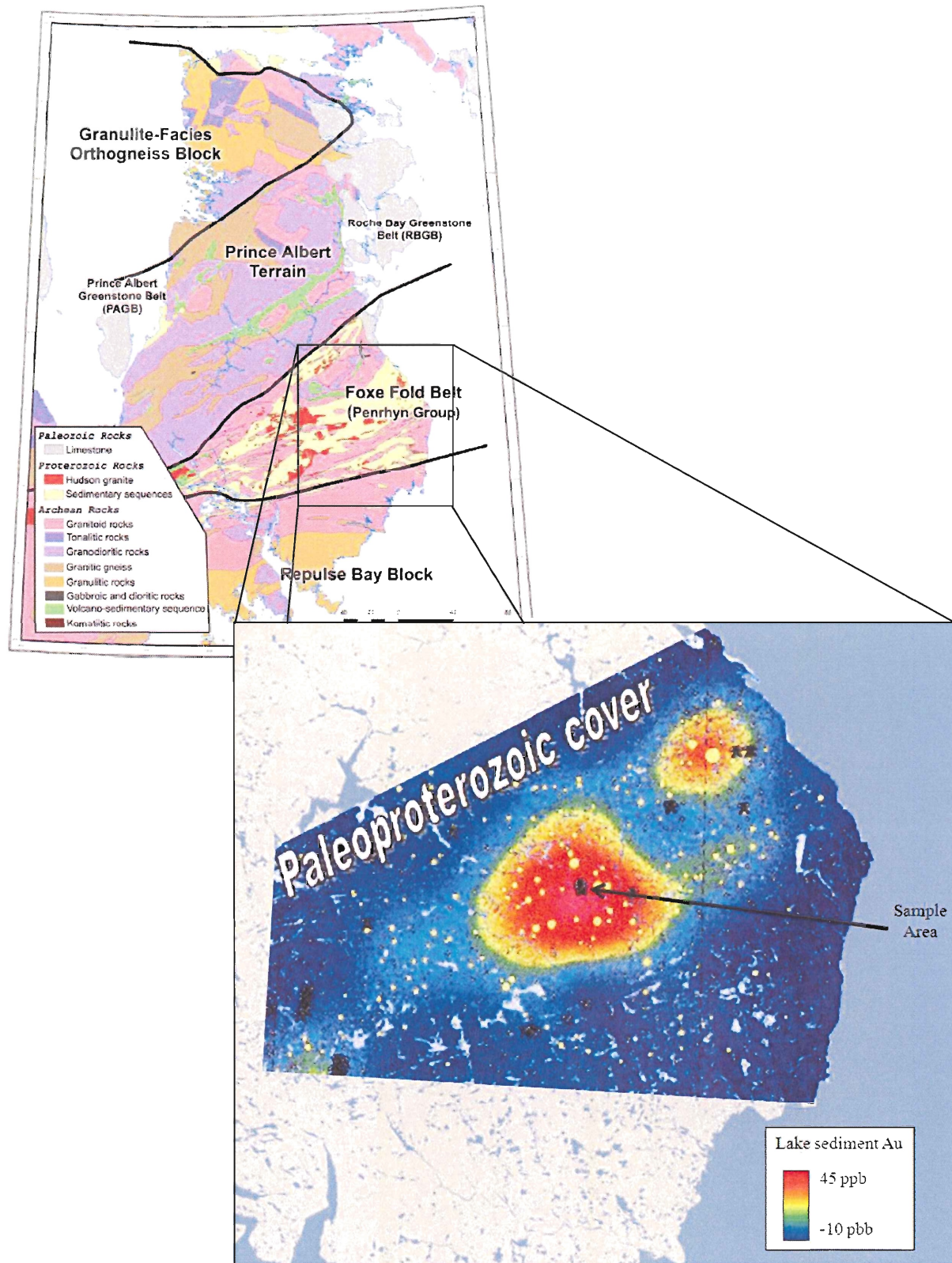


Figure 5.9: Lake sediment samples of Au concentrations through S-E Melville Peninsula, with highest enrichment directly south of study area. Pyrrhotite and graphite within the study area however increases potential for base metal leaching from rocks and may be the cause of the anomaly.

CHAPTER 6: CONCLUSIONS

The extent of hydrothermal alteration and metamorphism is pervasive throughout the study area, with practically no primary deposition features preserved. Sedimentary protolith rocks were probably shales and pelites with minor intrusions of granite and diabase. Tourmaline is dravite to alkali-free dravite and formed in at least two stages: early more Fe-rich ($\text{Mg}/[\text{Mg}+\text{Fe}]=0.57$) and F-poor (0.07 apfu) olive cores, and later Fe-poor and Mg-rich ($\text{Mg}/[\text{Mg}+\text{Fe}]=0.96$) and higher F (0.2 apfu) colourless rims. Magnesium was probably derived from pre-metamorphic Mg-rich clays or dolomite, possibly Mg-rich basin fluids. Boron was supplied by the surrounding sediments and partitioned into hydrothermal fluids to precipitate as tourmaline. Early metamorphic tremolite crystals were later pseudomorphed mainly by tourmaline, muscovite and sillimanite during several stages of fluid infiltration. Sulphides in the study area consist of pyrite and pyrrhotite and appear to be secondary.

The study area was most likely deposited within a sedimentary-exhalative environment, as indicated by the presence of pyrite and pyrrhotite, amphibolites, tourmalinites and dravite. The setting was probably an intracontinental basin, where local rifting may have occurred. Further exploration in the area should be conducted to determine if a large deposit is present or if near-surface leaching conditions are the cause for base metal concentrations in surrounding lakes and soils.

Further work should involve better examination of field characteristics. Field relationships are an important feature of SEDEX-type deposits, but detailed fieldwork was not possible during the study. The sample area and surroundings should be mapped to greater detail. Footwall and hanging wall relationships and mineralization sequences are important for the

proper analysis of mineralization and metamorphism of SEDEX-type areas. If possible footwall and hanging wall sections should be discovered and mapped for better classification.

Further questions of tourmaline composition include the mechanism for such widespread deficiency of Fe within tourmalines. No previous research encountered during this study reported consistent $Mg/(Mg+Fe)$ values as high as 0.94-0.98. More fluid composition and analysis should be conducted to better determine reasons for substitutions of Mg, Fe, Ca, K and Na to create the pseudomorph from tremolite. Also more insight into possible sources of fluid would be useful.

More extensive study of isotopic signatures of both boron and sulfur minerals would provide a more thorough analysis and comparison of study area tourmalines to global tourmaline SEDEX compositions. Boron isotope abundances can be used as comparison to other global deposits for further comparison sedimentary-ore deposits. Boron isotopes can differ within minerals, specifically tourmaline, depending on temperature of formation, proportions of dissolved boron in the water, proportion of boron taken into the crystal lattice (Rayleigh Fractionation), seawater entrainment and post-ore metamorphism (Palmer and Slack, 1999). Sulfur isotope analysis would be useful to confine the basin environment during deposition. Analysing for ^{34}S could also provide useful comparison with other global SEDEX deposits on the basis of water composition and anoxia.

APPENDIX A: MICROPROBE ANALYSES

Tables A.1 – A.11 present electron microprobe (EMP) analyses from apatite, potassium-feldspar, plagioclase, muscovite, phlogopite, chlorite, pumpellyite, rutile, titanite, tourmaline and tremolite. A map illustrating sample locations is provided in Appendix C. The analyses were done at the Dalhousie University Regional Electron Microprobe Laboratory using the JEOL JXA-8200 electron microprobe. Tourmaline compositions are assumed to have a weight percent of 10.5% oxide in tourmalines. The analyses were conducted with a 15kV acceleration voltage, 2µm spot size and 20nA beam current.

Abbreviations for rock types used in A.1 to A.13 are:

<u>Lithology</u>	<u>Abbreviation</u>	<u>Mineral</u>	<u>Abbreviation</u>
Amphibolite	Amph	Chlorite	chl
Granite	Grnt	Muscovite	ms
GraphitePelite	GPelite	Potassium-feldspar	kspar
Tourmaline-rich Pelite	TPelite	Plagioclase	pl
Tourmalinite	Tmlt	Phlogopite	phl
		Pumpellyite	pmp
		Pyrite	py
		Pyrrhotite	po
		Tourmaline	tour

Table A.1: Apatite Analyses

Sample	A003A	A004L	A004L	A004L	A003C	A003C	A019A
Lithology	Tmlt	Amph	Amph	Amph	Grnt	Grnt	TPelite
No.	21	9	30	31	67	86	102
Mineral	Apatite	Apatite	Apatite	Apatite	Apatite	Apatite	Apatite
Wt%							
SiO ₂	0.17	0.27	0.09	0.22	0.15	0.22	0.10
TiO ₂	0.04	0.11	0.08	0.06	0.00	0.04	0.05
FeO	0.05	0.10	0.08	0.06	0.02	0.05	0.13
CaO	54.01	53.68	54.39	54.29	55.52	55.04	54.35
Na ₂ O	0.09	0.11	0.03	0.03	0.03	0.04	0.09
F	3.57	3.74	3.54	3.20	3.87	4.00	2.64
O=F	1.50	1.57	1.49	1.35	1.63	1.68	1.11
Total	55.21	55.14	55.54	55.55	56.43	56.23	56.03

Cations (calculated on the basis of 12O)

Si	0.032	0.051	0.017	0.042	0.026	0.041	0.018
Ti	0.005	0.016	0.011	0.008	0.000	0.005	0.006
Fe	0.007	0.016	0.013	0.010	0.004	0.007	0.021
Ca	10.794	10.672	10.813	10.845	10.807	10.707	10.846
Na	0.007	0.020	0.015	0.013	0.004	0.010	0.009
F	2.107	2.194	2.078	1.887	2.221	2.297	1.555
Total	13.027	13.051	13.017	12.898	13.089	13.106	12.764

Table A.2: Feldspar Analyses

Sample	A003C	A003C	A003C	A003C	A003C	A003C	A003C	A004K	A004K	A004K	A004K	A004K
Lithology	Grnt	Grnt	Grnt	Grnt	Grnt	Grnt	Grnt	GPelite	GPelite	GPelite	GPelite	GPelite
No.	57	60	68	69	70	79	75	13	125	135	137	138
Mineral	Kfs	Kfs	Kfs	Kfs	Kfs	Kfs	Kfs	Kfs	Kfs	Kfs	Kfs	Kfs
Wt %												
SiO ₂	63.29	63.04	64.74	63.43	62.25	63.94	64.35	65.18	64.70	64.99	65.75	64.97
Al ₂ O ₃	17.89	17.78	18.27	17.84	17.53	17.93	18.24	18.51	18.15	18.33	18.26	18.20
CaO	0.06	0.06	0.00	0.15	0.02	0.00	0.03	0.02	0.06	0.14	0.00	0.00
Na ₂ O	0.32	0.22	0.22	0.28	0.15	0.07	0.56	0.67	0.74	0.77	0.61	0.50
K ₂ O	15.97	16.00	16.39	15.90	15.94	16.57	15.77	16.00	15.57	15.68	15.81	16.06
Total	97.68	97.42	99.68	97.71	96.04	98.82	99.14	100.45	99.22	99.93	100.43	99.72
Cations (calculated on the basis of 8O)												
Si	3.000	3.000	3.000	3.000	3.000	3.000	3.000	3.000	3.010	3.000	3.020	3.010
Al	1.000	1.000	1.000	0.990	1.000	0.990	1.000	1.000	0.990	1.000	0.990	0.990
Ca	0.000	0.000	0.000	0.010	0.000	0.000	0.000	0.000	0.000	0.000	0.000	0.000
Na	0.020	0.010	0.010	0.020	0.010	0.000	0.030	0.040	0.050	0.050	0.040	0.030
K	0.970	0.970	0.970	0.960	0.980	0.990	0.940	0.940	0.920	0.920	0.930	0.950
Total	4.990	4.990	4.980	4.990	4.990	5.000	4.980	4.980	4.980	4.980	4.970	4.980

Table A.2: Feldspar Analyses (Cont'd)

Sample	A004K	A004K	A004K	A004K	A004K	A004L	A004L	A019A	A003C	A003C	A004K	A019A
Lithology	GPelite	GPelite	GPelite	GPelite	GPelite	Amph	Amph	TPelite	Grnt	Grnt	GPelite	TPelite
No.	139	147	148	149	9	36	48	119	53	62	157	120
Mineral	Kfs	Kfs	Kfs	Kfs	Kfs	Kfs	Kfs	Kfs	Pl	Pl	Pl	Pl
Wt %												
SiO ₂	64.87	65.04	64.71	63.13	64.54	64.39	61.39	64.03	64.75	61.82	62.10	62.96
Al ₂ O ₃	18.40	18.11	17.90	17.75	18.28	18.14	17.32	18.20	21.16	23.03	21.85	22.65
FeO	0.00	0.00	0.00	0.00	0.00	0.05	0.05	0.23	0.01	0.02	0.00	0.26
CaO	0.00	0.00	0.07	0.13	0.02	0.04	0.04	0.07	2.50	4.76	3.77	4.30
Na ₂ O	0.73	1.35	0.65	0.73	0.37	0.64	0.44	0.66	9.18	8.34	8.59	8.44
K ₂ O	15.74	13.73	15.02	15.48	16.43	15.89	15.63	15.82	0.10	0.28	0.09	0.13
Total	99.75	98.25	98.35	97.10	99.70	99.26	94.93	99.17	97.70	98.31	96.40	98.83

Cations (calculated on the basis of 8O)

Si	3.000	3.030	3.020	3.010	3.000	3.000	3.000	2.990	2.930	2.820	2.880	2.850
Al	1.000	0.990	0.990	1.000	1.000	1.000	1.000	1.000	1.210	1.240	1.190	1.210
Ca	0.000	0.000	0.000	0.000	0.000	0.000	0.000	0.000	0.140	0.230	0.190	0.210
Na	0.040	0.080	0.040	0.050	0.020	0.040	0.030	0.040	0.330	0.500	0.520	0.500
K	0.930	0.820	0.900	0.940	0.970	0.950	0.970	0.940	0.040	0.020	0.010	0.010
Total	4.980	4.920	4.950	4.990	4.990	4.990	5.000	4.990	4.650	4.810	4.780	4.790

Table A.3: Phlogopite Analyses

Sample	A003A	A003A	A003A	A003A	A004K	A004K	A004L	A004L	A004L	A019A	A019A	A019A
Lithology	Tmlt	Tmlt	Tmlt	Tmlt	GPelite	GPelite	Amph	Amph	Amph	TPelite	TPelite	TPelite
No.	17	19	20	29	11	136	17	37	41	97	106	105
Mineral	Phl	Phl	Phl	Phl	Phl	Phl	Phl	Phl	Phl	Phl	Phl	Phl
Wt%												
SiO ₂	39.88	40.85	41.28	40.35	40.14	41.63	40.85	40.04	40.98	38.64	38.44	37.84
TiO ₂	1.16	0.72	0.67	0.89	1.24	1.05	0.77	0.81	0.80	0.92	0.95	0.80
Al ₂ O ₃	17.03	15.90	16.33	16.53	16.25	14.91	15.74	16.00	16.04	19.25	19.16	18.67
FeO	3.63	2.72	2.92	3.01	3.34	3.04	2.62	2.58	2.74	3.99	4.03	4.03
MgO	21.29	22.57	22.72	22.05	22.32	22.80	23.65	23.26	23.93	20.18	20.50	20.29
Na ₂ O	0.05	0.07	0.06	0.07	0.04	0.07	0.06	0.03	0.03	0.13	0.09	0.14
K ₂ O	10.58	10.49	10.62	10.06	10.43	10.30	9.59	8.97	9.46	9.91	9.97	9.09
F	1.70	1.09	2.07	1.91	1.20	1.67	0.67	0.72	0.78	0.22	0.32	0.30
O=F	0.72	0.46	0.87	0.80	0.50	0.70	0.28	0.30	0.33	0.09	0.14	0.13
Total	94.20	93.84	95.17	93.57	94.36	94.41	93.52	91.95	94.22	93.17	93.26	91.14
Cations (calculated on the basis of 22O)												
Si	5.620	5.780	5.700	5.680	5.660	5.820	5.780	5.740	5.740	5.560	5.520	5.540
Ti	0.120	0.080	0.060	0.100	0.140	0.120	0.080	0.080	0.080	0.100	0.100	0.080
Al	2.820	2.640	2.660	2.740	2.700	2.460	2.620	2.700	2.660	3.260	3.240	3.220
Fe	0.420	0.320	0.340	0.360	0.400	0.360	0.320	0.300	0.320	0.480	0.480	0.500
Mg	4.480	4.760	4.680	4.620	4.700	4.760	4.980	4.980	5.000	4.320	4.380	4.440
Na	0.000	0.020	0.020	0.020	0.000	0.020	0.020	0.000	0.000	0.020	0.020	0.020
K	1.900	1.900	1.880	1.800	1.880	1.840	1.740	1.640	1.700	1.820	1.820	1.700
F	0.760	0.480	0.900	0.840	0.540	0.740	0.300	0.320	0.340	0.100	0.140	0.140
Total	16.120	15.980	16.240	16.160	16.020	16.120	15.840	15.760	15.840	15.660	15.700	15.640
Mg#	0.914	0.937	0.932	0.928	0.922	0.930	0.940	0.943	0.940	0.900	0.901	0.899

Table A.3: Phlogopite Analyses (Cont'd)								Table A.3: Chlorite Analyses				
Sample	A019A	A019A	A019A	A019A	A019A	A019A	A019A	A003C	A003C	A003C	A003C	A003C
Lithology	TPelite	TPelite	TPelite	TPelite	TPelite	TPelite	TPelite	Grnt	Grnt	Grnt	Grnt	Grnt
No.	112	113	114	116	117	91	92	64	65	76	81	71
Mineral	Phl	Phl	Phl	Phl	Phl	Phl	Phl	Chl	Chl	Chl	Chl	Chl
Wt %												
SiO ₂	38.96	37.60	36.71	39.50	38.38	38.91	38.50	29.71	30.92	30.98	30.24	30.11
TiO ₂	0.89	0.81	0.78	1.03	1.01	0.92	0.97	0.00	0.00	0.00	0.02	0.00
Al ₂ O ₃	19.17	18.70	19.16	19.50	18.94	19.45	18.99	18.22	17.87	17.37	17.52	18.00
FeO	4.19	4.11	5.01	4.21	4.08	4.03	4.04	9.68	9.09	9.23	10.85	10.03
MgO	20.73	20.43	22.19	20.92	19.95	20.39	20.64	27.28	28.41	28.56	27.20	26.93
Na ₂ O	0.10	0.24	0.13	0.13	0.19	0.08	0.13	0.00	0.00	0.00	0.00	0.00
K ₂ O	9.78	8.93	7.70	10.00	9.92	10.07	9.21	0.00	0.02	0.02	0.03	0.00
F	0.26	0.28	0.28	0.31	0.25	0.28	0.27	0.24	0.22	0.27	0.27	0.24
O=F	0.11	0.12	0.12	0.13	0.10	0.12	0.11	0.10	0.09	0.11	0.11	0.10
Total	94.08	91.20	91.92	95.59	92.75	94.02	92.63	85.03	86.47	86.31	86.18	85.24
Cations (calculated on the basis of 22O)								Cations (calculated on the basis of 18 O)				
Si	5.540	5.500	5.340	5.540	5.560	5.540	5.540	3.800	3.870	3.890	3.840	3.840
Ti	0.100	0.080	0.080	0.100	0.100	0.100	0.100	0.000	0.000	0.000	0.000	0.000
Al	3.220	3.220	3.280	3.220	3.220	3.260	3.220	2.740	2.640	2.570	2.620	2.710
Fe	0.500	0.500	0.600	0.500	0.500	0.480	0.480	1.030	0.950	0.970	1.150	1.070
Mg	4.400	4.460	4.800	4.360	4.300	4.340	4.440	5.200	5.300	5.340	5.150	5.120
Na	0.020	0.040	0.020	0.020	0.040	0.020	0.020	0.000	0.000	0.000	0.000	0.000
K	1.780	1.660	1.420	1.780	1.840	1.840	1.700	0.000	0.000	0.000	0.000	0.000
F	0.120	0.140	0.120	0.140	0.120	0.120	0.120	0.100	0.090	0.110	0.110	0.100
Total	15.680	15.600	15.660	15.660	15.680	15.700	15.620	12.880	12.860	12.880	12.900	12.850
Mg#	0.898	0.899	0.889	0.897	0.896	0.900	0.902	0.835	0.848	0.846	0.817	0.827

Table A.4: Muscovite Analyses

Sample	A003C	A004K	A004K	A004K	A004K	A004K	A004K	A004K	A004K	A004K	A004K	A004K
Lithology	Grnt	GPelite	GPelite	GPelite	GPelite	GPelite	GPelite	GPelite	GPelite	GPelite	GPelite	GPelite
No.	72	10	16	120	121	123	5	6	133	134	129	7
Mineral	Ms	Ms	Ms	Ms	Ms	Ms	Ms	Ms	Ms	Ms	Ms	Ms
Wt %												
SiO ₂	46.29	46.31	46.77	47.88	47.60	47.70	48.25	46.01	47.35	47.66	47.90	46.34
Al ₂ O ₃	35.68	36.07	36.07	37.12	36.48	36.82	36.21	35.98	35.67	35.27	35.43	37.37
FeO	0.53	0.19	0.18	0.22	0.19	0.23	0.22	0.18	0.19	0.14	0.13	0.12
MgO	0.02	0.70	0.90	0.68	0.84	0.64	0.90	0.67	0.94	0.97	0.96	0.26
Na ₂ O	0.01	0.21	0.22	0.18	0.21	0.19	0.17	0.19	0.16	0.16	0.22	0.25
K ₂ O	11.32	10.44	11.11	10.79	11.12	11.09	10.79	10.77	10.95	10.91	10.82	10.83
Total	93.87	94.10	95.38	97.17	96.63	96.92	96.72	93.99	95.38	95.25	95.55	95.35

Cations (calculated on the basis of 22O)												
Si	6.230	6.190	6.180	6.190	6.200	6.200	6.270	6.170	6.250	6.300	6.300	6.120
Al	5.660	5.680	5.620	5.660	5.600	5.640	5.540	5.690	5.550	5.490	5.490	5.820
Fe	0.060	0.020	0.020	0.020	0.020	0.020	0.020	0.020	0.020	0.010	0.010	0.010
Mg	0.000	0.140	0.180	0.130	0.160	0.120	0.170	0.130	0.190	0.190	0.190	0.050
Na	0.000	0.040	0.040	0.030	0.040	0.030	0.030	0.030	0.030	0.030	0.040	0.040
K	1.940	1.780	1.880	1.780	1.850	1.840	1.790	1.840	1.840	1.840	1.820	1.830
Total	13.900	13.870	13.950	13.860	13.930	13.900	13.850	13.910	13.930	13.870	13.900	13.890

Table A.5: Pumpellyite Analyses

Sample	A003C	A003C	A003C
Lithology	Grnt	Grnt	Grnt
No.	66	73	78
Mineral	pmp	pmp	pmp
Wt%			
SiO ₂	38.02	38.04	37.97
Al ₂ O ₃	24.83	24.59	25.05
FeO	0.98	0.59	0.73
MgO	4.70	5.21	4.66
CaO	23.44	23.34	22.93
F	0.47	0.81	0.34
O=F	0.20	0.34	0.14
Total	92.13	91.91	91.58

Cations (calculated on the basis of 14 O)

Si	3.460	3.460	3.470
Al	2.670	2.630	2.700
Fe	0.070	0.050	0.060
Mg	0.640	0.710	0.640
Ca	2.290	2.270	2.250
F	0.140	0.230	0.100
Total	9.270	9.340	9.230
Mg#	0.901	0.934	0.914

Table A.6: Pyrite Analyses

Sample	A003-A	A003-A	A003-A	A003-A	A003-A	A003-A	A003-A	A003-C	A003-C	A003-C	A003-C	A003-C	A003-C
Lithology	Tmlt	Tmlt	Tmlt	Tmlt	Tmlt	Tmlt	Tmlt	Grnt	Grnt	Grnt	Grnt	Grnt	Grnt
No.	226	213	236	230	211	226	232	179	178	194	205	191	198
Mineral	Pyrite	Pyrite	Pyrite	Pyrite	Pyrite	Pyrite	Pyrite	Pyrite	Pyrite	Pyrite	Pyrite	Pyrite	Pyrite
Wt%													
S	51.98	51.01	51.26	49.51	50.50	46.45	48.74	50.32	50.74	50.42	50.02	49.92	49.74
Fe	45.71	45.21	43.71	45.49	44.09	44.46	41.28	44.97	44.54	44.54	44.42	44.27	44.43
Co	0.28	0.15	0.17	0.20	0.17	0.10	0.15	0.28	0.26	0.21	0.24	0.23	0.18
Ni	0.32	0.28	0.22	0.14	0.15	0.05	0.08	0.16	0.14	0.10	0.13	0.16	0.12
Pb	0.15	0.04	0.11	0.04	0.00	0.11	0.15	0.10	0.10	0.14	0.09	0.07	0.06
Cu	0.00	0.00	0.00	0.00	0.00	0.12	0.00	0.00	0.00	0.00	0.00	0.00	0.00
Total	98.49	96.70	95.53	95.43	94.92	91.30	90.48	95.82	95.78	95.40	94.94	94.75	94.55
Cations (Calculated on the basis of 3 ions)													
S	1.980	1.980	2.010	1.960	1.990	1.930	2.010	1.980	1.990	1.990	1.980	1.980	1.980
Fe	1.000	1.010	0.980	1.030	1.000	1.060	0.980	1.010	1.000	1.010	1.010	1.010	1.010
Co	0.010	0.000	0.000	0.000	0.000	0.000	0.000	0.010	0.010	0.000	0.010	0.010	0.000
Ni	0.010	0.010	0.000	0.000	0.000	0.000	0.000	0.000	0.000	0.000	0.000	0.000	0.000
Pb	0.000	0.000	0.000	0.000	0.000	0.000	0.000	0.000	0.000	0.000	0.000	0.000	0.000
Cu	0.000	0.000	0.000	0.000	0.000	0.000	0.000	0.000	0.000	0.000	0.000	0.000	0.000
Total	3.000	3.000	3.000	3.000	3.000	3.000	3.000	3.000	3.000	3.000	3.000	3.000	3.000

Table A.6: Pyrite Analyses Cont'd

Sample	A003-C	A003-C	A003-C
Lithology	Grnt	Grnt	Grnt
No.	195	180	187
Mineral	Pyrite	Pyrite	Pyrite
Wt%			
S	49.62	48.35	48.05
Fe	44.28	45.24	44.51
Co	0.28	0.30	0.24
Ni	0.15	0.11	0.09
Pb	0.10	0.11	0.07
Cu	0.00	0.00	0.00
Total	94.51	94.10	92.96

Cations (Calculated on the basis of 3 ions)

S	1.980	1.950	1.950
Fe	1.010	1.050	1.040
Co	0.010	0.010	0.010
Ni	0.000	0.000	0.000
Pb	0.000	0.000	0.000
Cu	0.000	0.000	0.000
Total	3.000	3.000	3.000

Table A.7: Pyrrhotite Analyses

Sample	A003-A	A003-A	A003-A	A003-A	A003-A	A003-A	A003-A	A003-A	A003-A	A003-A	A003-A	A003-A
Lithology	Tmlt	Tmlt	Tmlt	Tmlt	Tmlt	Tmlt	Tmlt	Tmlt	Tmlt	Tmlt	Tmlt	Tmlt
No.	233	223	189	231	212	221	238	216	220	217	214	235
Mineral	Pyrrhotite	Pyrrhotite	Pyrrhotite	Pyrrhotite	Pyrrhotite	Pyrrhotite	Pyrrhotite	Pyrrhotite	Pyrrhotite	Pyrrhotite	Pyrrhotite	Pyrrhotite
Wt%												
S	38.76	38.86	38.72	38.66	38.20	38.52	38.50	38.09	38.54	37.85	37.94	37.63
Fe	59.53	59.32	59.37	59.34	59.76	59.37	59.25	59.70	59.28	59.74	59.54	59.42
Co	0.26	0.21	0.27	0.18	0.18	0.21	0.22	0.19	0.21	0.18	0.21	0.18
Ni	0.09	0.12	0.15	0.07	0.22	0.11	0.06	0.17	0.12	0.17	0.14	0.13
Pb	0.06	0.05	0.03	0.13	0.02	0.07	0.13	0.07	0.07	0.11	0.05	0.01
Cu	0.00	0.00	0.00	0.00	0.00	0.00	0.00	0.00	0.00	0.00	0.01	0.00
Total	98.73	98.59	98.58	98.46	98.43	98.36	98.29	98.29	98.24	98.13	97.99	97.46

Cations (Calculated on the basis of 1 ion)

S	0.530	0.530	0.530	0.530	0.530	0.530	0.530	0.520	0.530	0.520	0.520	0.520
Fe	0.470	0.470	0.470	0.470	0.470	0.470	0.470	0.470	0.470	0.470	0.470	0.470
Co	0.000	0.000	0.000	0.000	0.000	0.000	0.000	0.000	0.000	0.000	0.000	0.000
Ni	0.000	0.000	0.000	0.000	0.000	0.000	0.000	0.000	0.000	0.000	0.000	0.000
Pb	0.000	0.000	0.000	0.000	0.000	0.000	0.000	0.000	0.000	0.000	0.000	0.000
Cu	0.000	0.000	0.000	0.000	0.000	0.000	0.000	0.000	0.000	0.000	0.000	0.000
Total	1.000	1.000	1.000	1.000	1.000	1.000	1.000	1.000	1.000	1.000	1.000	1.000

Table A.7: Pyrrhotite Analyses Cont'd

Sample	A003-C	A003-C	A003-C	A003-C	A003-C	A003-C	A003-C	A003-C	A003-C	A003-C	A003-C	A003-C	A003-C
Lithology	Grnt	Grnt	Grnt	Grnt	Grnt	Grnt	Grnt	Grnt	Grnt	Grnt	Grnt	Grnt	Grnt
No.	209	207	167	175	171	168	181	188	162	160	210	164	161
Mineral	Pyrrhortite	Pyrrhortite	Pyrrhotite	Pyrrhotite	Pyrrhotite	Pyrrhotite	Pyrrhotite	Pyrrhotite	Pyrrhotite	Pyrrhotite	Pyrrhotite	Pyrrhotite	Pyrrhotite
Wt%													
S	38.16	37.63	38.98	38.73	38.75	39.11	38.79	38.90	38.26	38.47	38.70	38.62	38.02
Fe	56.65	56.38	59.60	59.52	59.53	59.10	59.28	59.25	60.00	59.80	59.28	59.45	59.99
Co	0.25	0.21	0.22	0.27	0.24	0.21	0.26	0.11	0.19	0.13	0.28	0.25	0.17
Ni	0.13	0.10	0.10	0.13	0.11	0.15	0.13	0.16	0.05	0.00	0.14	0.09	0.12
Pb	0.00	0.05	0.07	0.02	0.01	0.02	0.02	0.01	0.00	0.02	0.00	0.00	0.06
Cu	0.00	0.00	0.00	0.00	0.00	0.00	0.00	0.00	0.00	0.00	0.00	0.00	0.00
Total	95.27	94.41	98.98	98.79	98.67	98.62	98.58	98.56	98.55	98.49	98.46	98.44	98.38
Cations (Calculated on the basis of 1 ion)													
S	0.540	0.540	0.530	0.530	0.530	0.530	0.530	0.530	0.530	0.530	0.530	0.530	0.520
Fe	0.460	0.460	0.470	0.470	0.470	0.460	0.470	0.470	0.470	0.470	0.470	0.470	0.470
Co	0.000	0.000	0.000	0.000	0.000	0.000	0.000	0.000	0.000	0.000	0.000	0.000	0.000
Ni	0.000	0.000	0.000	0.000	0.000	0.000	0.000	0.000	0.000	0.000	0.000	0.000	0.000
Pb	0.000	0.000	0.000	0.000	0.000	0.000	0.000	0.000	0.000	0.000	0.000	0.000	0.000
Cu	0.000	0.000	0.000	0.000	0.000	0.000	0.000	0.000	0.000	0.000	0.000	0.000	0.000
Total	1.000	1.000	1.000	1.000	1.000	1.000	1.000	1.000	1.000	1.000	1.000	1.000	1.000

Table A.7: Pyrrhotite Analyses Cont'd

Sample	A003-C	A003-C	A003-C	A003-C	A003-C	A003-C	A003-C	A003-C	A003-C	A003-C	A003-C	A003-C
Lithology	Grnt	Grnt	Grnt	Grnt	Grnt	Grnt	Grnt	Grnt	Grnt	Grnt	Grnt	Grnt
No.	208	197	204	165	176	163	170	196	206	202	166	174
Mineral	Pyrrhotite	Pyrrhotite	Pyrrhotite	Pyrrhotite	Pyrrhotite	Pyrrhotite	Pyrrhotite	Pyrrhotite	Pyrrhotite	Pyrrhotite	Pyrrhotite	Pyrrhotite
Wt%												
S	38.79	38.80	38.56	38.89	38.51	38.64	38.34	38.39	38.58	38.35	38.55	38.52
Fe	59.17	58.99	59.17	58.85	59.23	59.21	59.25	59.20	59.00	59.15	59.00	58.84
Co	0.21	0.25	0.26	0.21	0.25	0.18	0.22	0.26	0.27	0.29	0.15	0.18
Ni	0.14	0.13	0.12	0.15	0.15	0.03	0.14	0.12	0.14	0.10	0.12	0.17
Pb	0.00	0.05	0.01	0.02	0.01	0.00	0.09	0.03	0.00	0.05	0.07	0.01
Cu	0.00	0.00	0.00	0.00	0.00	0.00	0.00	0.00	0.00	0.00	0.00	0.00
Total	98.33	98.27	98.21	98.18	98.16	98.11	98.07	98.04	98.01	97.95	97.88	97.80

Cations (Calculated on the basis of 1 ion)

S	0.530	0.530	0.530	0.530	0.530	0.530	0.530	0.530	0.530	0.530	0.530	0.530
Fe	0.470	0.460	0.470	0.460	0.470	0.470	0.470	0.470	0.470	0.470	0.470	0.470
Co	0.000	0.000	0.000	0.000	0.000	0.000	0.000	0.000	0.000	0.000	0.000	0.000
Ni	0.000	0.000	0.000	0.000	0.000	0.000	0.000	0.000	0.000	0.000	0.000	0.000
Pb	0.000	0.000	0.000	0.000	0.000	0.000	0.000	0.000	0.000	0.000	0.000	0.000
Cu	0.000	0.000	0.000	0.000	0.000	0.000	0.000	0.000	0.000	0.000	0.000	0.000
Total	1.000	1.000	1.000	1.000	1.000	1.000	1.000	1.000	1.000	1.000	1.000	1.000

Table A.8: Rutile Analysis

Sample	A004-K	A004-K	A004-K	A004-K	A004-K	A004-K	A004-K	A004-K	A004-K
Lithology	GPelite	GPelite	GPelite	GPelite	GPelite	GPelite	GPelite	GPelite	GPelite
No.	243	244	245	246	247	248	249	250	251
Mineral	Rutile	Rutile	Rutile	Rutile	Rutile	Rutile	Rutile	Rutile	Rutile
Wt%									
SiO ₂	0.00	0.02	0.00	0.00	0.00	0.00	0.00	0.00	0.00
Al ₂ O ₃	0.00	0.00	0.00	0.00	0.00	0.00	0.00	0.00	0.00
TiO ₂	92.55	92.60	92.25	92.56	92.41	92.91	92.28	92.69	91.67
FeO	0.02	0.00	0.00	0.00	0.03	0.01	0.00	0.01	0.01
CaO	0.01	0.00	0.04	0.01	0.01	0.00	0.00	0.00	0.00
Cr ₂ O ₃	0.24	0.25	0.25	0.26	0.28	0.25	0.30	0.29	0.29
Total	95.48	95.48	95.17	95.47	95.33	95.82	95.34	95.71	94.80

Cations (Calculated on the basis of 2O)

Si	0.000	0.000	0.000	0.000	0.000	0.000	0.000	0.000	0.000
Al	0.000	0.000	0.000	0.000	0.000	0.000	0.000	0.000	0.000
Ti	1.000	1.000	1.000	1.000	1.000	1.000	1.000	1.000	1.000
Fe	0.000	0.000	0.000	0.000	0.000	0.000	0.000	0.000	0.000
Ca	0.000	0.000	0.000	0.000	0.000	0.000	0.000	0.000	0.000
Cr	0.000	0.000	0.000	0.000	0.000	0.000	0.000	0.000	0.000
Total	1.000	1.000	1.000	1.000	1.000	1.000	1.000	1.000	1.000

Table A.9: Tourmaline Analyses

Sample	A003A	A003A	A003A	A003A	A003A	A003A	A004K	A004K	A004K	A004K	A004K	A004K
Lithology	Tmlt	Tmlt	Tmlt	Tmlt	Tmlt	Tmlt	GPelite	GPelite	GPelite	GPelite	GPelite	GPelite
No.							127	130	122	124	126	142
Mineral	Tour	Tour	Tour	Tour	Tour	Tour	Tour	Tour	Tour	Tour	Tour	Tour
Wt %												
SiO ₂	37.34	37.38	37.44	37.49	37.70	37.33	39.51	37.33	37.56	36.83	38.92	37.06

Table A.9: Tourmaline Analyses (Cont'd)

Sample	A004K	A004K	A004K	A004K	A004K	A004K	A004K	A004K	A004K	A004K	A004K	A004K
Lithology	GPelite	GPelite	GPelite	GPelite	GPelite	GPelite	GPelite	GPelite	GPelite	GPelite	GPelite	GPelite
No.	144	145	150	151	152	153	154	155	156	158	128	4
Mineral	Tour	Tour	Tour	Tour	Tour	Tour	Tour	Tour	Tour	Tour	Tour	Tour
Wt%												
SiO ₂	37.33	36.54	35.69	36.37	36.61	35.75	36.77	36.39	36.13	35.94	36.87	37.60
TiO ₂	0.00	0.08	0.31	0.15	0.00	0.00	0.00	0.00	0.00	0.00	0.00	0.00
B ₂ O ₃	10.50	10.50	10.50	10.50	10.50	10.50	10.50	10.50	10.50	10.50	10.50	10.50
Al ₂ O ₃	33.67	33.33	33.17	32.45	34.70	33.63	35.00	33.65	33.50	32.70	34.81	34.75
FeO	0.53	0.55	4.77	0.49	0.50	0.65	0.63	0.83	1.06	1.06	0.73	0.71
MgO	9.50	9.24	6.57	9.82	8.62	9.48	8.39	9.12	9.28	9.49	9.05	8.91
CaO	0.66	0.72	0.18	1.32	0.55	0.81	0.56	0.79	1.08	0.90	0.64	0.34
Na ₂ O	2.05	1.98	2.21	1.74	2.05	2.11	2.04	2.05	2.00	2.07	1.98	1.90
K ₂ O	0.01	0.03	0.05	0.05	0.02	0.02	0.02	0.03	0.03	0.02	0.04	0.04
F	0.32	0.28	0.27	0.41	0.26	0.35	0.20	0.38	0.37	0.42	0.23	0.24
O=F	0.13	0.12	0.11	0.17	0.11	0.15	0.08	0.16	0.15	0.18	0.10	0.00
Total	94.57	93.25	93.72	93.30	93.81	93.30	94.11	93.74	93.95	93.10	94.85	94.99
Cations (calculated on the basis of 29O)												
Si	6.060	6.020	5.960	6.000	5.990	5.900	6.000	5.980	5.940	5.960	5.980	6.060
Ti	0.000	0.010	0.040	0.020	0.000	0.000	0.000	0.000	0.000	0.000	0.000	0.000
B	2.940	2.990	3.030	2.990	2.960	2.990	2.950	2.980	2.980	3.010	2.940	2.920
Al	6.450	6.470	6.530	6.310	6.690	6.550	6.720	6.510	6.490	6.390	6.650	6.600
Fe	0.070	0.080	0.670	0.070	0.070	0.090	0.090	0.110	0.150	0.150	0.100	0.120
Mg	2.300	2.270	1.640	2.420	2.100	2.330	2.040	2.230	2.270	2.350	2.190	2.140
Ca	0.110	0.130	0.030	0.230	0.100	0.140	0.100	0.140	0.190	0.160	0.110	0.060
Na	0.430	0.430	0.480	0.370	0.440	0.460	0.430	0.440	0.430	0.450	0.420	0.400
K	0.000	0.010	0.010	0.010	0.000	0.000	0.000	0.010	0.010	0.000	0.010	0.010
F	0.160	0.150	0.140	0.210	0.130	0.180	0.100	0.200	0.190	0.220	0.120	0.000
Total	18.540	18.530	18.530	18.630	18.480	18.650	18.430	18.600	18.640	18.680	18.500	18.340

Table A.9: Tourmaline Analyses (Cont'd)

Sample	A004L	A004L	A004L	A004L	A004L	A004L	A004L	A004L	A004L	A004L	A004L	A004L
Lithology	Amph	Amph	Amph	Amph	Amph	Amph	Amph	Amph	Amph	Amph	Amph	Amph
No.	45	1	11	14	16	18	2	24	3	33	6	5
Mineral	Tour	Tour	Tour	Tour	Tour	Tour	Tour	Tour	Tour	Tour	Tour	Tour
Wt %												
SiO ₂	35.91	36.39	36.65	36.63	36.59	36.70	36.82	35.94	35.51	36.30	35.72	36.33
TiO ₂	0.37	1.10	0.71	1.11	0.82	0.94	0.83	1.09	0.85	0.49	0.87	1.16
B ₂ O ₃	10.50	10.50	10.50	10.50	10.50	10.50	10.50	10.50	10.50	10.50	10.50	10.50
Al ₂ O ₃	29.35	28.52	29.65	28.86	29.46	29.26	29.53	28.29	29.96	32.06	30.38	28.50
FeO	7.61	0.85	0.92	0.88	0.89	0.90	0.89	0.90	7.78	5.40	8.03	0.88
MgO	7.57	12.07	11.79	11.86	11.74	11.85	11.88	11.83	6.33	7.20	6.02	12.00
CaO	2.05	3.01	2.37	2.99	2.63	2.84	2.70	2.98	0.45	0.54	0.43	2.96
Na ₂ O	1.85	1.22	1.58	1.30	1.57	1.44	1.52	1.26	2.55	2.30	2.56	1.33
K ₂ O	0.05	0.14	0.17	0.11	0.13	0.09	0.14	0.08	0.14	0.06	0.10	0.28
F	0.21	0.33	0.39	0.35	0.36	0.31	0.39	0.30	0.14	0.11	0.14	0.37
O=F	0.09	0.14	0.16	0.15	0.15	0.13	0.16	0.13	0.06	0.04	0.06	0.15
Total	95.47	94.13	94.73	94.59	94.69	94.83	95.20	93.17	94.21	94.96	94.75	94.31
Cations (calculated on the basis of 29O)												
Si	6.020	6.010	6.010	6.020	6.010	6.020	6.020	6.000	6.020	6.020	6.030	6.000
Ti	0.050	0.140	0.090	0.140	0.100	0.120	0.100	0.140	0.110	0.060	0.110	0.140
B	3.030	2.990	2.960	2.970	2.970	2.960	2.950	3.020	3.070	3.000	3.060	2.980
Al	5.800	5.560	5.730	5.590	5.700	5.660	5.690	5.560	5.990	6.270	6.040	5.550
Fe	1.070	0.120	0.130	0.120	0.120	0.120	0.120	0.130	1.100	0.750	1.130	0.120
Mg	1.890	2.970	2.880	2.910	2.880	2.900	2.900	2.940	1.600	1.780	1.520	2.960
Ca	0.370	0.530	0.420	0.530	0.460	0.500	0.470	0.530	0.080	0.100	0.080	0.520
Na	0.410	0.260	0.340	0.280	0.340	0.310	0.330	0.280	0.570	0.500	0.560	0.290
K	0.010	0.030	0.040	0.020	0.030	0.020	0.030	0.020	0.030	0.010	0.020	0.060
F	0.110	0.170	0.200	0.180	0.190	0.160	0.200	0.160	0.080	0.060	0.070	0.190
Total	18.770	18.800	18.820	18.780	18.810	18.780	18.820	18.780	18.670	18.560	18.640	18.840
Mg#	0.64	0.96	0.96	0.96	0.96	0.96	0.96	0.96	0.59	0.70	0.57	0.96

Table A.9: Tourmaline Analyses (Cont'd)

Sample	A004L	A004L	A004L	A004L	A004L	A004L	A004L	A019A	A019A	A019A	A019A	A019A
Lithology	Amph	Amph	Amph	Amph	Amph	Amph	Amph	TPelite	TPelite	TPelite	TPelite	TPelite
No.	34	38	39	10	40	43	44	101	95	96	99	94
Mineral	Tour	Tour	Tour	Tour	Tour	Tour	Tour	Tour	Tour	Tour	Tour	Tour
Wt %												
SiO ₂	36.44	36.40	37.34	36.70	36.58	36.52	36.99	36.63	36.48	37.03	35.88	36.39
TiO ₂	1.26	1.11	0.66	0.84	0.78	0.97	0.70	0.40	0.40	0.35	0.30	0.71
B ₂ O ₃	10.50	10.50	10.50	10.50	10.50	10.50	10.50	10.50	10.50	10.50	10.50	10.50
Al ₂ O ₃	28.99	28.64	30.29	29.45	29.14	29.03	29.59	32.97	32.98	33.55	32.69	32.01
FeO	0.99	0.98	0.61	0.89	0.91	0.88	0.97	0.70	0.60	0.61	0.56	4.32
MgO	11.94	12.05	11.64	11.74	12.07	11.90	11.79	9.61	9.61	9.68	9.33	7.38
CaO	3.08	2.99	2.27	2.71	3.02	2.89	2.40	0.91	0.86	0.97	0.85	0.19
Na ₂ O	1.27	1.31	1.64	1.46	1.29	1.38	1.61	1.99	1.95	2.02	1.94	2.16
K ₂ O	0.09	0.08	0.06	0.18	0.08	0.08	0.08	0.05	0.04	0.05	0.05	0.04
F	0.26	0.32	0.26	0.41	0.28	0.35	0.33	0.10	0.08	0.06	0.08	0.05
O=F	0.11	0.13	0.11	0.17	0.12	0.15	0.14	0.04	0.03	0.03	0.03	0.02
Total	94.82	94.38	95.27	94.88	94.65	94.50	94.96	93.86	93.50	94.82	92.18	93.75
Cations (calculated on the basis of 29O)												
Si	5.990	6.000	6.070	6.010	6.010	6.010	6.050	6.010	6.000	6.020	5.980	6.070
Ti	0.160	0.140	0.080	0.100	0.100	0.120	0.090	0.050	0.050	0.040	0.040	0.090
B	2.970	2.980	2.940	2.960	2.970	2.970	2.960	2.970	2.980	2.940	3.020	3.020
Al	5.610	5.570	5.810	5.690	5.640	5.630	5.710	6.380	6.390	6.420	6.420	6.290
Fe	0.140	0.130	0.080	0.120	0.130	0.120	0.130	0.100	0.080	0.080	0.080	0.600
Mg	2.920	2.960	2.820	2.870	2.960	2.920	2.880	2.350	2.360	2.340	2.320	1.830
Ca	0.540	0.530	0.400	0.480	0.530	0.510	0.420	0.160	0.150	0.170	0.150	0.030
Na	0.270	0.280	0.350	0.310	0.280	0.300	0.340	0.430	0.420	0.430	0.420	0.470
K	0.020	0.020	0.010	0.040	0.020	0.020	0.020	0.010	0.010	0.010	0.010	0.010
F	0.140	0.170	0.140	0.210	0.150	0.180	0.170	0.050	0.040	0.030	0.040	0.030
Total	18.770	18.800	18.710	18.830	18.790	18.790	18.780	18.510	18.490	18.490	18.490	18.440
Mg#	0.95	0.96	0.97	0.96	0.96	0.96	0.96	0.96	0.97	0.97	0.97	0.75

Table A.9: Tourmaline Analyses (Cont'd)

Sample	A019A	A019A	A019A	A019A	A019A	A019A	A019A	A019A	A019A	A019A	A019A
Lithology	TPelite	TPelite	TPelite	TPelite	TPelite	TPelite	TPelite	TPelite	TPelite	TPelite	TPelite
No.	104	106	107	108	109	110	111	118	89	90	93
Mineral	Tour	Tour	Tour	Tour	Tour	Tour	Tour	Tour	Tour	Tour	Tour
Wt%											
SiO ₂	36.91	36.29	36.77	37.00	37.06	36.86	37.07	37.25	36.28	36.79	35.96
TiO ₂	0.43	0.47	0.39	0.46	0.43	0.42	0.39	0.39	0.36	0.44	0.39
B ₂ O ₃	10.50	10.50	10.50	10.50	10.50	10.50	10.50	10.50	10.50	10.50	10.50
Al ₂ O ₃	33.05	32.47	33.17	33.24	33.66	32.05	33.94	33.30	33.38	31.21	32.46
FeO	0.62	0.70	0.58	0.62	0.67	3.76	0.60	0.77	0.55	1.10	0.65
MgO	9.60	9.49	9.55	9.64	9.57	8.39	9.56	9.90	9.27	10.20	9.27
CaO	0.93	0.88	0.95	0.84	1.14	1.16	0.93	0.92	0.94	1.94	1.05
Na ₂ O	1.88	1.82	1.92	2.00	1.85	1.95	1.92	1.94	1.94	1.43	1.86
K ₂ O	0.05	0.25	0.06	0.04	0.05	0.05	0.07	0.06	0.05	0.05	0.06
F	0.07	0.14	0.06	0.09	0.09	0.10	0.11	0.13	0.07	0.16	0.08
O=F	0.03	0.06	0.03	0.04	0.04	0.04	0.04	0.05	0.03	0.07	0.04
Total	94.04	93.01	93.95	94.43	95.02	95.24	95.09	95.16	93.34	93.82	92.28
Cations (calculated on the basis of 29O)											
Si	6.030	6.000	6.020	6.030	6.000	6.050	6.000	6.030	5.970	6.060	5.990
Ti	0.050	0.060	0.050	0.060	0.050	0.050	0.050	0.050	0.040	0.050	0.050
B	2.960	2.990	2.960	2.950	2.930	2.970	2.930	2.930	2.980	2.980	3.020
Al	6.370	6.330	6.400	6.380	6.430	6.200	6.470	6.350	6.480	6.060	6.370
Fe	0.080	0.100	0.080	0.080	0.090	0.520	0.080	0.100	0.080	0.150	0.090
Mg	2.340	2.340	2.330	2.340	2.310	2.050	2.310	2.390	2.280	2.510	2.300
Ca	0.160	0.160	0.170	0.150	0.200	0.200	0.160	0.160	0.170	0.340	0.190
Na	0.400	0.390	0.410	0.430	0.390	0.420	0.410	0.410	0.420	0.310	0.400
K	0.010	0.050	0.010	0.010	0.010	0.010	0.010	0.010	0.010	0.010	0.010
F	0.040	0.070	0.030	0.050	0.050	0.050	0.050	0.070	0.040	0.080	0.040
Total	18.470	18.530	18.470	18.480	18.480	18.550	18.490	18.520	18.470	18.560	18.490
Mg#	0.97	0.96	0.97	0.97	0.96	0.80	0.97	0.96	0.97	0.94	0.96

Table A.10: Tremolite Analyses

Sample	A003C	A003C	A004L	A004L	A004L	A004L	A004L	A004L	A004L	A004L
Lithology	Grnt	Grnt	Amph	Amph	Amph	Amph	Amph	Amph	Amph	Amph
No.	80	83	13	19	20	23	26	35	46	8
Mineral	Tremolite	Tremolite	Tremolite	Tremolite	Tremolite	Tremolite	Tremolite	Tremolite	Tremolite	Tremolite
Wt%										
SiO ₂	56.72	55.98	56.33	56.47	55.05	55.70	55.86	56.71	55.36	56.41
Al ₂ O ₃	0.64	0.79	1.72	1.89	2.54	1.82	2.00	1.75	1.70	1.82
FeO	5.05	6.26	1.48	1.60	1.75	1.72	1.65	1.65	1.65	1.60
MgO	20.95	19.96	22.78	22.58	22.23	22.78	22.69	22.83	22.67	22.76
CaO	13.36	13.31	13.58	13.49	13.38	13.52	13.41	13.69	13.31	13.49
F	0.19	0.22	0.17	0.17	0.20	0.15	0.17	0.12	0.20	0.24
Total	97.08	96.94	96.47	96.59	95.81	96.18	96.21	97.25	95.21	96.78

Cations (calculated on the basis of 24 O)

Si	8.240	8.200	8.120	8.130	8.010	8.070	8.080	8.130	8.090	8.100
Al	0.110	0.140	0.290	0.320	0.430	0.310	0.340	0.300	0.290	0.310
Fe	0.610	0.770	0.180	0.190	0.210	0.210	0.200	0.200	0.200	0.190
Mg	4.540	4.360	4.900	4.840	4.820	4.920	4.900	4.880	4.940	4.870
Ca	2.080	2.090	2.100	2.080	2.090	2.100	2.080	2.100	2.080	2.080
F	0.090	0.100	0.080	0.080	0.090	0.070	0.080	0.050	0.090	0.080
Total	15.720	15.750	15.750	15.730	15.800	15.780	15.770	15.740	15.780	15.770
Mg#	0.882	0.850	0.965	0.962	0.958	0.959	0.961	0.961	0.961	0.962

Table A.11: Titanite Analysis

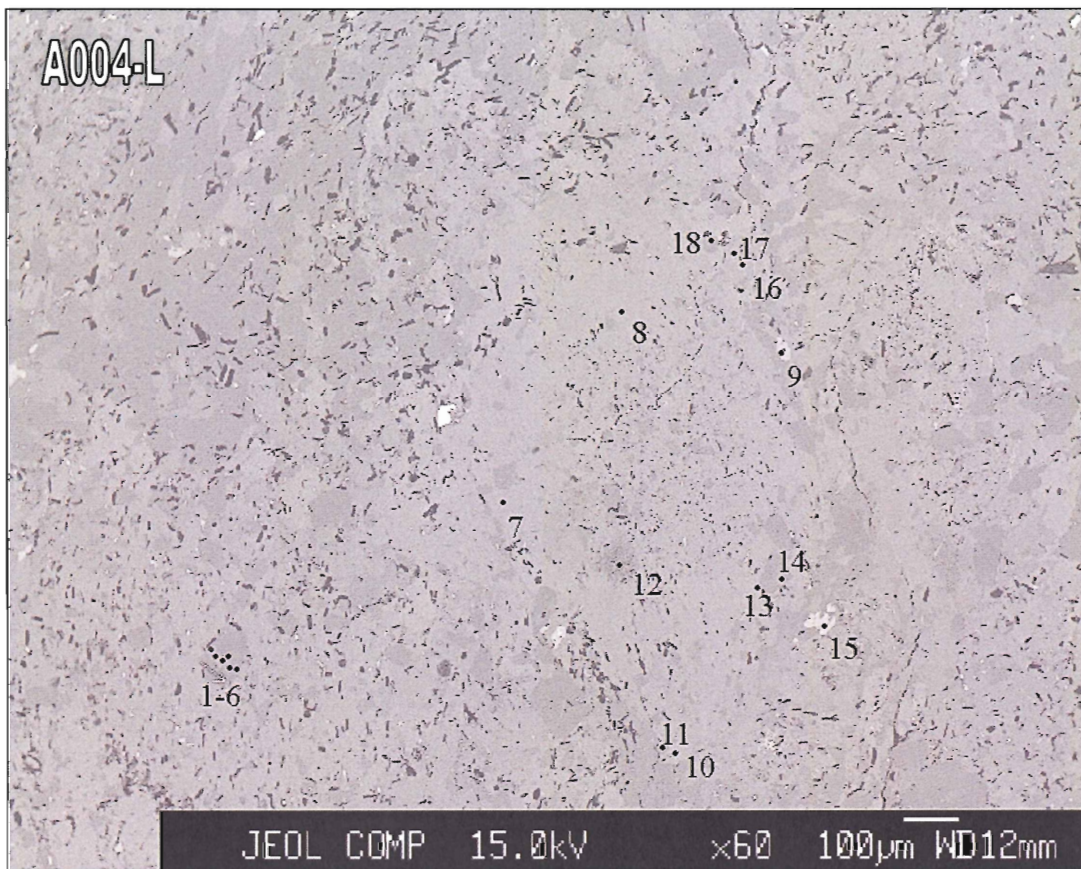
Sample	A003-C	A003-C	A003-C	A003-C	A003-C	A003-C	A003-C	A003-C	A003-C	A003-C
Lithology	Granite	Granite	Granite	Granite	Granite	Granite	Granite	Granite	Granite	Granite
No.	252	253	254	255	256	258	261	264	265	266
Mineral	Titanite	Titanite	Titanite	Titanite	Titanite	Titanite	Titanite	Titanite	Titanite	Titanite
Wt%										
SiO ₂	29.35	30.45	30.22	30.70	29.98	30.08	30.11	29.19	29.66	29.79
TiO ₂	35.57	35.34	34.25	27.87	34.71	32.26	34.47	30.10	31.27	31.26
Al ₂ O ₃	1.36	1.90	2.04	6.54	1.74	2.41	1.92	3.24	3.56	3.56
FeO	0.14	0.38	0.32	0.36	0.20	0.46	0.24	0.65	0.55	0.61
CaO	28.04	29.33	29.04	29.77	28.78	28.78	29.28	27.10	28.47	28.44
Total	94.90	97.78	96.29	95.81	95.84	94.35	96.41	90.85	94.07	94.22

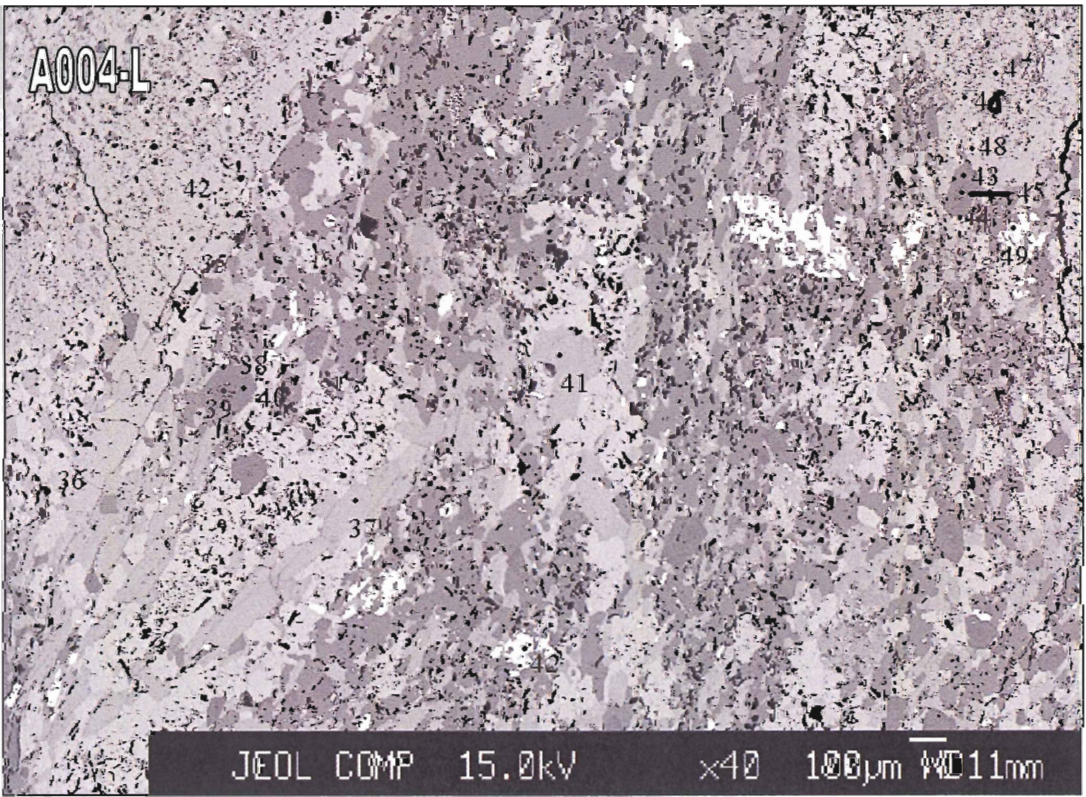
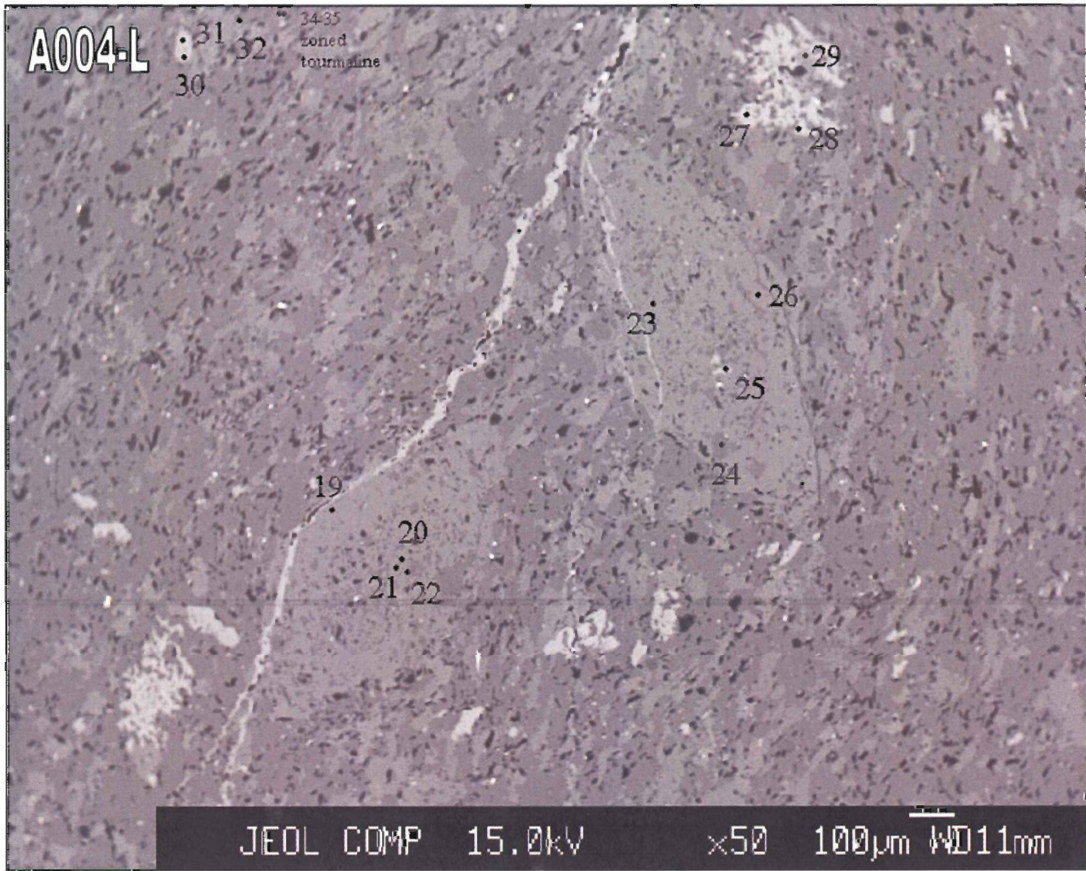
Cations (Calculated on the basis of 5O)

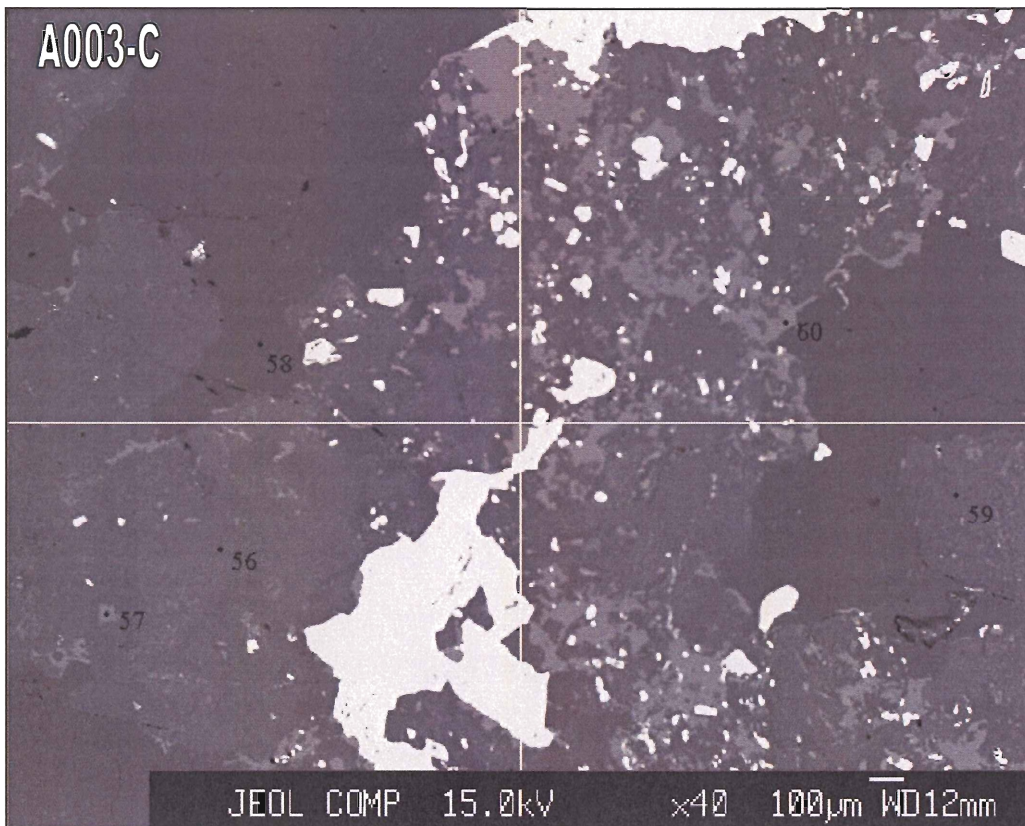
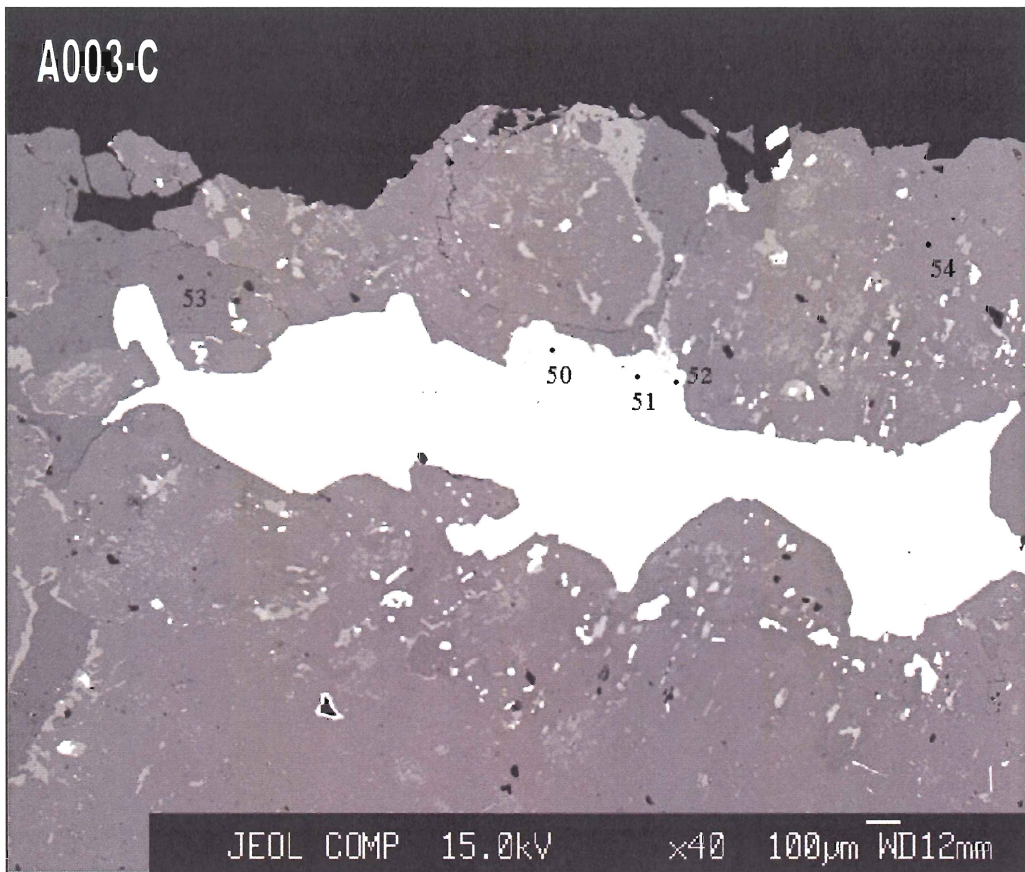
Si	0.620	0.630	0.640	0.650	0.630	0.650	0.630	0.650	0.640	0.640
Ti	1.180	1.140	1.130	0.920	1.150	1.090	1.130	1.050	1.060	1.050
Al	0.070	0.090	0.100	0.330	0.090	0.120	0.090	0.170	0.180	0.180
Fe	0.010	0.010	0.010	0.010	0.010	0.020	0.010	0.020	0.020	0.020
Ca	1.280	1.300	1.310	1.350	1.300	1.330	1.320	1.300	1.320	1.310
Total	3.160	3.180	3.190	3.260	3.180	3.200	3.190	3.210	3.210	3.210

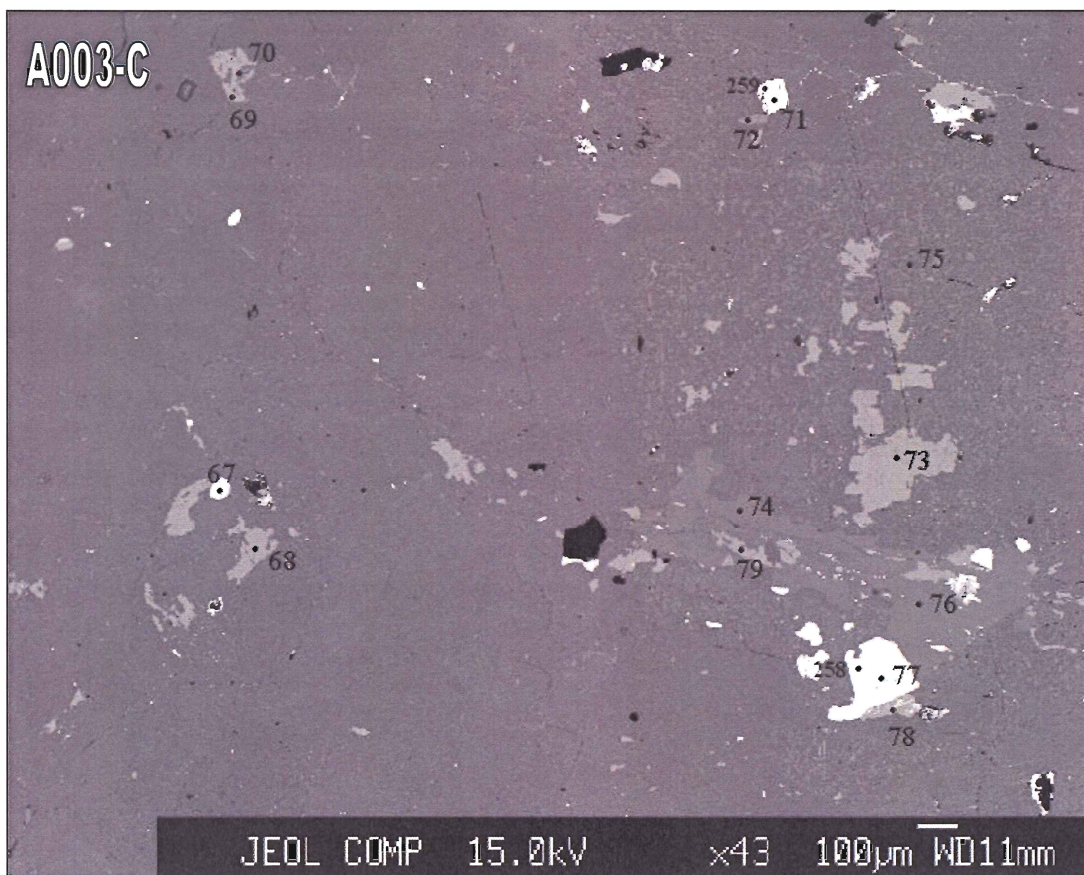
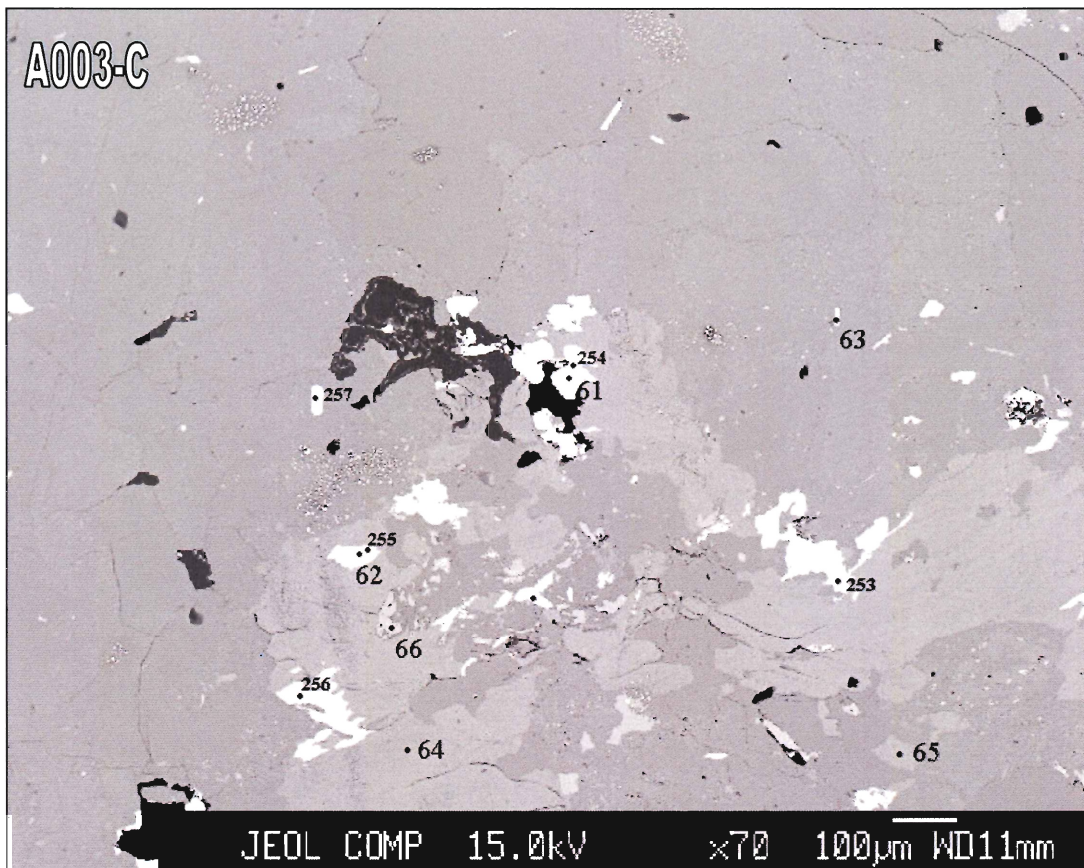
APPENDIX B: MICROPROBE IMAGES

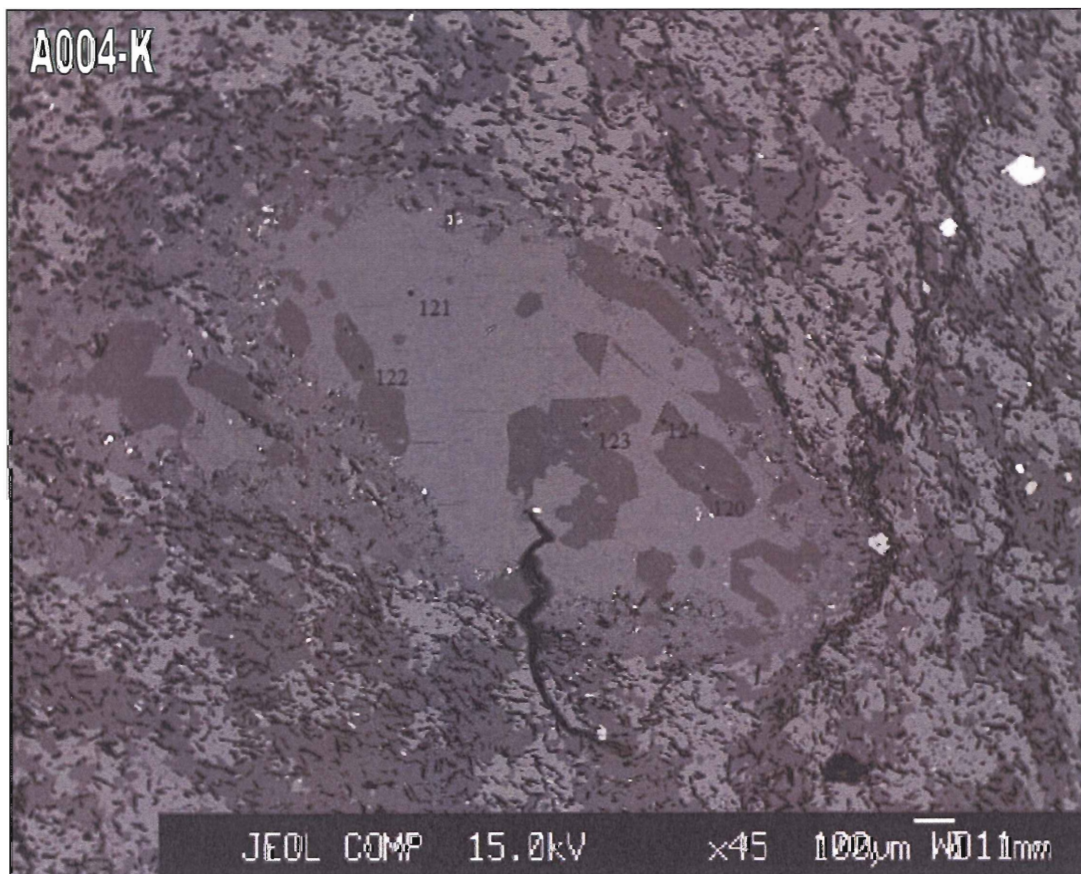
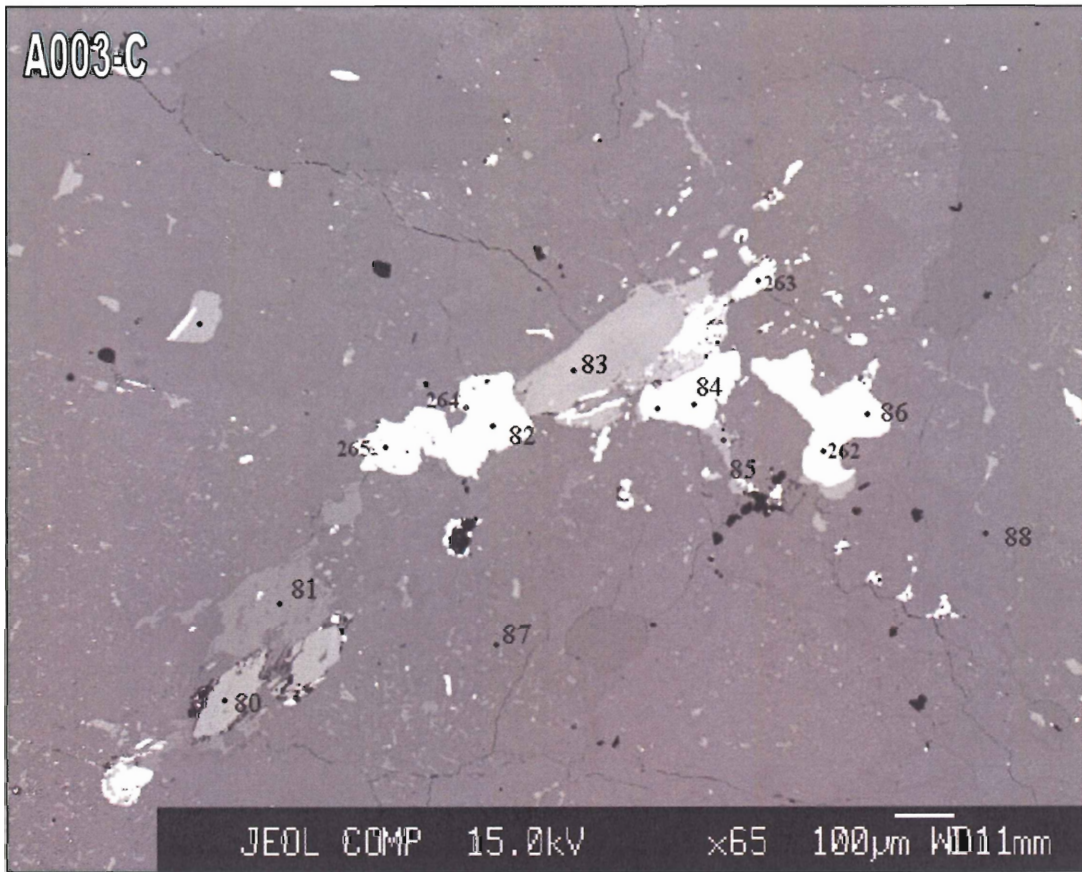
The following are backscattered electron (BSE) images obtained during electron microprobe analyses of study samples. The sample number in the upper left of the photos and the numbered points correspond to the sample and analysis 'No.' in Appendix A.



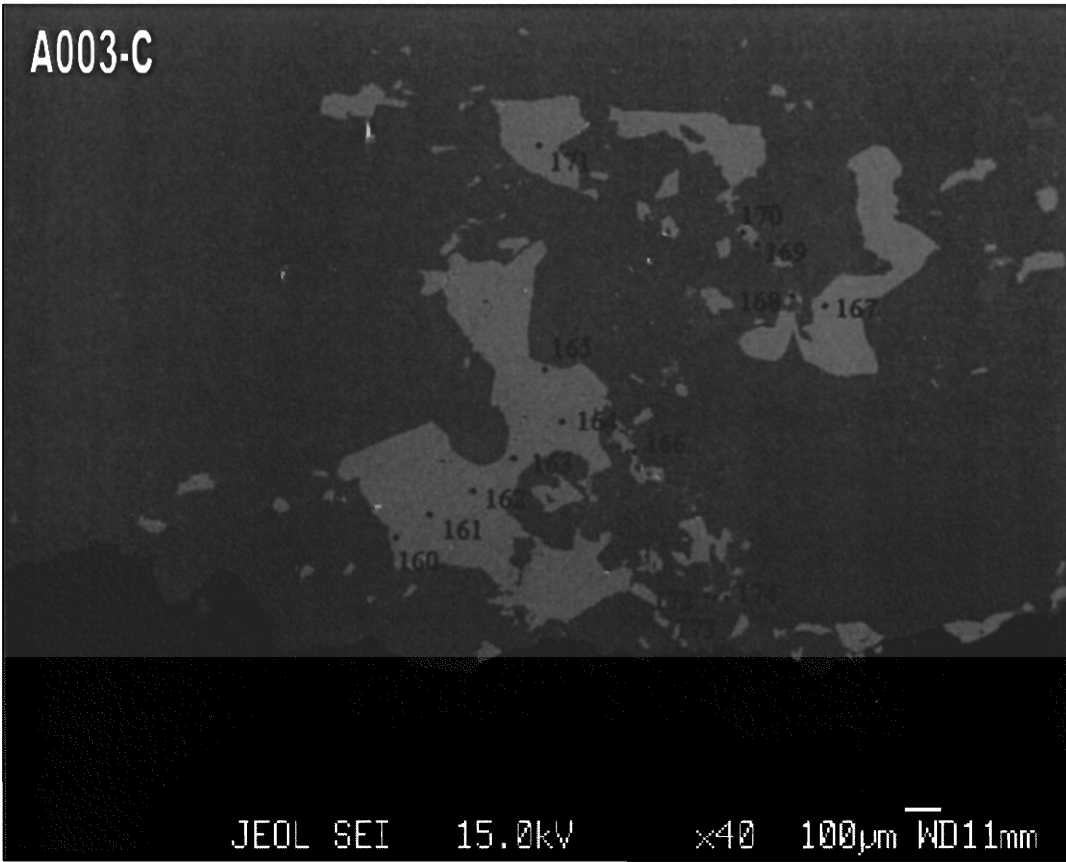




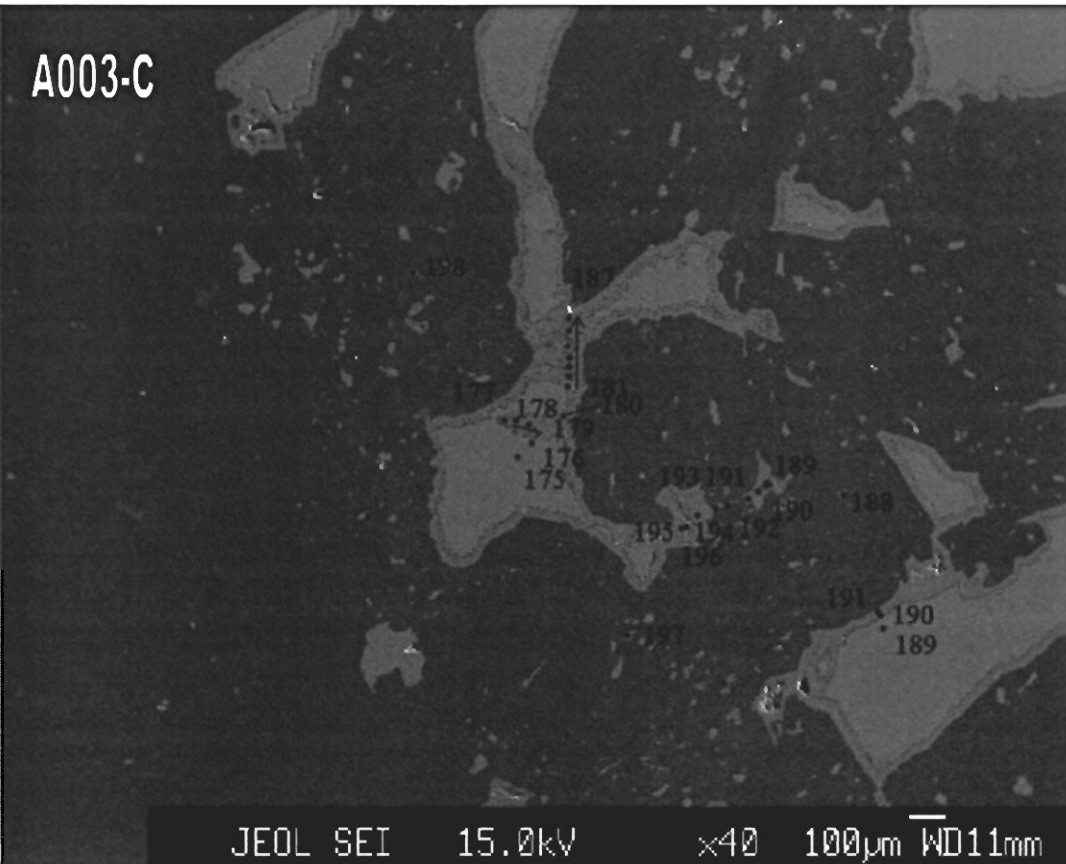


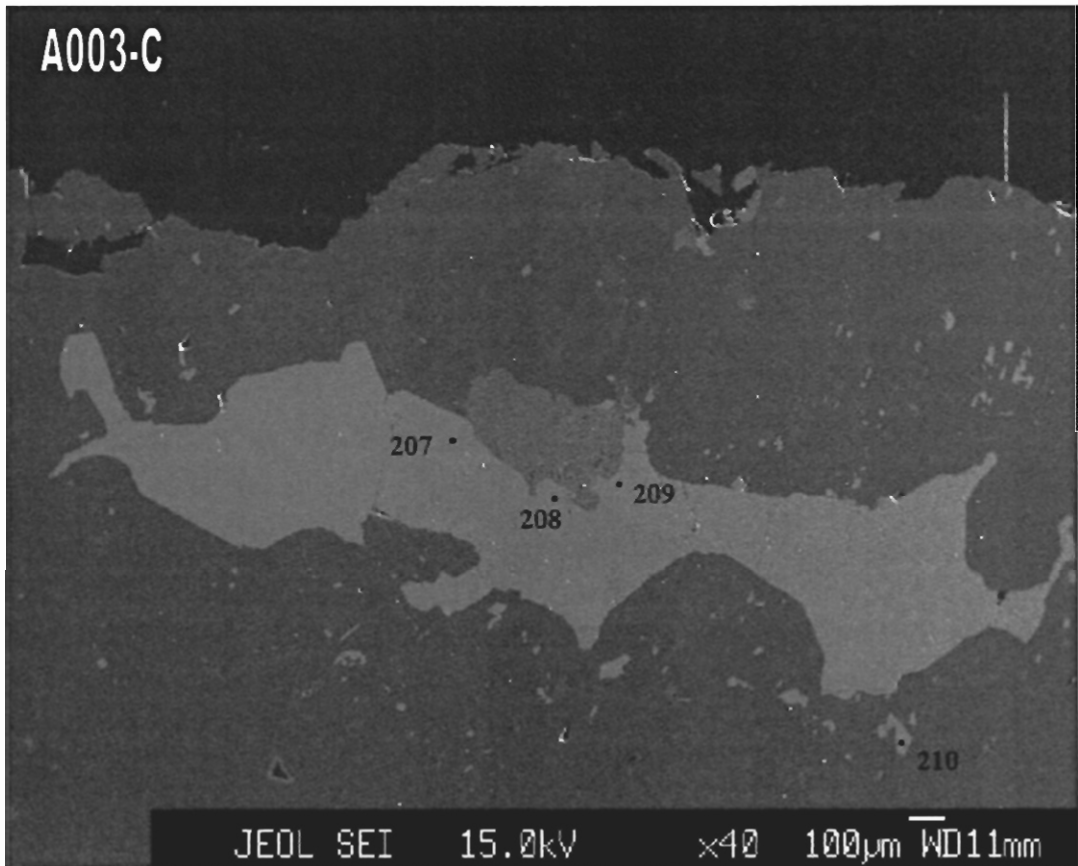
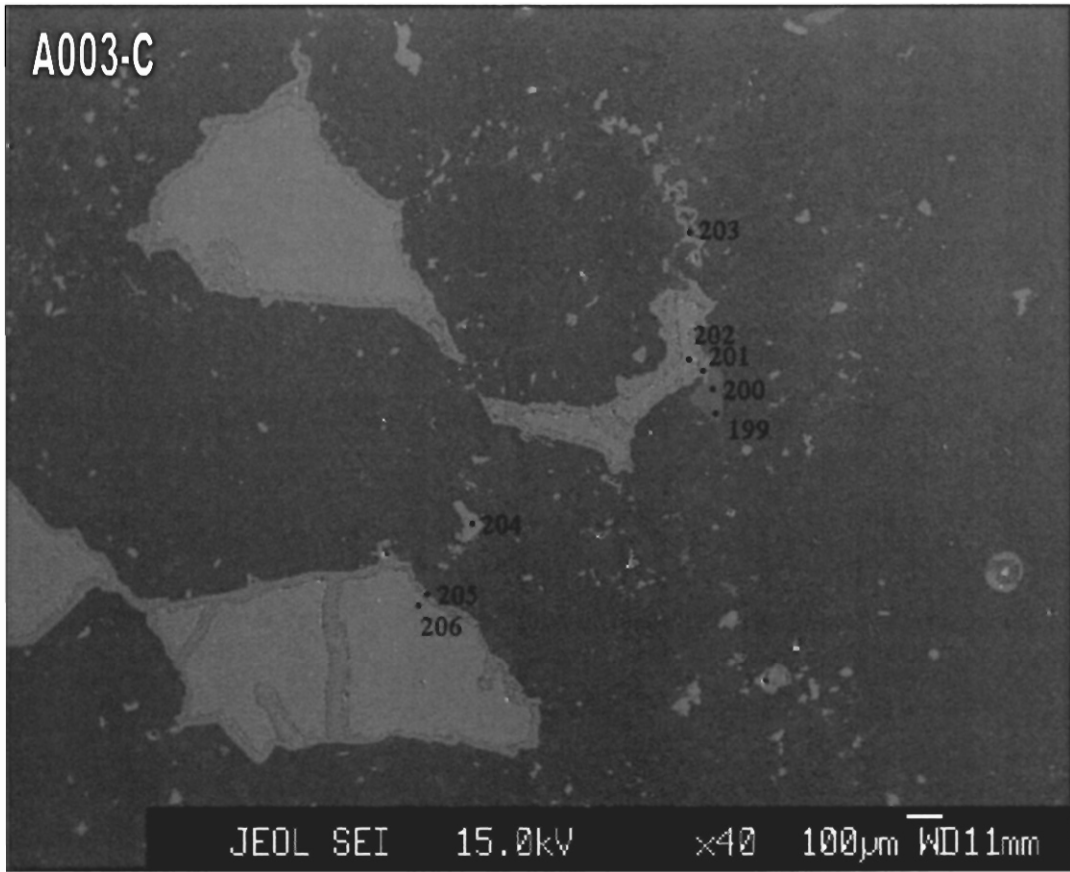


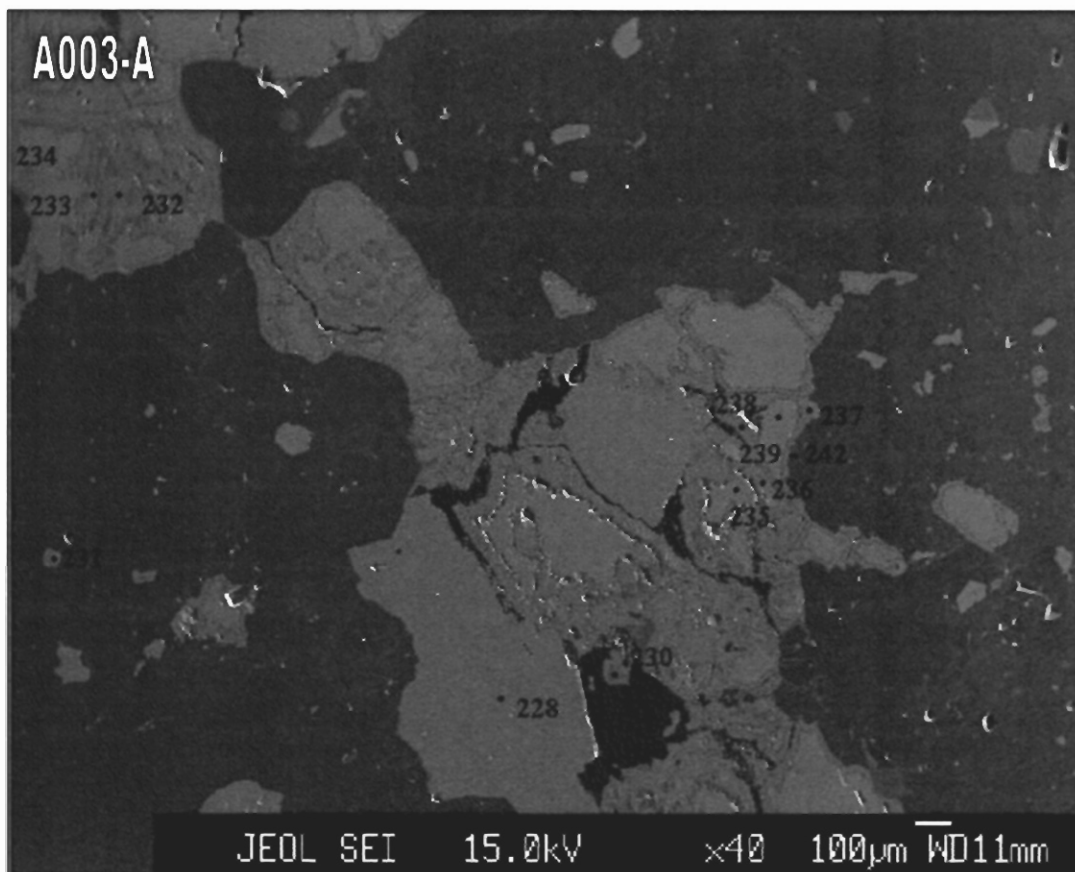
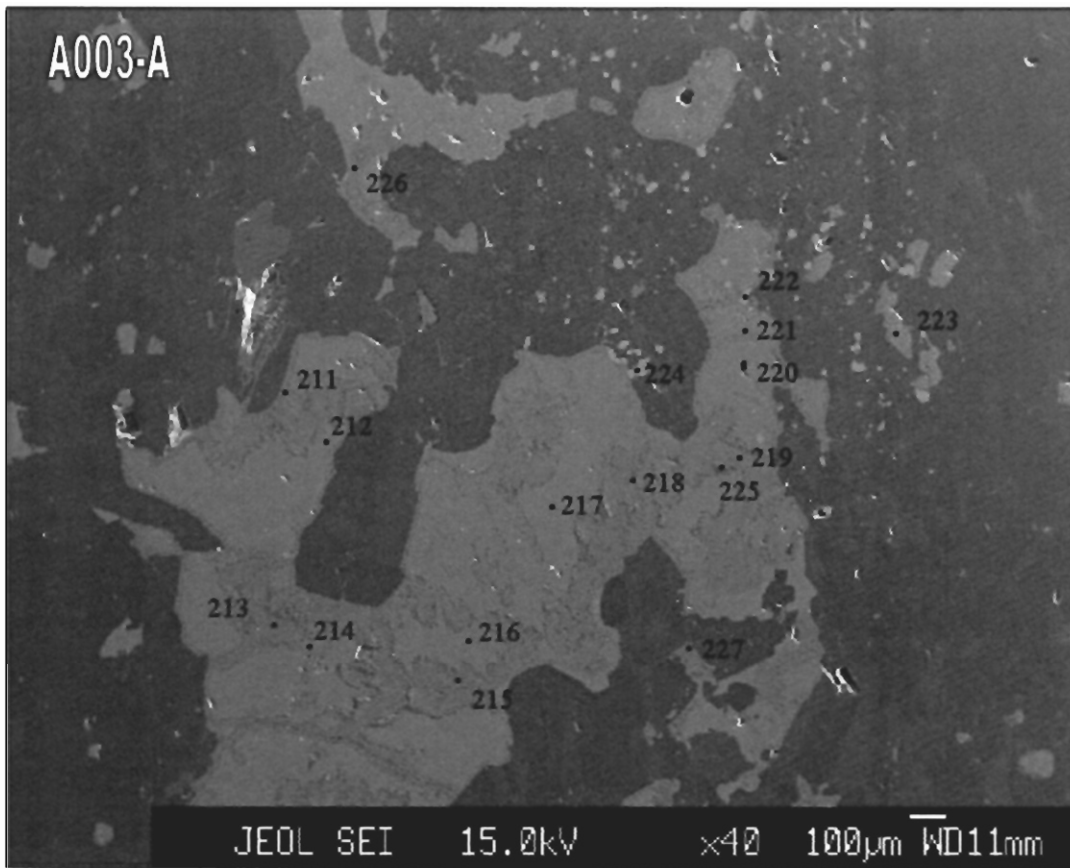
A003-C



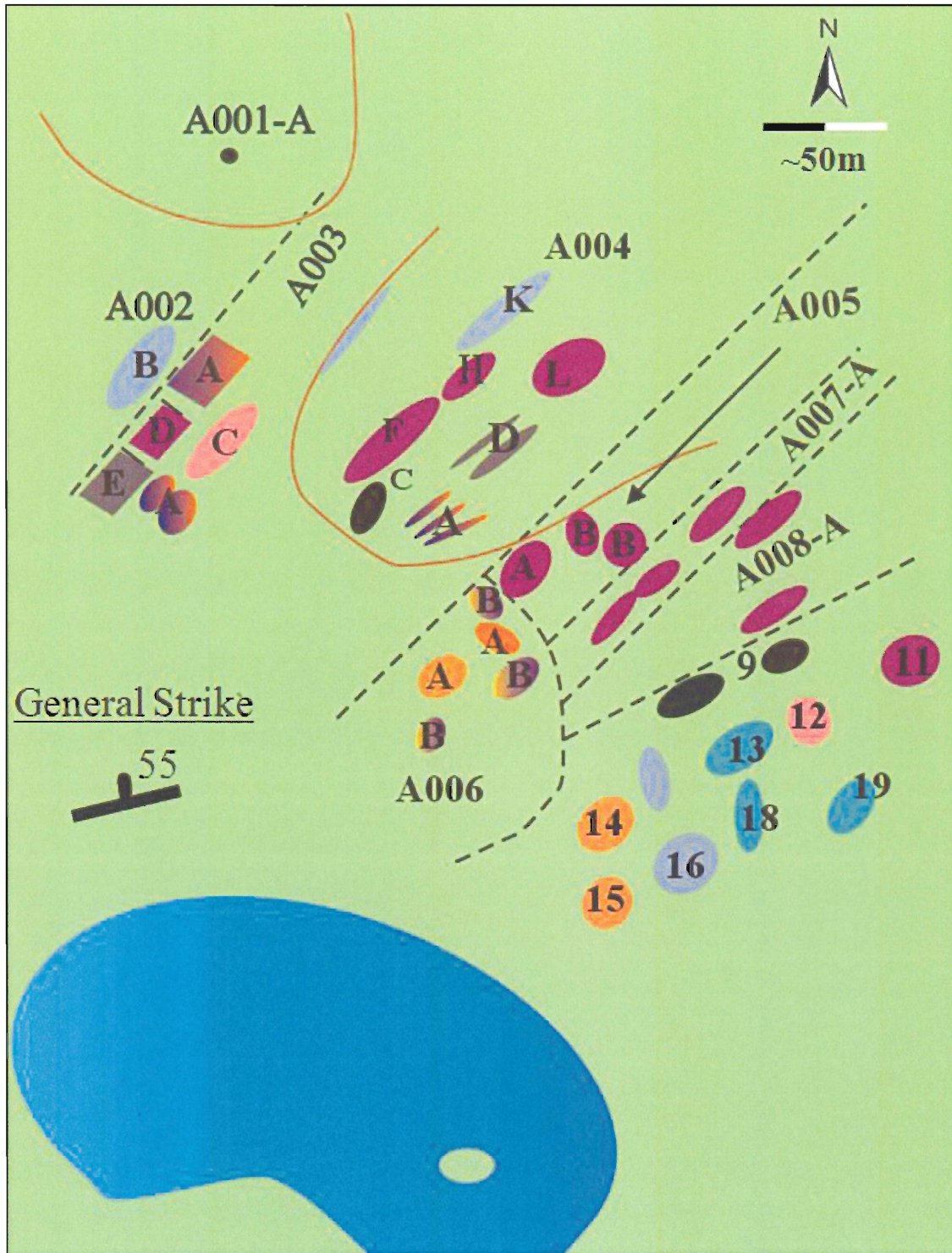
A003-C















APPENDIX C: SAMPLE AREA MAP



- | | | |
|--|--|---|
|  Graphite-rich pelite |  Granite |  Tourmaline-rich pelite |
|  Amphibolite |  Tourmalinite |  Greywacke |
|  Musc-schist |  Gabbro | |

REFERENCES

- Alonso, C V. (1997). The variation of tourmaline chemistry with metamorphic grade in southwest maine. *Keck Research Symposium in Geology*, 10, 183-186.
- Barnes, H.L. (1997) *Geochemistry of Hydrothermal Ore Deposits*. New York: Wiley.
- Berman, R.G., Camacho, A. & Sandeman, H.A. (2010) Diachronous Palaeoproterozoic deformation and metamorphism in the Committee Bay belt, Rae Province, Nunavut: insights from ^{40}Ar - ^{39}Ar cooling ages and thermal modelling. *Journal of Metamorphic Geology*, 28, 439.
- Clarke, D.B., Reardon, N.C., Chatterjee, A.K. & Gregoire, D.C. (1989) Tourmaline composition as a guide to mineral exploration; a reconnaissance study from Nova Scotia using discriminant function analysis. *Economic Geology and the Bulletin of the Society of Economic Geologists*, 84, 1921-1935
- Corrigan, D., Nadeau, L. & Tremblay, T. (2010) The GEM-minerals program on Melville Peninsula: project summary and preliminary report. Geological survey of Canada. Web. <<http://www.nunavutminingsymposium.ca/wp-content/uploads/2010/04/Corrigan-and-Tremblay-C-NGO.pdf>>.
- Corrigan, D., St-Onge, M.R. & Scott, D.J. (2001) Geology of the Northern Margin of the Trans-Hudson Orogen (Foxe Fold Belt), Central Baffin Island, Nunavut. Lecture. Ottawa. Natural Resources Canada. Web.<<http://dsp-psd.pwgsc.gc.ca/Collection/M44-2001-C23E.pdf>>.
- Day, S. J. (2009) Regional lake sediment and water geochemical data, Melville Peninsula, Nunavut (parts of NTS 046N, O, P, 047A and B). *Geological Survey of Canada Open-File Report*.
- Deer, W. A., Howie, R.A., & Zussman, J. (1997) *Rock Forming Minerals: Orthosilicates and Ring Silicates*. London: Geological Society.
- Dietrich, R. V. (1985) *The tourmaline group*. Van Nostrand Reinhold Co., New York, NY, United States (USA)
- Edgar, A. & Arima, M. (1985) Fluorine and chlorine contents of phlogopites crystallized from ultrapotassic rock compositions in high pressure experiments; implication for halogen reservoirs in source regions. *The American Mineralogist*, 70, 529.
- Galbraith, C.G., Clarke, D.B., Trumbull, R.B., & Wiedenbeck, M. (2009) Assessment of tourmaline compositions as an indicator of emerald mineralization at the Tsa da Glisza Prospect, Yukon Territory. *Canada Economic Geology and the Bulletin of the Society of Economic Geologists*, 104, 713-731.

- Garda, G.M., Beljavskis, P., Juliani, C., and Silva, D. (2003) Geochemistry associated with iron formation and quartz veins of the Morro da Pedra Preta Formation, Serro do Itaberaba Group: *Anais da Academia Brasileira de Ciencias*, 75, 209–234.
- Goodfellow, W. D. & Lydon, J. (2007) Sedimentary Exhalative Deposits. Mineral Deposits of Canada: a Synthesis of Major Deposit-types, District Metallogeny, the Evolution of Geological Provinces, and Exploration Methods. St. John's, NL: *Geological Association of Canada, Mineral Deposits Division*, 163-85.
- Henderson, J.R. (1983) Geology, southeastern Melville Peninsula, District of Franklin, Northwest Territories; *Geological Survey of Canada, Map 1655A*, scale 1:100 000.
- Henderson, J.R. (1983) Structure and metamorphism of the Aphebian Penryhn Group and its Archean basement complex in the Lyon Inlet area, Melville Peninsula, District of Franklin; *Geological Survey of Canada, Bulletin 324*.
- Henry, D.J. & Dutrow, B.L. (1996) Metamorphic Tourmaline and its Petrologic Applications. In *Boron: Mineralogy, Petrology and Geochemistry Review Minerals*. 33, 503-557.
- Henry, D. & Guidotti, C.V. (1985) Tourmaline as a petrogenetic indicator mineral: an example from the staurolite-grade metapelites of NW Maine. *The American Mineralogist*, volume 70, 1-15.
- Hill, B.F. (1996) Geological and Geochemical Report for the Bar Grid NTS 46 0/7; Melville Peninsula, Nunavut. Report.
- Hitzman, M.W., Selley, D. & Bull, S. (2010) Formation of Sedimentary Rock-Hosted Stratiform Copper Deposits through Earth History. *Economic Geology*, 105, 627-639.
- Holler, W. & Gandhi S.M. (1997) Origin of tourmaline and oxide minerals from the metamorphosed Rampura Agucha Zn-Pb-(Ag) deposit, Rajasthan, India. *Mineral Petrol*, 60, 99–119.
- Houlé, M G; Gibson, H L; Richan, L; Bécu, V; Corrigan, D; Nadeau, L. (2010) A new nickel discovery in the Prince Albert Hills, Melville Peninsula, Nunavut: implications for Ni-Cu-(PGE) exploration in the Prince Albert Group; *Geological Survey of Canada, Open File 6729*.
- Jiang, S.Y., Palmer, M.R., Slack, J.F. & Shaw, D.R. (1999) Boron isotope systematics of tourmaline formation in the Sullivan Pb-Zn-Ag deposit, British Columbia, Canada. *Chemical Geology*, 158, 131-144.
- Johns, S. M., Helmstaedt, H.H. & Kyser, K.T. (2006) Paleoproterozoic submarine intrabasinal rifting, Baffin Island, Nunavut, Canada; volcanic structure and geochemistry of the Bravo Lake Formation. *Canadian Journal of Earth Sciences* 43, 593-616.

- Jolliff, B.L., Papike, J.J., and Shearer, C.K. (1986) Tourmaline as a recorder of pegmatite evolution: Bob Ingersoll pegmatite, Black Hills, South Dakota: *American Mineralogist*, 71, 472–500.
- Keller, P., Robles, E.R., Pérez, A.P., and Fontan, F. (1999) Chemistry, paragenesis and significance of tourmaline in pegmatites of the southern tin belt, central Namibia. *Chemical Geology*, 158, 203–225.
- Kesler, S. (2005) Ore-forming fluids. *Elements*, 1, 13-18.
- Lyons, T. W., Gellatly, A.M., McGoldrick, P.J., Kah, L.C. (2004) Proterozoic sedimentary exhalative (sedex) deposits and their links to evolving global ocean chemistry. *Geological Society of America Memoir 198*, 36, 200.
- Mallio, W. & Gheith, M.A. (1972) Textural and chemical evidence bearing on sulfide-silicate reactions in metasediments. *Mineralium deposita*, 7, 13-17.
- Marmot, C. (1994) Geochemical and Geological Report; Nagvaak Project, Melville Peninsula . BHP Minerals Canada Ltd.
- Okulitch, A. V., Gordon, T., Henderson, J.R., Reesor, J.E. & Hutcheon, I.E. (1997) Geology of the Barrow River map-area, Melville Peninsula, District of Franklin. *Geological Survey of Canada*, 77, 213-215.
- Palmer, M. & Slack, J.F. (1989) Boron isotopic composition of tourmaline from massive sulfide deposits and tourmalinites. *Contributions to Mineralogy and Petrology*, 103, 434-451.
- Pirajno, F., and Smithies, R.H.(1992) The FeO/(FeO + MgO) ratio of tourmaline: A useful indicator of spatial variations in granite-related hydrothermal mineral deposits. *Journal of Geochemical Exploration*, 42, 371–381
- Sanborn-Barrie, M. (2009) New Insights into the Precambrian Geology of NE Laurentia from GSC CNGO Framework Mapping Projects." Speech. Nunavut Mining Symposium. Web. <<http://www.nunavutminingsymposium.ca/wp-content/uploads/2009/06/mary-sanborn-barrie-130-pm.pdf>>.
- Scott, D. I. (2008) An Overview of the Geology of Nunavut. Instructional Web Server. <<http://instruct.uwo.ca/earth-sci/300b-001/seg/scott.htm>>.
- Slack, J.F. (1996) Tourmaline associations with hydrothermal ore deposits: Boron; mineralogy, petrology and geochemistry. *Reviews in Mineralogy*, 33, 559-643
- Slack, J. F., Herriman, N., Barnes, R.G. & Plimer, I.R (1984) Stratiform tourmalinites in metamorphic terranes and their geologic significance. *Geology*, 12, 713-716.

- St-Onge, M.R., Wodicka, N. & Ijewliw, O. (2007) Polymetamorphic Evolution of the Trans-Hudson Orogen, Baffin Island, Canada: Integration of Petrological, Structural and Geochronological Data. *Journal of Petrology*, 48, 271–302.
- Taylor, B. and Slack, J.F. (1984) Tourmalines from Appalachian-Caledonian massive sulfide deposits; textural, chemical, and isotopic relationships. *Economic geology and the bulletin of the Society of Economic Geologists*, 79, 1703-1726.
- van Hinsberg, V.J., Henry, D.J. & Marschall, H.R. (2011) Tourmaline; an ideal indicator of its host environment. *The Canadian Mineralogist*, 49, 1-16.
- White, W. M. (2009) Chapter 13: Reactions at the Earth's Surface: Weathering, Soils, and Stream Chemistry. Lecture. Cornell University; Geochemistry. *International Mine Water Association*. Web. <<http://www.imwa.info/white-geochemistry.html>>.
- Yavuz, F. (1999) A revised program for microprobe-derived amphibole analyses using the IMA rules. *Computers & geosciences*, 25, 909-927.